Минералдық шикізаттарды кешенді пайдалану

2 (321)

Комплексное Использование Минерального Сырья

Complex Use of Mineral Resources

Address:
Institute of Metallurgy and Ore Beneficiation
29/133 Shevchenko Street, corner of Ch. Valikhanov Street,
Almaty, 050010, Kazakhstan
Fax. +7 (727) 298-45-03, Tel. +7-(727) 298-45-02, +7 (727) 298-45-19
E mail: journal@kims-imio.kz, product-service@kims-imio.kz
www.kims-imio.kz

Investigation of the properties of oxide coatings on titanium alloys obtained by plasma electrolytic oxidation

1,2* Ramazanova Zh.M., 2 Zamalitdinova M.G., 3 Kovalenko M.V.

1 S. Seifullin Kazakh Agro Technical University, Nur-Sultan, Kazakhstan
2 JSC "National Center for Space Research and Technology", Almaty, Kazakhstan
3 L.N. Gumilyov Eurasian National University, Nur-Sultan, Kazakhstan

* Corresponding author email: zh_ram@mail.ru

ABSTRACT

The use of structures made of titanium and its alloys, which have improved corrosion, physical and mechanical properties, are in demand in many industries. In this regard, the processes of modifying the surface of metals are of interest. One of the modern and promising methods of metal surface treatment is plasma electrolytic oxidation. Currently, there is a problem of widespread use of this process when DC modes are used in the implementation of the process. This is due to the large consumption of electricity. The purpose of this work is to study the morphological and corrosion properties of oxide coatings obtained in the pulsed anode-cathode mode on titanium alloys VT1-0 and VT5 in various electrolyte solutions. Modification of the surface of titanium alloys was carried out at the duration of the anode current pulse of 250 ± 25 microseconds, the duration of the cathode current pulse of 5 ± 0.5 ms, the repetition frequency of the anode and cathode pulses of 50 ± 0.5 Hz. Alkaline solutions served as electrolytes. Oxide coatings obtained in various electrolytes are characterized by different porosity and coating thickness. Coatings with a finely porous structure, with an average pore diameter from 0.09 microns to 0.4 microns, and larger pore sizes of $0.6 - 0.7$ microns were obtained. The porosity of the coatings ranges from 6.12% to 12.2%. According to the data of energy dispersion analysis, it was found that the structure of oxide coatings includes both components of the processed metal and components of the electrolyte solution. The main components, in this case, are oxygen and processed metal, as well as other elements such as boron, phosphorus, aluminium, fluorine, sodium, silicon and others. Corrosion tests according to GOST 9.308-85 under the influence of neutral salt mist at a temperature of (35 ± 2) °C with 1500 hours in the Ascott CC 450 chamber, it was shown that there was no corrosion damage to the coatings.

Keywords: oxide coating, electrolyte, plasma-electrolytic oxidation, corrosion tests, coating morphology, porosity.

	Information about authors:
Ramazanova Zhanat Musanovna	Candidate of Chemical Sciences, Associate Professor of S. Seifullin Kazakh Agro Technical University, Head of the Space Monitoring Center Nur-Sultan city, JSC "National Center of Space Research and Technology". E-mail: zh_ram@mail.ru, ORCID ID: 0000-0003-1419-2886
Zamalitdinova Marina Grigorievna	Master of Information Systems, Researcher at the Space Monitoring Center Nur-Sultan city, JSC "National Center of Space Research and Technology". E-mail: kazncsm@yandex.ru, ORCID ID: 0000-0002-8746-1664
Kovalenko Maria Vitalievna	Master student of L.N. Gumilyov Eurasian National University, Nur-Sultan, Kazakhstan. E-mail: maria.kovalenko.98@mail.ru, ORCID ID: 0000-0003-1838-6338

Introduction

Titanium and its alloys are widely used in many sectors of the manufacturing economy. However, to create promising and modernize existing products, it is necessary to give them a set of properties, such as a combination of corrosion resistance and good physical and mechanical properties. By introducing alloying additives, the properties of titanium alloys are improved [[1], [2]]. Aluminum, vanadium, molybdenum, silicon, chromium, zirconium and others can be used as alloying additives. The introduction of alloying additives during titanium smelting positively affects its corrosion resistance and other properties [2]. However, this leads to an increase in the cost of the product and the weight of the structure.

Currently, classical materials science is giving way to methods of modifying the properties of materials, such as surface treatment, since the

surface characteristics determine the level of product properties [[3], [4]]. In addition, surface modification is more attractive compared to other methods of changing the characteristics of materials and products.

Currently, plasma electrolytic oxidation (PEO) is one of the promising methods for modifying the surface of titanium [[5], [6], [7]]. This method allows you to change the surface condition of valve metals significantly, which makes it possible to replace traditional materials with inexpensive and non-scarce materials. At the same time, there is a significant improvement in the operational properties of products [[8], [9], [10]].

A distinctive feature of the PEO method is the participation in the modification process of surface micro-discharges, which have a significant and specific effect on the phase and structural properties of the coating [11]. The obtained oxide coatings by the PEO method in electrolyte solutions have high adhesion to the substrate, wear resistance, and heat resistance [[12], [13]].

The implementation of the PEO process can be carried out in various modes using stationary and slowly changing energy influences. In these modes, the application of the method is not widely used due to the large consumption of electricity. Recently, PEO modes based on fast-flowing (pulsed) energy effects have been used [14]. With a small value of the duration of the anode current pulse of the order of 250 microseconds, coatings characterized by low roughness are formed [15]. The use of these modes does not require a large consumption of electricity, and can contribute to a wider application of the PEO method in production.

It is known that the properties of oxide coatings are influenced by the composition of electrolyte solutions [16]. In view of this, it is relevant to study the corrosion resistance and morphology of coatings obtained in various electrolytes. This makes it possible to purposefully form functional coatings with certain properties.

This work aims to study the properties of complex oxide coatings, consisting of two or more elements obtained in the pulsed anode-cathode mode of PEO in various electrolyte solutions.

Experimental part

Samples from titanium alloys VT1-0 and VT5 were subjected to surface treatment by plasma electrolytic oxidation. The samples had a rectangular shape with a thickness of 3 mm and a size of 20 x 40 mm and 15 x 40 mm. The samples were ground

before the PEO process to remove irregularities and scratches. Further, the surfaces of the samples were degreased using ethyl alcohol. Drying was carried out at room temperature. The scheme of the installation for obtaining oxide coatings by the PEO method is shown in Figure 1.
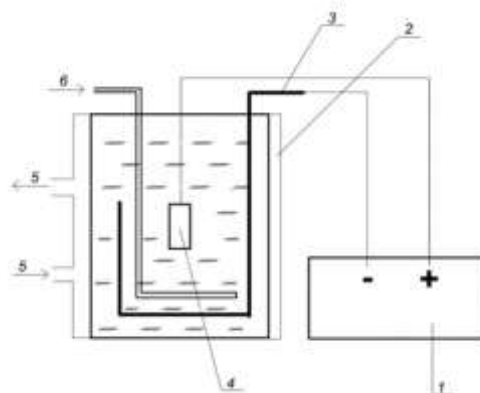
Figure 1 - Installation diagram: 1 - power supply, 2 - electrochemical bath with water cooling jacket, 3 - auxiliary electrode (cathode), 4 - coated sample (anode), 5 - water, 6 – air

The research facility consisted of a bath with a cooling system. Stainless steel was used as the cathode. The processed samples served as the anode. A switching power supply "Corundum M0", not mass-produced, was used to obtain oxide coatings. The power supply generates positive and negative voltage pulses of trapezoidal shape. The PEO processing of titanium samples took place under the following conditions: the duration of the anode current pulse is 250 ± 25 microseconds; the duration of the cathode current pulse is 5 ± 0.5 ms; the interval between the anode and cathode current pulses is 250 ± 25 microseconds; the frequency of the anode and cathode pulses is 50 ± 0.5 Hz, the voltage is within 360-365 V. The current density was in the range of 109 - 115 A/dm^2, and this parameter depends on the composition of the electrolyte and the metal alloy. Processing time 600 sec. The electrolyte temperature was maintained within 20 ^{o}C – 25 ^{o}C. To obtain coatings, electrolytes were used, the compositions of which are presented in Table 1.

Electrolyte solutions were prepared from chemical substances of the chemically pure grade, analytical grade. Electrolytes were prepared in distilled water. The thickness of the oxide coatings was measured using a NOVOTEST TP-1 thickness gauge with an NF-2 sensor with a digital indicator indication. When measuring the thickness of oxide coatings, 7 measurements were carried out on both sides of the sample. Next, the arithmetic mean of the coating thickness was calculated.

Table 1 - Compositions of electrolytes

No. electrolyte	Name of the component	Concentration, g/l
1	Sodium silicate (metasilicate) 9 aqueous	100
	NaOH	8
	Aluminum oxide (1.1-1.5 microns) powder	20
2	Sodium phosphoric acid 3- substituted, 12 aqueous	70
	Aluminium hydroxide (0.6 μm)	20
3	Sodium phosphoric acid, two-substituted, 12 aqueous	40
	Sodium tetraborate 10 aqueous	30
	Boric acid	22
	Ammonium fluoride (NH$_4$F)	10
	Aluminium oxide	20

Micrographs and energy dispersion analysis of oxide coatings on titanium alloys were obtained using a Hitachi TM3030 scanning electron microscope in SEI mode at an accelerating voltage of 15 kV with an Oxford Instruments energy dispersion analysis prefix.

When calculating porosity, the number of pores per surface unit, and evaluating their shapes, the planimetry method was used by processing micrographs of the surface of oxide coatings [17]. In this case, porosity was determined as the ratio of the sum of the pore areas F_P to the total area of the observation site F_{total}: $\Pi = \dfrac{\sum F_P}{F_{total}} 100\%$.

The corrosion resistance of samples with oxide coatings was carried out under the influence of neutral salt mist at a temperature of (35 ± 2) $^{\circ}$C for 1000 hours in the Ascott CC 450 chamber according to GOST 9.308-85. In the Ascott CC 450 chamber, the distance between the test samples was 20 mm; the distance from the chamber walls was at least 100 mm, and from the day of the chamber – at least 200 mm. The tests were carried out at a (35 ± 2) °C. According to GOST 9.308-85, a sodium chloride solution was continuously sprayed in the chamber (concentration 50 ± 5 g / dm3, pH of the solution 6.5 – 7.2). Spraying of salt mist was carried out so that the condensate volume during the chamber's operation for 24 hours was maintained within 1.2 - 1.5 cm^3/hour. The state of the oxide coatings was monitored visually through 2, 24, 96, 294, 460, 720, 1000 and 1500 hours of testing. During the control of coatings, samples were removed from the chamber, washed with tap water, dried.

The appearance was assessed for the presence of corrosion damage by the following signs: discolouration, pitting corrosion, peeling of the coating, etc.

Results and discussion

As a result of the PEO process, dense oxide layers are formed on the surface of titanium alloys VT1-0 and VT5, the thickness data given in Table 2. The thickness of the oxide coatings is uniform over the entire surface of the samples.

Table 2 - Data on the thickness of oxide coatings on titanium alloys

No. electrolyte	Coating thickness on VT1-0 alloy, microns	Coating thickness on VT5 alloy, microns
1	5.0	7.5
2	15.0	9.5
3	21.0	19.5

Energy dispersion analysis of the coatings obtained on titanium alloys showed that the main elements included in their composition are both components of the processed material (base) and the electrolyte solution. The composition of the coating mainly consists of oxygen and processed metal. Other elements are boron, phosphorus, aluminium, fluorine, sodium, silicon, etc. (Tables 3, 4).

In the work of researchers [18], the production of complex PEO coatings is confirmed. The authors have shown that the composition of the oxide layers formed on titanium from the calcium phosphate electrolyte system contains the elements Ti, P, Ca and O [18].

It is known that the pores in the PEO are formed at the place of micro-arc combustion [19]. During the initial period of the plasma electrolytic oxidation process, when a positive voltage is applied to the sample, a porous, thin barrier layer forms on the surface of the processed material according to the mechanism of electrochemical oxidation. Micro-

Table 3 - Composition of coatings on VT1-0 alloys

Electrolytes	Content of elements, at. %							
	O	Ti	B	P	F	Na	Al	Si
1	65.42	15.7	-	-	-	1.62	0.53	13.2
2	64.74	31.48	-	2.66	-	0.95	0.17	-
3	63.84	27.47	4.75	2.42	0.5	0.42	0.6	-

Table 4 - Composition of coatings on VT5 alloys

Electrolytes	Content of elements, at. %							
	O	Ti	B	P	F	Na	Al	Si
1	60.45	20.26	-	-	-	1.55	1.02	16.76
2	64.39	31.42	-	2.21	-	0.76	1.22	-
3	65.84	20.79	5.61	3.22	1.21	1.63	1.70	-

discharges do not occur when a barrier layer is formed (Figure 2a). Provided that the electrical strength of the barrier layer is less than the voltage at the electrode-solution interface, a breakdown occurs, a spark discharge occurs (Figure 2b), which, as the coating thickness increases, turns into a micro-arc (Figure 2c). High temperatures develop on the arc axis [[20], [21]].

When using the pulse mode, the burning time of the micro-arc depends on the duration of the anode pulse of the anode current pulse. As the coating thickness increases, the size of the micro-discharges may increase, and their number may decrease. This leads to the formation of pores of large diameters.

Morphological studies of the surface of the oxide coating have shown that as a result of PEO under pulsed anode-cathode mode in electrolyte No.1, both on the VT1-0 alloy and the VT5 alloy, many small pores with an average diameter of 0.09 microns on the VT1-0 alloy, and 0.2 microns on the VT5 alloy are formed (Figure 3 a- b; Table 5). The porosity of the coatings is 6.12% and 6.25%. The pores mostly have a rounded shape. Almost under the same conditions of the PEO process for all

electrolyte solutions, a thinner coating is formed in this electrolyte. This is due to the formation of a finely porous coating structure. To obtain coatings with a more significant value of its thickness, it requires a further increase in voltage from an external power source.

A finely porous structure also characterizes the oxide coatings obtained in electrolyte No.2. The average pore diameter for the VT1-0 alloy is 0.4 microns, and the porosity is 7.7% (Figure 3c; Table 6). On the VT5 alloy, the average pore diameter is 0.2 microns, and the porosity is 7.7%. (Figure 3d; Table 6). The pores are evenly distributed over the entire surface of the sample. It should be noted that the pore sizes in this electrolyte are larger than on the coating obtained in the first electrolyte, and, accordingly, the coating thickness is more significant. Small pores contribute to the reduction of mechanical stresses in the coating [22].

Larger pores are formed in electrolyte No.3 (Figure 3 e - f). The average pore diameter is 0.7 microns on the VT1-0 alloy, 0.6 microns on the VT5 alloy. The porosity of the coatings is 11.3% on the VT1-0 alloy, and 12.2% on the VT5 alloy (Table 7).
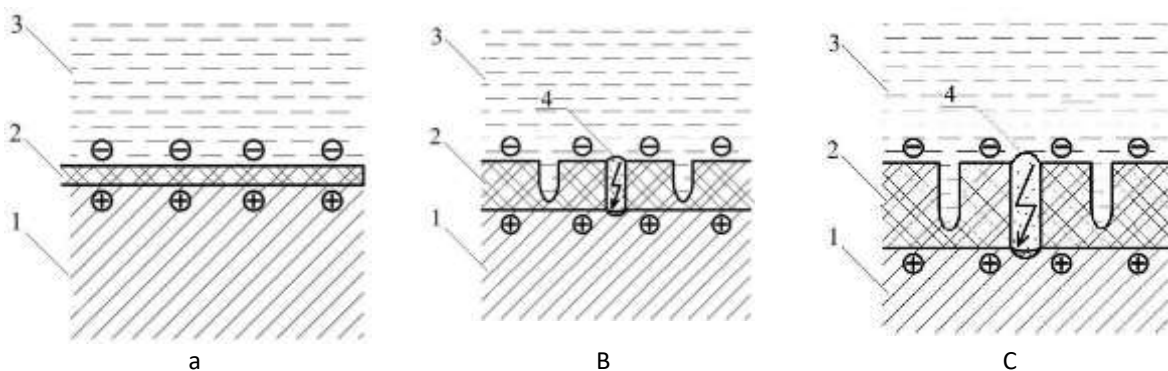
a – barrier layer formation; b - spark discharge stage; c - micro-arc discharge stage; 1 - metal, 2 – an oxide layer, 3 - electrolyte solution, 4 - plasma formation

Figure 2 - Scheme of the development of plasma formations

a

b

c

d

e

f
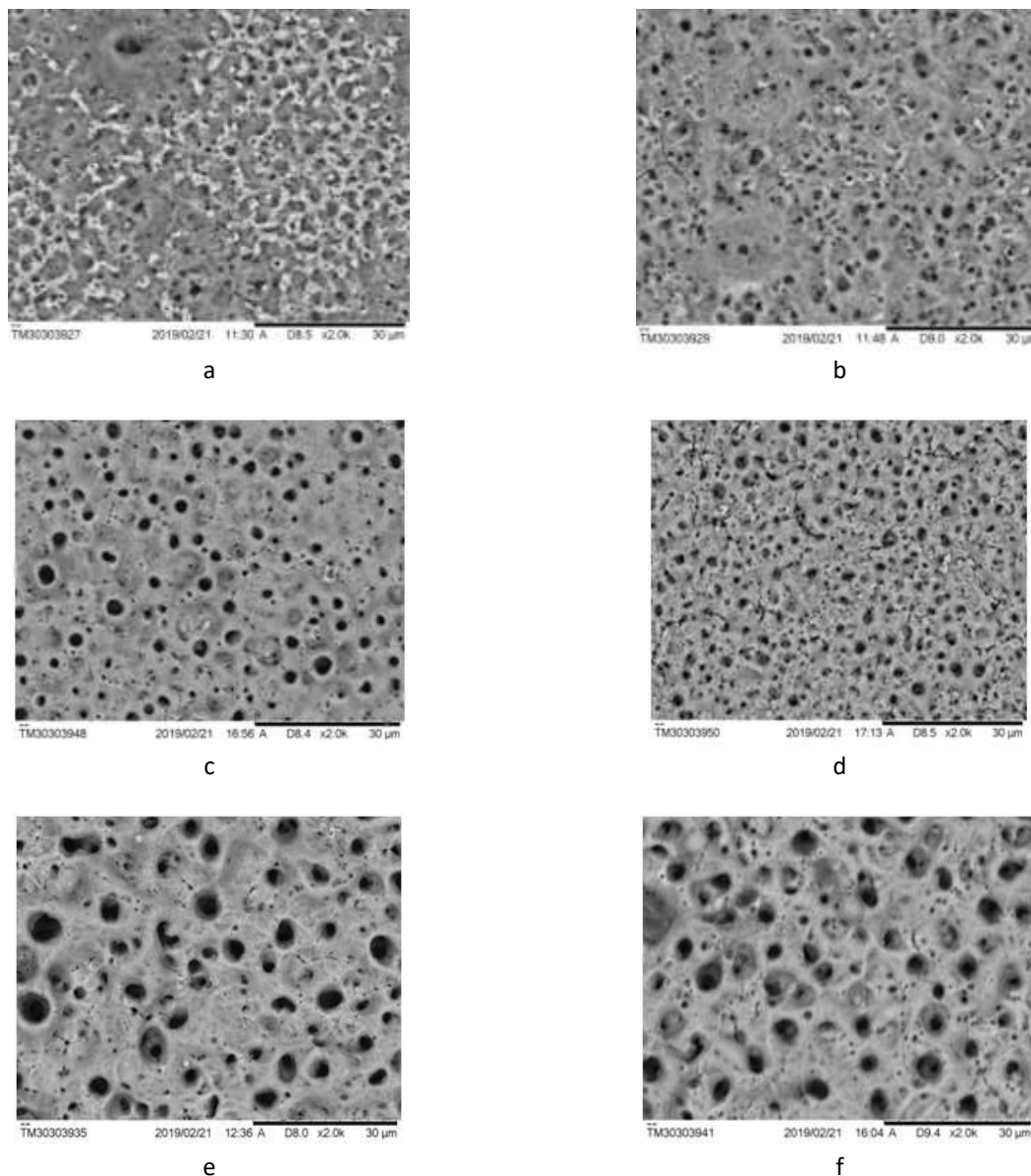
Figure 3 - Micrographs of oxide coatings obtained: a – in electrolyte 1 on VT1-0 alloy; b - in electrolyte 1 on VT5 alloy; c - in electrolyte 2 on VT1-0 alloy; d - in electrolyte 2 on VT5 alloy; e - in electrolyte 3 on VT1-0 alloy; f - in electrolyte 3 on VT5 alloy

Calculated data on the porosity of oxide coatings obtained in various electrolytes on titanium alloys VT1-0 and VT5 are given in Tables 5-7.

During corrosion tests, the change in the condition of the coatings was determined by visual inspection through 2, 24, 96, 294, 460, 720, 1000 and 1500 hours (Table 8).

Thus, at all stages of the test under the influence of neutral salt mist at a temperature of 35°C for 1500 hours at a solution concentration of 50 g/l of sodium chloride, the pH of the solution is 6.5 – 7.2, there is no corrosion damage on samples with oxide coatings, no traces of corrosion damage are observed. Oxide coatings have proven to be corrosion resistant.

Table 5 - Data on porosity of oxide coatings obtained in electrolyte 1

Alloy	Porosity ΔS, %	Number of pores per 1 cm² of coating	Average pore diameter, microns
VT1-0	6.12	$2.2 \cdot 10^7$	0.09
VT5	6.25	$1.3 \cdot 10^7$	0.2

Table 6 - Data on porosity of oxide coatings obtained in electrolyte 2

Alloy	Porosity ΔS, %	Number of pores per 1 cm² of coating	Average pore diameter, microns
VT1-0	7.7	$1.3 \cdot 10^7$	0.4
VT5	7.7	$1.6 \cdot 10^7$	0.2

Table 7 - Data on porosity of oxide coatings obtained in electrolyte 3

Alloy	Porosity ΔS, %	Number of pores per 1 cm² of coating	Average pore diameter, microns
VT1-0	11.3	$7.0 \cdot 10^6$	0.7
VT5	12.2	$7.8 \cdot 10^6$	0.6

Table 8 - Results of corrosion tests

Test stage, hours	The appearance of the samples treated with PEO	Appearance of coatings
0		Initial samples
2		Without changes
24		Without changes
96		Without changes
294		Without changes
460		Without changes
720		Without changes
1000		Without changes
1500		Without changes
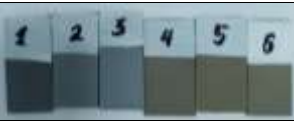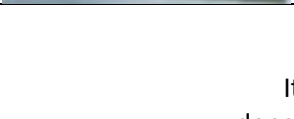
Conclusions

The process of obtaining oxide coatings on titanium alloys VT1-0 and VT5 by plasma electrolytic oxidation has been studied. Uniform porous oxide coatings were obtained in the pulsed mode of the PEO process.

It is shown that the porosity of the coatings depends on the composition and nature of the electrolyte. In electrolytes containing sodium silicic acid, sodium hydroxide, aluminium oxide (electrolyte No.1), as well as sodium phosphoric acid and aluminium hydroxide (electrolyte No.2), the coatings are finely porous. The average pore

diameter of oxide coatings on titanium alloys in electrolyte No.1 is 0.09 microns and 0.2 microns, respectively, at VT1-0 and VT5. In electrolyte No.2, the average pore diameter of oxide coatings is 0.4 microns (alloy VT1-0) and 0.2 microns (alloy VT5). In electrolyte No.3, pores of a larger size of 0.6 – 0.7 microns are formed.

The coating composition includes both components of the processed material and components of the electrolyte solution. Oxide coatings are corrosion resistant when tested in accordance with GOST 9.308-85 under the influence of neutral salt fog at a temperature of (35 ± 2) °C for 1500 hours in an Ascott CC 450 chamber.

Conflict of interests. On behalf of all authors, the correspondent author declares that there is no conflict of interests.

Плазмалық электролиттік оксидтеу арқылы алынған титан қорытпаларындағы оксидті жабындардың қасиеттерін зерттеу

[1,2] Рамазанова Ж.М., [2] Замалитдинова М.Г., [3] Коваленко М.В.

[1] С. Сейфуллин атындағы Қазақ Агротехникалық Университеті, Нұр-Сұлтан қ, Қазақстан
[2] «Ұлттық ғарыштық зерттеулер мен технологиялар орталығы» АҚ, Алматы қ, Қазақстан
[3] Л.Н.Гумилев атындағы Еуразия Ұлттық Университеті, Нұр-Сұлтан қ, Қазақстан

ТҮЙІНДЕМЕ

Жақсартылған коррозиялық, физика-механикалық қасиеттері бар титан мен оның қорытпаларынан жасалған құрылымдарды пайдалану көптеген салаларда сұранысқа ие. Осыған байланысты металдардың бетін түрлендіру процестері қызығушылық тудырады. Металл бетін өңдеудің заманауи және перспективті әдістерінің бірі-плазмалық электролиттік тотықтыру. Қазіргі уақытта процесті жүзеге асырғанда тұрақты ток режимдері қолданылады. Бұдан процесті кеңінен қолдану проблемасы туындайды, себебі электр энергиясы көп тұтынылады. Бұл жұмыстың мақсаты-электролиттердің әртүрлі ерітінділеріндегі ВТ1-0 және ВТ5 титан қорытпаларында импульсті анод-катод режимінде алынған оксид жабындарының морфологиялық және коррозиялық қасиеттерін зерттеу. Титан қорытпаларының бетін модификациялау 250 ± 25 мкс токтың анодты импульсінің ұзақтығы, 5 ± 0.5 мс токтың катодты импульсінің ұзақтығы, 50 ± 0,5 Гц анодты және катодты импульстардың өту жиілігі кезінде жүзеге асырылды. Сілтілік ерітінділер электролит қызметін атқарды. Әртүрлі электролиттерде алынған оксидті жабындар әртүрлі кеуектілікпен және жабын қалыңдығымен сипатталады. Қаптамалар орташа кеуек диаметрі 0,09 мкм-ден 0,4 мкм-ге дейінгі жіңішке кеуекті құрылымымен де, 0,6 – 0,7 мкм үлкен кеуек өлшемдерімен де алынған. Қаптамалардың кеуектілігі 6,12%-дан 12,2%-ға дейін. Энергетикалық дисперсиялық талдау деректері бойынша оксидті жабындардың құрамына өңделетін металдың құрамдас бөліктері де, электролит ерітіндісінің компоненттері де кіретіні анықталды. Негізгі құрамдастарға оттегі және өңделетін металл, сонымен қатар бор, фосфор, алюминий, фтор, натрий, кремний және т.б. жатады. Ascott CC 450 камерасында 1500 сағат бойы (35 ± 2) °C температурада бейтарап тұзды тұманның әсерінен ГОСТ 9,308-85 сәйкес жүргізілген коррозиялық сынаулар жабындарда коррозиялық зақымданулардың жоқтығын көрсетті.

Түйін сөздер: *оксидті жабын, электролит, плазмалық-электролиттік оксидтеу, коррозиялық сынау, жабындардың морфологиясы, кеуектілік.*

Авторлар туралы ақпарат:

Рамазанова Жанат Мусановна	*Химия ғылымдарының кандидаты, С.Сейфуллин атындағы Қазақ агротехникалық университетінің доценті, Нұр-Сұлтан қаласы ғарыштық мониторинг орталығының басшысы, «Ұлттық ғарыштық зерттеулер мен технологиялар орталығы» АҚ. E-mail: zh_ram@mail.ru, ORCID ID: 0000-0003-1419-2886*
Замалитдинова Марина Григорьевна	*Ақпараттық жүйелер магистрі, Нұр-Сұлтан қаласы ғарыштық мониторинг орталығының ғылыми қызметкері, «Ұлттық ғарыштық зерттеулер мен технологиялар орталығы» АҚ. E-mail: kazncsm@yandex.ru, ORCID ID: 0000-0002-8746-1664*
Коваленко Мария Витальевна	*Л.Н.Гумилев атындағы Еуразия ұлттық университетінің магистранты, Нұр-Сұлтан қ, Қазақстан. E-mail: maria.kovalenko.98@mail.ru, ORCID ID: 0000-0003-1838-6338*

Исследование свойств оксидных покрытий на сплавах титана, полученных плазменным электролитическим оксидированием

[1,2] Рамазанова Ж.М., [2] Замалитдинова М.Г., [3] Коваленко М.В.

[1] Казахский Агротехнический Университет имени С. Сейфуллина, Нур-Султан, Казахстан
[2] АО «Национальный центр космических исследований и технологий», Алматы, Казахстан
[3] Евразийский национальный университет им. Л.Н. Гумилева, Нур-Султан, Казахстан

АННОТАЦИЯ

Использование конструкций из титана и его сплавов, которые имеют улучшенные коррозионные, физико-механические свойства, востребованы во многих отраслях производства. В связи с этим представляет интерес процессы модифицирования поверхности металлов. Одним из современных и перспективных методов обработки поверхности металлов является плазменное электролитическое оксидирование. В настоящее время существует проблема широкого применения данного процесса, когда при реализации процесса используются режимы на постоянном токе. Это связано с большим потреблением электроэнергии. Целью данной работы является исследование морфологических и коррозионных свойств оксидных покрытий, полученных в импульсном анодно-катодном режиме на сплавах титана ВТ1-0 и ВТ5 в различных растворах электролитов. Модифицирование поверхности сплавов титана осуществлялось при продолжительности анодного импульса тока 250 ± 25 мкс, продолжительности катодного импульса тока 5 ± 0.5 мс, частоте следования анодных и катодных импульсов 50 ± 0.5 Гц. Электролитами служили щелочные растворы. Оксидные покрытия, полученные в различных электролитах, характеризуются различной пористостью и толщиной покрытия. Покрытия характеризуются мелкопористой структурой, со средним диаметром пор от 0,09 мкм до 0,4 мкм, так и с более крупными размерами пор 0,6 − 0,7 мкм. Пористость покрытий составляет от 6,12% до 12,2%. По данным энергодисперсионного анализа было установлено, что в состав оксидных покрытий включаются как компоненты обрабатываемого металла, так и компоненты раствора электролита. Основными компонентами при этом являются кислород и обрабатываемый металл, а также другие элементы как бор, фосфор, алюминий, фтор, натрий, кремний и другие. Коррозионные испытания согласно ГОСТ 9,308-85 под воздействием нейтрального соляного тумана при температуре (35±2) °С в течение 1500 часов в камере Ascott CC 450 показали, что коррозионных разрушений покрытий нет.

Ключевые слова: оксидное покрытие, электролит, плазменно-электролитическое оксидирование, коррозионные испытания, морфология покрытий, пористость.

	Информация об авторах:
Рамазанова Жанат Мусановна	*Кандидат химических наук, доцент Казахского агротехнического университета им. С. Сейфуллина, начальник Центра космического мониторинга г. Нур-Султан, АО «Национальный центр космических исследований и технологий». E-mail: zh_ram@mail.ru, ORCID ID: 0000-0003-1419-2886*
Замалитдинова Марина Григорьевна	*Магистр информационных систем, научный сотрудник Центра космического мониторинга г. Нур-Султан АО «Национальный центр космических исследований и технологий». E-mail: kazncsm@yandex.ru, ORCID ID: 0000-0002-8746-1664*
Коваленко Мария Витальевна	*Магистрант Евразийского национального университета им. Л.Н. Гумилева, Нур-Султан, Казахстан. E-mail: maria.kovalenko.98@mail.ru, ORCID ID: 0000-0003-1838-6338*

References

[1] Duyunova VA, Leonov AA, Molodcov SV. Vklad VIAM v razrabotku legkih splavov i bor'bu s korroziej izdelij raketno-kosmicheskoj tekhniki [Contribution of the All-Russian Research Institute of Aviation Materials to the development of light alloys and the fight against corrosion of rocket and space technology products]. Trudy VIAM = Proceedings of the All-Russian Research Institute of Aviation Materials 2020. 2, (86). (in Russ.). http://dx.doi./10.18557/2307-6046-2020-0-2-22-30 (in Russ.).

[2] Aleksandrov VM. Materialovedenie i tekhnologiya konstrukcionnyh materialov: uchebnoe posobie. CHast' 1. Materialovedenie. Standart tret'ego pokoleniya [Materials science and technology of structural materials: textbook. Part 1. Materials science. Third generation standard]. Arhangel'sk: Severnyj (Arkticheskij) federal'nyj universitet, 2015, 327. (in Russ.).

[3] Rúa JM, Zuleta AA, Ramírez J, Fernández-Morales P. Micro-arc oxidation coating on porous magnesium foam and its potential biomedical applications. Surface and Coatings Technology 2019;360(25):213-221. https://doi.org/10.1016/j.surfcoat.2018.12.106

[4] Kemelzhanova A, Mukasev K, Yar-Mukhamedova G, Lampke Th. Investigation of the anticorrosion properties of nano-CEC in amine environments. Kompleksnoe Ispol'zovanie Mineral'nogo Syr'a = Complex Use of Mineral Resources 2020;313(2):52–57. https://doi.org/10.31643/2020/6445.17

[5] Mamaeva AA, Kenzhegulov AK, Panichkin AV, Shah A. Obtaining hydroxyapatite coatings by mechanochemical interaction. Kompleksnoe Ispol'zovanie Mineral'nogo Syr'a = Complex Use of Mineral Resources 2020;314(3):76-83. https://doi.org/10.31643/2020/6445.29

[6] Ramazanova ZhM, Zamalitdinova MG. Study of the Properties of Oxide Coatings Formed on Titanium by Plasma Electrolytic Oxidation Method. Eurasian Chemico-Technological Journal 2020;22(1):51-58. https://doi.org/10.18321/ectj930

[7] WeiZhanWang, ShunShan Feng, ZhongMing Li, ZhiGang Chen, TaiYong Zhao. Microstructure and properties of micro-arc oxidation ceramic films on AerMet100 steel. Journal of Materials Research and Technology 2020;9(3):6014-6027. https://doi.org/10.1016/j.jmrt.2020.04.005

[8] Zhou T, Ding Y, Luo Q, Qin Z, Zhang Q, Shen B, Hu W, Liu L. The Effects of Sodium Tungstate on the Characteristics of Microarc Oxidation Coating on Ti6Al4V. Journal of Materials Engineering and Performance 2018;27:5489–5499. http://dx.doi. org/ 10.1007/s11665-018- 3613-2

[9] Ramazanova JM, Zamalitdinova MG. Physical and mechanical properties investigation of oxide coatings on titanium. Kompleksnoe Ispol'zovanie Mineral'nogo Syr'a = Complex Use of Mineral Resources 2019;2:34-41. https://doi.org/10.31643/2019/6445.14

[10] Xiaoben Qi, Hailong Shang, Bingyang Ma, Rulin Zhang, Leyang Guo, Bo Su. Microstructure and Wear Properties of Micro Arc Oxidation Ceramic Coatings. Material (Basel) 2020;13(4):970. https://doi.org/10.3390/ma13040970

[11] Yong Lian, Xianyi Dai, Jin Zhang. Characterization of micro-arc oxidation coatings on Ti6Al4V with addition of SiC particle. Materials Research Express 2020. 7, 1. https://doi.org/10.1088/2053-1591/ab6c9a

[12] Ramazanova Zh, Zamalitdinova M, Kozlovskiy A, Butyagin P, Arbuzova S. Synthesis and properties of coatings obtained by plasma electrolytic oxidation of titanium alloys in alkaline solutions. Journal of Advanced Research in Dynamical and Control Systems 2020;12(06):858-865.

[13] Subbotina VV, Belozerov VV. The effect of electrolysis conditions during microarc oxidation on the phase-structural state, hardness and corrosion resistance of magnesium alloys. Physics and Chemistry of Solid State 2020;21(3):545-551. https://doi.org/10.15330/pcss.21.3.545-551.

[14] Mamaev AI, Dolgova YuN, Beletskaya EYu, Mamaeva VA. Synthesis of Nanostructured Nonmetallic Inorganic Coatings at High Energy Localization in Interfacial Nanolayers. Russian Physics Journal 2021;63(9/2):1605-1014. https://doi.org/10.1007/s11182-021-02212-w

[15] Ramazanova ZhM, Kirgizbayeva KZh, Akhmedyanov AU, Jaxymbetova MA, Yergaliyev D, Zhakupova A, Abdirashev O. Influence of the process of microplasma treatment in electrolyte solutions on the oxide coating properties. International Journal of Mechanical Engineering and Technology 2018;12(9):709–721. http://iaeme.com/Home/jornal/IJMET

[16] Chunyan Du, Hui Zhao, Zhiyong Dai, Zhiyu Tian, Jinchuan Wang, ZhenWang. The preparation and properties of black coating by micro arc oxidation on 2A12 aluminum alloy. Materials Letters 2019;236(1):723-726. https://doi.org/10.1016/j.matlet.2018.11.019

[17] Saltykov SA. Stereometricheskaya metallografiya [Stereometric metallography]. Moscow: Metallurgiya. 1970, 375. (in Russ.).

[18] Jingtao Wang, Yaokun Pan, Rui Feng, Hongwei Cui, Benkui Gong, Lei Zhang, Zengli Gao, Xiaoli Cui, Hongbin Zhang, Zhiqiang Jia. Effect of electrolyte composition on the microstructure and bio-corrosion behavior of micro-arc oxidized coatings on biomedical Ti6Al4V alloy. Journal of Materials Research and Technology 2020;9(2):1477-1490. https://doi.org/10.1016/j.jmrt.2019.11.073

[19] Shankar MP, Sokkalingam R, Sivaprasad K, Veerappan Muthupandi. Effect of Electrolyte on Micro Arc Oxidation Coating of Al-2014 Alloy. Advanced Materials Research 2018;1148:159-164. https://doi.org/:ord/10.4028/www.scientific.net/AMR.1148.159

[20] Wang DD, Liu XT, Wu YK, Han HP, Yang Z, Su Y, Zhang XZ, Wu GR, Shen DJ. Evolution Process of the Plasma Electrolytic Oxidation (PEO) Coating Formed on Aluminum in an Alkaline Sodium Hexametaphosphate ((Napo3)6) Electrolyte. Journal of Alloys and Compounds 2019;798:129 – 143. https://doi.org/10.1016/j.jallcom.2019.05.253

[21] Guo-rui WU, Dong-dong WANG, Xin-tong LIU, Mingjia WANG, Dong CHEN, Yekang WU, Dejiu Shen. New Formation Mechanisms of Pores and Cracks in Micro-arc Oxidation Coatings on 6061 Aluminum Alloy with High Temperature Oxide Prefab Film. Materials Science (Medžiagotyra) 2021;27(1):37-41. http://dx.doi.org/10.5755/j02.ms.24210

[22] Yeshmanova GB, Smagulov DU, Blawert C. Plasma electrolytic oxidation technology for producing protective coatings of aluminum alloys. Kompleksnoe Ispol'zovanie Mineral'nogo Syr'a = Complex Use of Mineral Resources 2021;317(2):78-93. https://doi.org/10.31643/2021/6445.21 (in Russ.).

![Crossref]

![creative commons]

Granular materials based on expanded sands and their production waste

¹* Miryuk O.A., ² Zagorodnyuk L.H.

¹ Rudny Industrial Institute, Rudny, Kazakhstan
² Belgorod State Technological University named after V.G. Shukhov, Belgorod, Russia

* Corresponding author email: psm58@mail.ru

ABSTRACT

The article presents the results of studies of granular materials obtained by non-firing technology. For the formation of granules, composite cement and magnesia binders containing waste products of expanded perlite and expanded clay are proposed. Mechanical activation of composite binders intensifies the processes of hydration and structure formation, contributes to increasing the strength of materials. The combination of a binder with a filler in the form of waste from the production of porous aggregates ensures a decrease in the density of the binder, the formation of a finely dispersed porous structure of the composite material, the formation of stable hydrates. The porous structure of the granules is provided by the use of porous sand to form the core of the granules. Studies of the structure of granules by electron microscopy revealed that the reliable adhesion of particles of porous sand with a composite binder stone provides high strength of porous granular materials. Cement granules based on expanded perlite sand are characterized by a density of $300 - 400$ kg/m^3 and a compressive strength of $1.8 - 2.6$ MPa. Magnesia granules based on expanded clay sand have a density of $450 - 500$ kg/m^3 and compressive strength of $3.5 - 5.7$ MPa. The work is aimed at creating effective building materials using resource-saving technology, at the rational use of production waste.

Keywords: granular material, expanded perlite, expanded clay sand, composite binders, porous structure.

	Information about authors:
Miryuk Olga Aleksanrovna	*Doctor of Technical Sciences, Professor. Head of the department of building construction materials, Rudny Industrial Institute, Rudny, Kazakhstan. Email: psm58@mail.ru, orcid id: https://orcid.org /0000-0001-6892-2763*
Zagorodnyuk Lilia Hasanovna	*Doctor of Technical Sciences, Professor of the Department of Building Materials Science, Products and Structures. Belgorod State Technological University named after V.G. Shukhov, Belgorod, Russia. Email: LHZ47@mail.ru, orcid id: https://orcid.org/0000-0001-9840-4414*

Introduction

To ensure energy efficiency of construction, we need materials that provide not only the required bearing capacity of structures, but also have heat-shielding properties. These materials include lightweight concrete. Lightweight concretes are characterized by low density, the values of which, as a rule, do not exceed 2000 kg/m^3. Main physical and mechanical properties of lightweight concrete are due to a highly developed porous structure, which is formed using foam and gas formers (cellular concrete) or due to porous aggregates.

Lightweight concretes based on porous aggregates, compared to cellular concretes, have increased strength, lower shrinkage and creep, which expand the scope of their application [[1], [2], [3], [4], [5]]. The structure of lightweight concretes based on porous aggregates is mainly controlled by the aggregate. Porous aggregates

have been used since ancient times in the form of volcanic rocks. Modern porous aggregates are artificial materials made with a variety of raw materials and manufacturing processes. The characteristics of lightweight aggregates vary widely.

In modern technology of lightweight concretes, expanded clay is the most common. Optimization of technological process ensures expanded clay gravel production with a bulk density of $350 - 600$ kg/m^3; expanded clay concrete is characterized by a density of $600 - 1200$ kg/m^3 and strength of $2 - 12$ MPa [[6], [7], [8], [9], [10], [11], [12]]. Possibilities for further improvement of expanded clay technology are often limited by the state of raw material base [[13], [14], [15]].

Among the promising porous aggregates is expanded perlite, which is used to produce lightweight concrete with a density of $450 - 900$ kg/m^3 [[16], [17], [18], [19]]. Expanded perlite is

distributed mainly in regions where aggregates are produced. When producing porous aggregates, waste is generated at various stages of technological process; chemical and disperse composition of which depends on the conditions of formation. The problem of rational use of such waste remains relevant.

Along with porous firing concrete aggregates, granular materials which are made without the use of high-temperature technological processes have become widespread [[20], [21]]. Unfired porous aggregates favorably differ in reduced cost due to exclusion of an energy-intensive process. Non-firing porous aggregates are obtained by hardening granular raw mixtures, which include a binder and components that provide pores formation. The variety of components of the raw mix provides extensive raw material base for granular materials production. The growth of requirements for construction and technical properties of lightweight concretes necessitates the improvement of porous aggregates technology and expansion of the raw material base due to available sources.

The purpose of the work is to study influence of material composition of the raw mixture on formation and properties of unfired granules.

Experimental part

To obtain granulated materials, raw mixtures consisting of a composite binder and porous particles were used. Composite binders were prepared on the basis of Portland cement and production wastes of expanded perlite sand, caustic magnesite and expanded clay production wastes. Expanded perlite sand (cement mixes) and expanded clay sand (magnesia mixes) served as porous particles for granulated raw mixes.

The main characteristics of Portland cement CEM I 42.5N (GOST 31108 – 2016): specific surface 330 ± 10 m^2/kg, initial setting time is 1 hour and 40 minutes, time of final setting is 3 hours, activity is 26 MPa at the age of 2 days.

Caustic magnesite PMK – 75 brand contains $75 - 80\%$ of MgO, is characterized by specific surface of 300 ± 10 m^2/kg, initial setting time is 25 minutes, time of final setting is 2 hours 10 minutes, compressive strength at the age of 2 days is 34 MPa, at the age of 28 days – 52 MPa.

Expanded perlite production waste is a dispersed material with an average particle size of 0.1 - 1.2 mm («Oskolsnab» JSC, Stary Oskol) Chemical composition of waste, wt. %: SiO_2 – 75;

Al_2O_3 – 12.5; Fe_2O_3 – 0.7; CaO – 1.6; MgO – 0.6; $(K_2O + Na_2O)$ – 4.6; others – 5.0.

Wastes of expanded clay production are mainly represented by particles of $0.2 - 1.0$ mm (Ust-Kamenogorsk expanded clay plant). Chemical composition of waste, wt.%: SiO_2 – 67.5; Al_2O_3 – 10.8; Fe_2O_3 – 5.7; CaO – 5.4; MgO – 2.3; $(K_2O + Na_2O)$ – 4.5; others – 3.8.

Expanded perlite sand is a granular material with a particle size of up to 5 mm, obtained by thermal treatment of crushed perlite, a volcanic rock. The bulk density of expanded perlite sand is $75 - 500$ kg/m^3. In this work, expanded perlite sand with a fraction of $0.16 - 1.25$ mm and a bulk density of 200 ± 10 kg/m^3 was used.

Expanded clay sand is a granular mass of particles 0-5 mm in size, obtained by crushing Keramzite grains. Bulk density is $500 - 650$ kg/m^3. In the experiments, particles of expanded clay sand with a fraction of $0.16 - 1.25$ mm with a bulk density of 510 ± 10 kg/m^3 were used.

Composite binders were being obtained by mechanical activation of a mixture of the original binder with waste products after porous filler production in «E-max» activator mill during 30 minutes. The specific surface area of the binders was evaluated using a photosedimentometer.

Water (cement mixtures) and magnesium chloride solution with a density of 1230 kg/m^3 (magnesia mixtures) were used to mix the molding masses.

Granules were molded on a drum-type laboratory unit. Rotation of the metal drum ensured pelletization of raw mixtures loaded into the unit. Presence of a restrictive mechanism prevented materials from sticking to the walls of the drum. The method of granules forming as follows: particles of porous sand with a part of mixing agent were placed in a pre-installed unit; then the composite binder was poured. After 2 minutes of rotation of the drum unit, the remaining amount of mixing agent and composite binder was added. Rotation of the granulating unit for 10 min ensured the formation of a dense shell on the surface of granules.

Raw mixture granulation includes the processes of wet rolling of a composite binder onto porous sand grains until raw pellets are formed.

Adjusting the duration allows you to get spherical granules with a size of $5 - 15$ mm.

The mode of hardening of raw granules was settled taking into account the nature of binders hardening. Cement granules hardened in the air-humid environment, magnesia granules in air,

the ambient temperature in both cases was 18 – 22°C. After 28 days of hardening, the granules were tested for strength by squeezing on a hydraulic press.

The microstructure of granular materials was studied by electron microscopy using TESCAN MIRA 3 LMU scanning electron microscope.

Discussion of the results

The working hypothesis of the study is based on the possibility of obtaining granules from porous sand and a composite binder, in which the filler has a composition related to porous particles. Combination of a binder with filler in the form of waste products of porous fillers will reduce binder's density and form a finely dispersed porous structure of the composite material. Mechanical activation of the binder-filler mixture can accelerate hardening and increase material's strength.

Mixes for cement granules.

Analysis of composite cement binders' properties made it possible to determine the rational combination of Portland cement with waste of expanded perlite sand production (Table 1). The content of waste in the composite binder does not exceed 10%. Introduction of a porous technogenic component is accompanied by increase in water demand, reduction in setting time of the cement paste, decrease in density and increase in strength of the binder stone. Mechanical activation of the cement composite binder contributes to additional amount of the dispersed phase, which activates hydration processes, accelerating the setting and structure formation of the binder.

Granulated material was obtained by applying a shell of a composite binder to a porous core. The core of the granules was particles of expanded perlite sand, held together by a composite binder.

Comparison of the properties of granules of various fractions obtained from perlite sand showed that with increase in the size of sand particles, density of granules increases (Table 2). Strength characteristics of granules are directly dependent on their density. Physical and mechanical properties of granules are largely determined by shell's state, thickness of which increases with transition to large fractions. Cleavage surface of cement granules was studied by electron microscopy. The central part of granules of 1.5 – 2.5 mm in size is formed by scaly particles bonded with a binder, has surgeless porosity (Figure 1).

Table 1 – Influence of expanded perlite production waste on the properties of cement composite binder

Content of filler in binder, %	Normal binder density, %	Setting period, min	Properties of a binder stone at the age of 28 days	
			density, kg/m³	*compressive strength, MPa*
0	28	120	2185	48
5	32	90	2060	50
10	40	70	2010	59
15	45	40	1815	38

Table 2 – Physical and mechanical characteristics of granular materials based on composite cement

Granule core fraction, mm	Granules properties	
	density, kg/m³	Granules properties
1.5 – 2.5	300±10	1.8
2.5 – 5.0	350±10	2.3
5.0 – 10.0	400±10	2.6
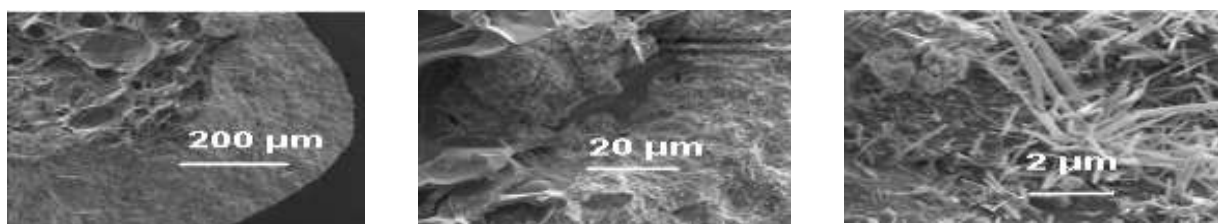
Figure 1 – Microstructure of granules from cement mixtures

Pores of the inner part of granules are permeated with hydration products of the binder. Shell thickness of fine fraction granules is 600 μm on average.

Structure of granules is formed with the participation of dense shells on the surface of porous sand due to dense fouling with binder hydration products (calcium hydrosilicates, calcium hydrosulfoaluminate), concentration of crystalline hydrates on the sand surface and in the pore space. Mechanical activation contributes to structural change of pearlite. As a result, reactivity of perlite in pozzolanization reactions is increased. According to X-ray phase analysis, calcite, tobermorite, gehlenite, and silica were found in the multicomponent granular material. Identification of the composition of all products of the pozzolanic reaction is difficult due to weak crystallization of most phases.

Shells are a kind of reinforcing element of composite binder's stone in the shell of the granule. Porosity of granules is represented by voids of perlite sand, which are overlapped by hydrates and form closed spaces. In this case, a special role belongs to fibrous calcium hydrosilicates, which form intergrowths due to the presence of a silicate technogenic component.

Mixtures for magnesia granules.

Properties of non-firing granules depend on the binder component that connects filler particles. Unfired granular aggregates for lightweight concretes are usually obtained using cements. Prevalence of cement-based granules is due to hydraulic properties of this binder.

The use of cements often causes complications in the molding process and provides relatively high values for density of granular materials. To develop porous granules technology, it is necessary to expand the range of binders.

Magnesia binders are distinguished by intense hardening, high strength properties, and expressive adhesion to various materials [[21], [22], [23]].

Composite magnesia binders were obtained by joint grinding in an activator mill of caustic magnesite with expanded clay production waste. Analysis of the test results revealed advantages of composite binders containing 40 – 50% of expanded clay production waste. Mechanical activation ensures the production of a high-strength composite binder containing up to 50% of the technogenic component. Such binders are distinguished by reduced consumption of salt grouting fluid - solution of magnesium chloride, of lower stone density with strength indicators comparable to caustic magnesite (Table 3). Introduction of technogenic component increases water resistance of the binder stone, which is estimated by the softening coefficient (the ratio of material's strength after being in water for 3 days to material's strength hardened in air).

Granules based on magnesia binders were obtained in the manner described above for cement granules. The core for granules formation was aggregates of expanded clay sand particles connected by a magnesian binder.

Table 3 – Influence of expanded clay production waste on the properties of composite magnesia binder

Content of filler in binder, %	Normal binder density, %	Setting period, min	Properties of a binder stone at the age of 28 days		
			density, kg/m³	*compressive strength, MPa*	*softening factor*
0	45	70	1930	52	0.45
10	45	75	1920	53	0.46
20	42	78	1900	54	0.52
30	40	82	1880	58	0.55
40	38	85	1865	62	0.65
50	37	85	1840	67	0.70
60	36	87	1825	46	0.73

Table 4 – Physical and mechanical characteristics of granular materials based on magnesia composite binder

Fraction of granules, mm	Granules properties	
	density, kg/m³	**Granules properties**
6.0 – 8.0	450±10	3.5
8.0 – 10.0	500±10	5.7
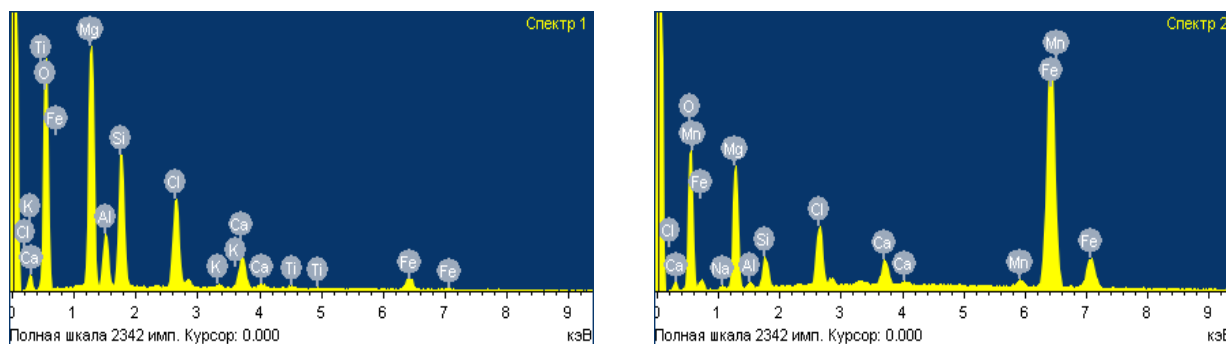
Figure 2 – Elemental composition of granules from magnesia mixtures
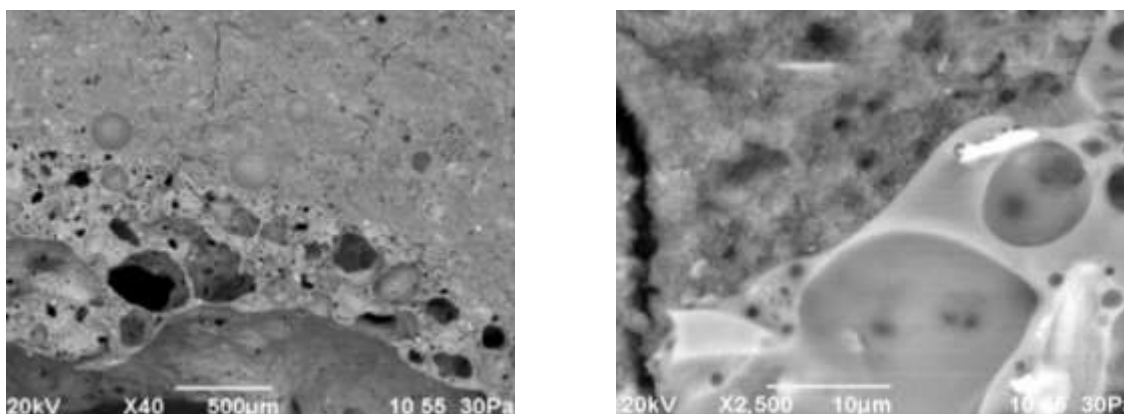
Figure 3 – Microstructure of granules from magnesia mixtures

Average size of a granule core was 5.5 – 7.5 mm. Thickness of the shell around the core reached 1.5 - 2.5 mm. Physical and mechanical properties of magnesia granules are shown in Table 4. Compared to cement granules (Table 2), magnesia granules are characterized by higher density, which is due to the lower porosity of expanded clay sand in contrast to expanded perlite particles.

Microconglomerate structure of the granular material is formed on the basis of intergrowth of crystals of magnesium hydroxide chlorides and predominantly amorphous sparingly soluble hydrates with the participation of a technogenic component. This creates a matrix of gel-crystalline structure of the stone and ensures its resistance to shrinkage and water.

High strength of magnesia granules is provided by crystalline structure of magnesium hydroxide chlorides, formation of weakly crystallized hydrosilicates, hydroaluminosilicates, magnesium hydroferrites (Figure 2), and reliable adhesion of the binder stone to the surface of expanded clay particles (Figure 3).

Practicability of magnesia granules obtaining is determined by low energy intensity of composite binders' production, which are half made up of technogenic filler, and by high strength of the porous granular material.

Conclusions

To obtain non-firing granular materials, mechanically activated composite binders containing porous aggregates production waste are proposed.

Porous structure of granular materials is formed with the participation of expanded sand connected by composite material into the core of granules.

The use of expanded perlite sand or crushed expanded clay particles in granules structure expands the area of rational use of fine-grained materials with high open porosity.

Granules strength is ensured by reliable adhesion of components, including due to genetic similarity of porous sand and technogenic component of the binder.

Қопсыған құмдар және олардың өндіру қалдықтарының негізінде алынған түйіршіктелген материалдар

¹ Мирюк О.А., ² Загороднюк Л.Х.

¹ Рудный индустриялық институты, Рудный, Қазақстан
² В.Г. Шухов атындағы Белгород мемлекеттік технологиялық университеті, Белгород, Ресей

ТҮЙІНДЕМЕ

Мақалада күйдірілмейтін технология бойынша алынған түйіршіктелген материалдарды зерттеу нәтижелері келтірілген. Түйіршіктерді қалыптастыру үшін құрамында қопсыған перлит пен керамзит өндірісінің қалдықтары бар композициялық цементті және магнезиалды тұтқыр заттар ұсынылады. Композициялық тұтқыр заттардың механикалық белсендірілуі гидратация және құрылымды қалыптастыру процестерін күшейтеді, материалдардың беріктігін арттыруға көмектеседі. Кеуекті агрегаттар өндірісінің қалдықтары түріндегі тұтқыр заттың толтырғышпен бірігуі тұтқыр заттың тығыздығының төмендеуін, композициялық материалдың ұсақ дисперсті кеуекті құрылымының қалыптасуын және тұрақты гидраттардың пайда болуын қамтамасыз етеді. Түйіршіктердің кеуекті құрылымы түйіршіктердің ядросын қалыптастыратын кеуекті құмды қолдану арқылы қамтамасыз етіледі. Түйіршіктердің құрылымын электронды микроскопия әдісімен зерттеу арқылы кеуекті құм бөлшектерінің композициялық байланыстырғышының таспен берік тұтасуы кеуекті түйіршікті материалдардың жоғары беріктігін қамтамасыз ететіндігін анықталды. Қопсыған перлит құмына негізделген цемент түйіршіктерінің тығыздығы 300 – 400 кг/м³ және сығылу күші 1,8 – 2,6 МПа болады. Керамзит құмына негізделген магнезия түйіршіктерінің тығыздығы 450 – 500 кг/м³ және беріктігі 3,5–5,7 МПа құрайды. Бұл жұмыс ресурс үнемдейтін технологияны пайдалана отырып, тиімді құрылыс материалдарын жасауға, өндіріс қалдықтарын ұтымды пайдалануға бағытталған.

Түйін сөздер: түйіршікті материал, қопсыған перлит, керамзит құмы, композициялық тұтқыр зат, кеуекті құрылым.

Авторлар туралы ақпарат:

Мирюк Ольга Александровна — *Техника ғылымдарының докторы, профессор. Құрылыс және құрылыстық материал тану кафедрасының меңгерушісі, Рудный индустриялық институты, Рудный, Қазақстан. Email: psm58@mail.ru, orcid id: https://orcid.org /0000-0001-6892-2763*

Загороднюк Лилия Хасановна — *Техника ғылымдарының докторы. Құрылыстық материалтану, бұйымдар мен конструкциялар кафедрасының профессоры. В.Г. Шухов атындағы Белгород мемлекеттік технологиялық университеті, Белгород, Ресей. Email: LHZ47@mail.ru, orcid id: https://orcid.org/0000-0001-9840-4414*

Гранулированные материалы на основе вспученных песков и отходов их производства

¹ Мирюк О.А., ² Загороднюк Л.Х.

¹ Рудненский индустриальный институт, Рудный, Казахстан
² Белгородский государственный технологический университет имени В.Г. Шухова, Белгород, Россия

АННОТАЦИЯ

В статье приведены результаты исследований гранулированных материалов, полученных по безобжиговой технологии. Для формирования гранул предложены композиционные цементные и магнезиальные вяжущие вещества, содержащие отходы производства вспученного перлита и керамзита. Механическая активация композиционных вяжущих интенсифицирует процессы гидратации и структурообразования, способствует повышению прочности материалов. Сочетание вяжущего с наполнителем в виде отходов производства пористых заполнителей обеспечивает

снижение плотности вяжущего, формирование мелкодисперсной пористой структуры композиционного материала, образование устойчивых гидратов. Пористая структура гранул обеспечивается использованием поризованного песка для образования ядра гранул. Исследованиями строения гранул методом электронной микроскопии выявлено, что надежное сцепление частиц поризованного песка с камнем композиционного вяжущего обеспечивает высокую прочность пористых гранулированных материалов. Цементные гранулы на основе вспученного перлитового песка характеризуются плотностью 300 – 400 кг/м³ и прочностью при сжатии 1,8 – 2,6 МПа. Магнезиальные гранулы на основе керамзитового песка имеют плотность 450 – 500 кг/м³ и прочность при сжатии 3,5 – 5,7 МПа. Работа направлена на создание эффективных строительных материалов по ресурсосберегающей технологии, на рациональное использование отходов производства.

Ключевые слова: гранулированный материал, вспученный перлит, керамзитовый песок, композиционные вяжущие, пористая структура.

Информация об авторах:

Мирюк Ольга Александровна	*Доктор технических наук, профессор. Заведующая кафедрой строительства и строительного материаловедения. Рудненский индустриальный институт, Рудный, Казахстан. Email: psm58@mail.ru, orcid id: https://orcid.org /0000-0001-6892-2763*
Загороднюк Лилия Хасановна	*Доктор технических наук. Профессор кафедры строительного материаловедения, изделий и конструкций. Белгородский государственный технологический университет имени В.Г. Шухова, Белгород, Россия. Email: LHZ47@mail.ru, orcid id: https://orcid.org/0000-0001-9840-4414*

References

[1] Kumar KN, Vijayan DS, Divahar R, Abirami R, Nivetha C. An experimental investigation on light-weight concrete blocks using vermiculite. Materials Today: Proceedings 2020;22(3):987–991. https://doi.org/10.1016/j.matpr.2019.11.237

[2] Min H-W, Kim S, Kim HS. Investigation on thermal and mechanical characteristics of concrete mixed with shape stabilized phase change material for mix design. Construction and Building Materials 2017;149:749–762. https://doi.org/10.1016/j.conbuildmat.2017.05.176

[3] Xu B, Li Z. Paraffin/diatomite composite phase change material incorporated cement-based composite for thermal energy storage. Applied Energy 2013;105:229–237. https://doi.org/10.1016/j.apenergy.2013.01.005

[4] Sangulova IB, Selyaev VP, Kuldeev EI, Nurlybaev RE, Orynbekov YS. Assessment of the influence of the structural characteristics of granular systems of microsilicon on the properties of thermal insulation materials. Kompleksnoe Ispol'zovanie Mineral'nogo Syr'a = Complex Use of Mineral Resources 2022;320(1):5–14. https://doi.org/10.31643/2022/6445.01

[5] Devecioglu AG, Bicer Y. The effects of tragacanth addition on the thermal and mechanical properties of light weight concretes mixed with expanded clay. Periodica Polytechnica Civil Engineering 2016;60(1):45–50. https://doi.org/10.3311/PPci.7984

[6] Borges A, Flores-Colen I, Brito J. Physical and mechanical performance of cement-based renders with different contents of fly ash, expanded cork granules and expanded clay. Construction and Building Materials 2018;191:535–543. https://doi.org/10.1016/j.conbuildmat.2018.10.043

[7] Miryuk O, Fediuk R, Amran M. Foam Glass Crystalline Granular Material from a Polymineral Raw Mix. Crystals 2021;11: 1447. https://doi.org/10.3390/cryst11121447

[8] Burbano-Garcia C, Hurtado A, Silva YF, Delvasto S, Araya-Letelier G. Utilization of waste engine oil for expanded clay aggregate production and assessment of its influence on lightweight concrete properties. Construction and Building Materials 2021;273:121677. https://doi.org/10.1016/j.conbuildmat.2020.121677

[9] Zhou J, Ji L, Gong C, Lu L, Cheng X. Ceramsite vegetated concrete with water and fertilizer conservation and light weight: Effect of w/c and fertilizer on basic physical performances of concrete and physiological characteristics of festuca arundinacea. Construction and Building Materials 2020;236(10):117785. https://doi.org/10.1016/j.conbuildmat.2019.117785

[10] Gao H, Xia S, Chen F, Stuedlein AW, Li X, Wang Z, Shen Z, Chen X. Dynamic shear modulus and damping of cemented and uncemented lightweight expanded clay aggregate (LECA) at low strains. Soil Dynamics and Earthquake Engineering 2021;142:106555. https://doi.org/10.1016/j.soildyn.2020.106555

[11] Sravya YL, Manoj T, Seshagiri RMV. Effect of temperature curing on lightweight expanded clay aggregate concrete. Materials Today: Proceedings 2021;38(5):3386–3391. https://doi.org/10.1016/j.matpr.2020.10.568

[12] Roces E, Muñiz-Menéndez M, González-Galindo J, Estaire J. Lightweight expanded clay aggregate properties based on laboratory testing. Construction and Building Materials 2021;313:125486. https://doi.org/10.1016/j.conbuildmat.2021.125486

[13] Bicer A. The effect of fly ash and pine tree resin on thermo-mechanical properties of concretes with expanded clay aggregates. Case Studies in Construction Materials 2021;15:e00624. https://doi.org/10.1016/j.cscm.2021.e00624

[14] Angelin AF, Lintz RCC, Osório WR, Gachet LA. Evaluation of efficiency factor of a self-compacting lightweight concrete with rubber and expanded clay contents. Construction and Building Materials 2020;257:119573. https://doi.org/10.1016/j.conbuildmat.2020.119573

[15] Xu M, Liu L, Deng Y, Zhou A, Gu S, Ding J. Influence of sand incorporation on unconfined compression strength of cement-based stabilized soft clay. Soils and Foundations 2021;61(4):1132–1141. https://doi.org/10.1016/j.sandf.2021.06.008

[16] Sun D, Wang L, Li C. Preparation and thermal properties of paraffin/expanded perlite composite as form-stable phase change material. Materials Letters 2013;108:247–249. https://doi.org/10.1016/j.matlet.2013.06.105

[17] Chung O, Jeong Su-G, Kim S. Preparation of energy efficient paraffinic PCMs/expanded vermiculite and perlite composites for energy saving in buildings. Solar Energy Materials and Solar Cells 2015;137:107–112. https://doi.org/10.1016/j.solmat.2014.11.001

[18] Zhang X, Wen R, Tang C, Wu B, Huang Z, Min X, Huang Y, Liu Y, Fang M, Wu X. Thermal conductivity enhancement of polyethylene glycol/expanded perlite with carbon layer for heat storage application. Energy and Buildings 2016;130:113–121. https://doi.org/10.1016/j.enbuild.2016.08.049

[19] Zhang N, Yuan Y, Li T, Cao X. Lauric–palmitic–stearic acid/expanded perlite composite as form-stable phase change material: Preparation and thermal properties. Energy and Buildings 2014;82:505–511. https://doi.org/10.1016/j.enbuild.2014.07.049

[20] Kocianova M, Drochytka R. Possibilities of lightweight high strength concrete production from sintered fly ash aggregate. Procedia Engineering 2017;195:9–16. https://doi.org/10.1016/j.proeng.2017.04.517

[21] Miryuk OA. Granular magnesia compositions. Kompleksnoe Ispol'zovanie Mineral'nogo Syr'a = Complex Use of Mineral Resources 2021;316(1):32–39. https://doi.org/10.31643/2021/6445.04

[22] Kumar S, Sonat C, Yang E-H, Unluer C. Performance of reactive magnesia cement formulations containing fly ash and ground granulated blast-furnace slag. Construction and Building Materials 2020;232:117275. https://doi.org/10.1016/j.conbuildmat.2019.117275

[23] Miryuk O. Porous magnesia compositions with various fillers. Lecture Notes in Civil Engineering 2021;147:344 – 350. https://doi.org/10.1007/978-3-030-68984-1_50

Geology and minerageny of the Bestobe deposit (Central Kazakhstan)

[1] Askarova N.S., [1] Portnov V.S., [1] Blyalova G.G., [1] Madisheva R.K., [2] Dyakonov V.V.

[1] *Karaganda Technical University, Karaganda, Kazakhstan*
[2] *Sergo Ordzhonikidze Russian State University for Geological Prospecting, Moscow, Russia*

* Corresponding author email: srajadin-nazym@mail.ru

ABSTRACT

Polygenic stratiform deposits are the largest in the world in terms of barite and manganese reserves, as well as lead and zinc reserves. In the mineral resource complex of the Republic of Kazakhstan, they are of great importance and are distinguished as an independent genetic Atasu type. In the article, the deposits of the Zhailma graben-syncline in a large riftogenic structure are considered as a reference for the Atasu type. The geological structure of the Bestobe stratiform polymetallic deposit located in the eastern part of the Zhailma synclinorium is presented. The stratigraphy of ore formations, mineralization features, morphology of the ore body and the pattern of zoning the distribution of elements in the ore-bearing rocks of the Bestobe deposit are shown. A feature of the deposit is the combination of layered iron-manganese and lead-zinc ores and superimposed zinc-lead-barite mineralization; the sharply subordinate role of hydrothermal-sedimentary ores in the total reserves of lead and zinc; comparative abundance of lead, copper and silver sulfosalts. The analysis of the materials indicates that mineralization at the Bestobe deposit is complex. Its main value is polymetallic ores. The role of iron ore mineralization of the deposit is insignificant. Manganese mineralization is practically absent. Polymetallic ores are conventionally subdivided into lead-zinc-barite, lead-barite, barite and lead-zinc. Strontium is a constant impurity in barites. Lead is mainly concentrated in galena; its insignificant amount is found in geocronite, boulangerite, jamsonite, bournonite, cerussite, anglesite, pyromorphite, plumboyarosite. The bulk of zinc is concentrated in the form of sphalerite.

Keywords: Atasu type, polymetallic, Zhayilma graben-syncline, lead-zinc-barite deposits.

	Information about authors:
Askarova Nazym Srajadinkyzy	*PhD student of Karaganda Technical University, Master of Engineering, Geology and Exploration of Mineral Deposits specialty, 100027, Karaganda, Republic of Kazakhstan, e-mail: srajadin-nazym@mail.ru. ORCID: 0000-0002-2103-6198*
Portnov Vassiliy Sergeevich	*Doctor of Technical Sciences, Professor of the Department of Geology and Exploration of Mineral Deposits at Karaganda Technical University, 100027, Karaganda, Republic of Kazakhstan, e-mail: vs_portnov@mail.ru. ORCID: 0000-0002-4940-3156*
Blyalova Gulim Galymzhanovna	*PhD student of Karaganda Technical University, Master in Science of Engineering, specialty Geology and Exploration of Mineral Resources, Karaganda Technical University, Karaganda, Republic of Kazakhstan; e-mail: krg_gulim@mail.ru. ORCID: 0000-0001-8801-8683*
Madisheva Rima Kopbosynkyzy	*PhD, senior lecturer of the Department of Geology and Exploration of Mineral Resources, Karaganda Technical University, Karaganda, Republic of Kazakhstan, e-mail: rimma_kz@mail.ru. ORCID: 0000-0002-5726-9567*
Dyakonov Victor Vasileevich	*Doctor of Geological and Mineralogical Sciences, Professor, Head of the Department of General Geology and Geological Mapping of the S Sergo Ordzhonikidze Russian State University for Geological Prospecting, 101000 Moscow, Russia, e-mail: mdf.rudn@mail.ru.*

Introduction

Polygenic stratiform ferromanganese and barite-lead-zinc deposits isolated as an independent genetic Atasu type, are of great importance in the mineral resource complex of the Republic of Kazakhstan [1]. Polygenic stratiform deposits are the largest in the world in terms of barite and manganese reserves, as well as lead and zinc reserves [1]. In terms of paragenetic associations, the deposits of the Atasu type are either complex ferromanganese and barite-polymetallic ones (Ushkatyn I, II, III, East Zhairem, West Kamys, Arap, Keregetas, South Karazhal), or (according to the prevalence of Fe, Mn) ferromanganese ones (West and East Karazhal, Big, Middle and Small Ktai, Zhomart, Vostochny Kamys, Yuzhny Klych, Akshagat, Kentobe, Bogach, Tur, Shoyntas), or by the predominance of Pb, Zn, Ba,

barite-polymetallic and polymetallic ones (Bestobe, Western and Far-West Zhairem, Karagayly , Akzhal, Uzunzhal, Mirgalimsay, Shalkiya, Achisay), or monobarite ones (Kentobe, Zhumanay, Zhalair), etc. (Figure 1) [1].

Experimental part

The deposits of the Zhailma graben-syncline (northwestern part of the Zhailma-Talkuduk rift zone) are considered as a reference for the Atasu type (Figure 2). The Zhailma graben-syncline (trough) is a large riftogenic structure, which is elongated from northwest to southeast. The rift-generating structure was formed in the Late Devonian during the destruction of the Epicaledonian Central Kazakhstan continental block [[2], [3], [4], [5], [6]].

The outer frame and the base of the graben-syncline (Figure 2) are composed of terrigenous-volcanogenic deposits of the Lower-Middle Devonian and volcanogenic-terrigenous deposits of the Daira Formation of the Upper Devonian. The total thickness of the Famennian and Tournaisian siliceous-terrigenous-carbonate deposits that make up the graben-syncline is more than 2500 m.

Rectilinear segments of its contours in the northwestern, latitudinal and less often northeastern and submeridional strike reflect the tectonic boundaries of the blocks of the rigid basement (Figure 2) [1].

The main value of the Atasu ore region is represented by stratiform complex deposits of iron-manganese, lead-zinc and barite ores of multi-stage and complex formation identified as an independent Atasu genetic type, one of which is the Bestobe deposit (Figure 3).

The Bestobe deposit is located in the eastern part of the Zhailma synclinorium (Zhairem, Ushkatyn, Zhumart are in the western part) and reveals a closer spatial relationship with the northeastern faults represented by barite, barite-polymetallic, polymetallic and iron-manganese deposits [[4], [9], [10], [11]]. Below iron-manganese ores, there are layered and secant bodies of lead-zinc-barite ores of the same two main stages of mineralization. Baritization was manifested in two stages: the first proceeded before folding, and the second one after it. Early fine-grained barites contain relict layered textures, sometimes they contain conformable interlayers with manganese mineralization. Late bodies of large-crystalline barite with sulfide mineralization replace even silicites, they are affected by shearing and faults associated with regional movements along the Uspenskaya mobile zone [8].
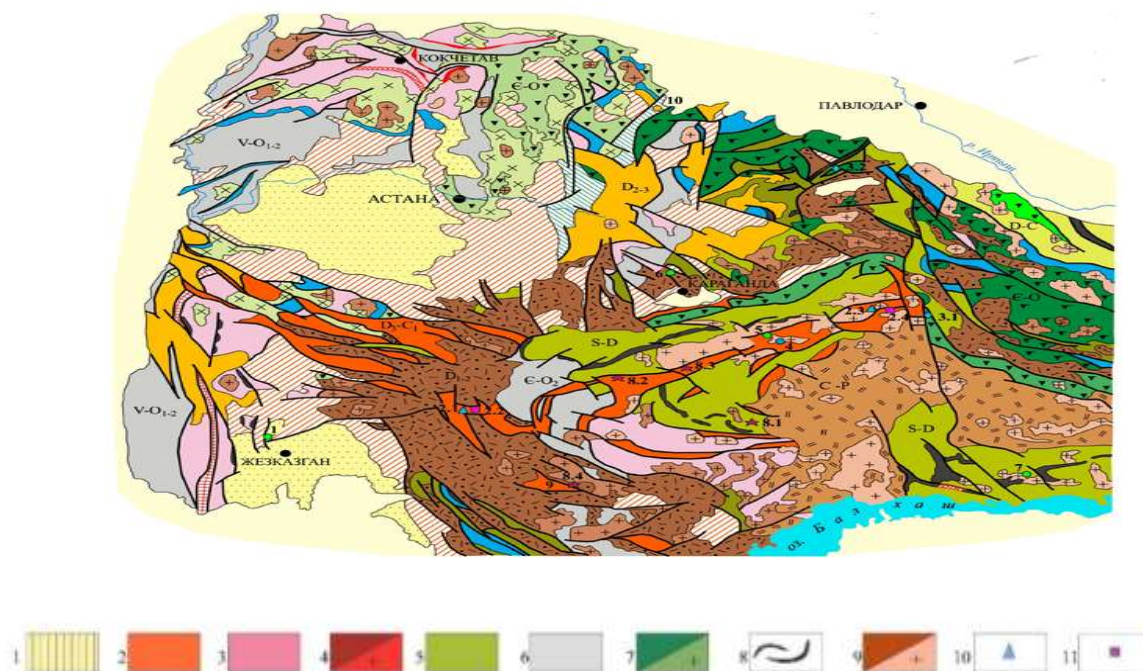
Figure 1 - Geodynamic position of the fields [[4], [5], [6]]:
1 - riftogenic structures (D₃-C₁); 2 - geological complexes of the inland sea basin (D₃-C₁); 3–7 - pre-Middle Devonian continental crust: Precambrian sialic massifs (3), Devonian runway (4), marginal sea basin (S₁-D₂) (5), passive continental margin (∈-O₃) (6), island arcs (∈-O₂) (7), tectonized ophiolite zones (8); Late Paleozoic runway (9); deposits: barite-polymetallic (10): Zhairem (2.1), Karagayly (2.3); ferromanganese (11): Ushkatyn (2.2), Kentobe (2.4) [[5], [6], [7]]
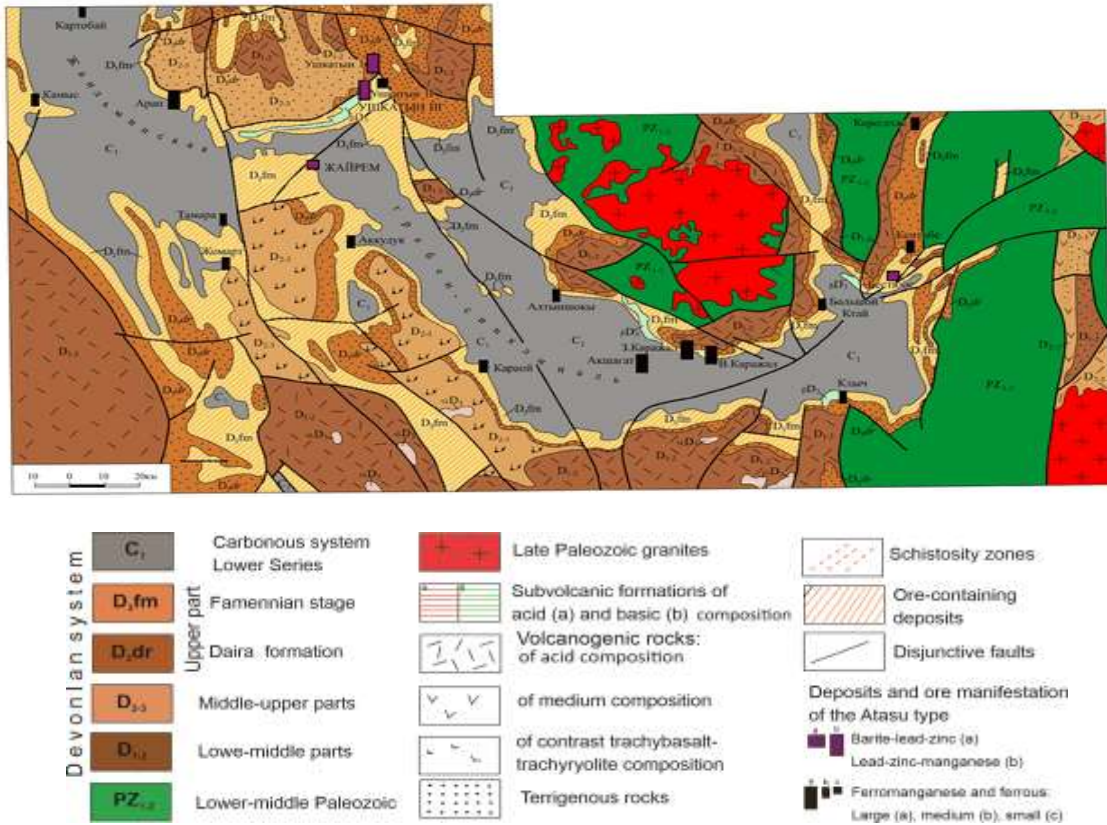
Figure 2 - Schematic geological map of the Zhailminsky and Karazhal ore clusters (according to A.A. Rozhnov et al.) [[3], [4], [5], [9]]
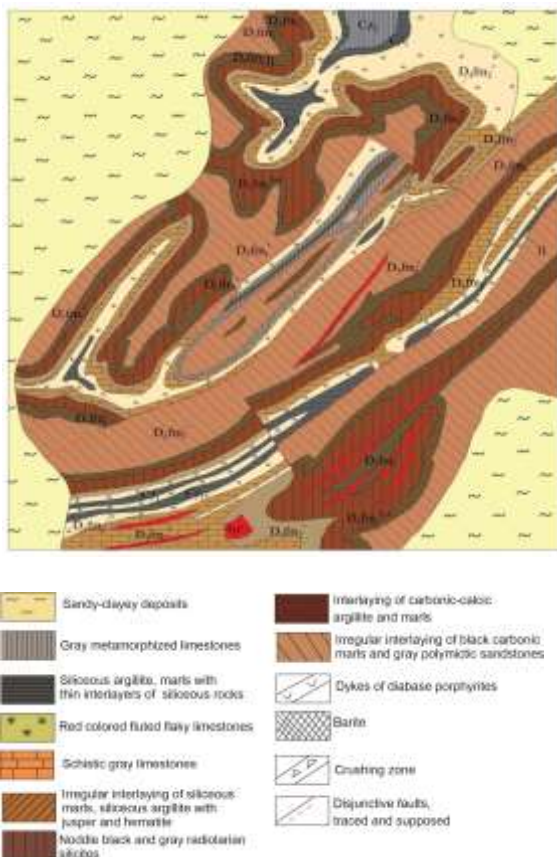
Figure 3 – Pattern of geological structure of the Bestobe deposit (acc. to N.S. Bozhukha) [[9], [11]]

As an occurrence of iron, it has been known since the late thirties. Zinc-lead-barite mineralization was discovered on it in 1952 by I.S. Syromyatnikov [[9], [11], [12], [13], [14]].

The deposit is composed of Upper Devonian and Lower Carboniferous sedimentary rocks containing an admixture of volcanic material [15].

There are distinguished the Daira Formation (D_3fm_1dr and Famennian deposits subdivided into five units: unevenly layered (D_3fm_1a), rhythmically layered (D_3fm_1b), flyschoid (D_3fm_1c), gray-colored (D_3fm_2a) and red-colored (D_3fm_2b), as well as Tournaisian rocks: dark gray pack (C_1t_1a) (Figure 4).

The features of the deposit are as follows: the combination of layered iron-manganese and lead-zinc ores and zinc-lead-barite mineralization superimposed on them; the sharply subordinate role of hydrothermal-sedimentary ores in the total reserves of lead and zinc; comparative abundance of sulfosalts of lead, copper and silver.

The deposits of the Famennian stage, according to lithological and petrographic features, are divided into horizons of terrigenous-carbonate rocks, black clayey marls, gray and black clayey silicites, ore, gray-colored and red-colored limestones (Figure 4).
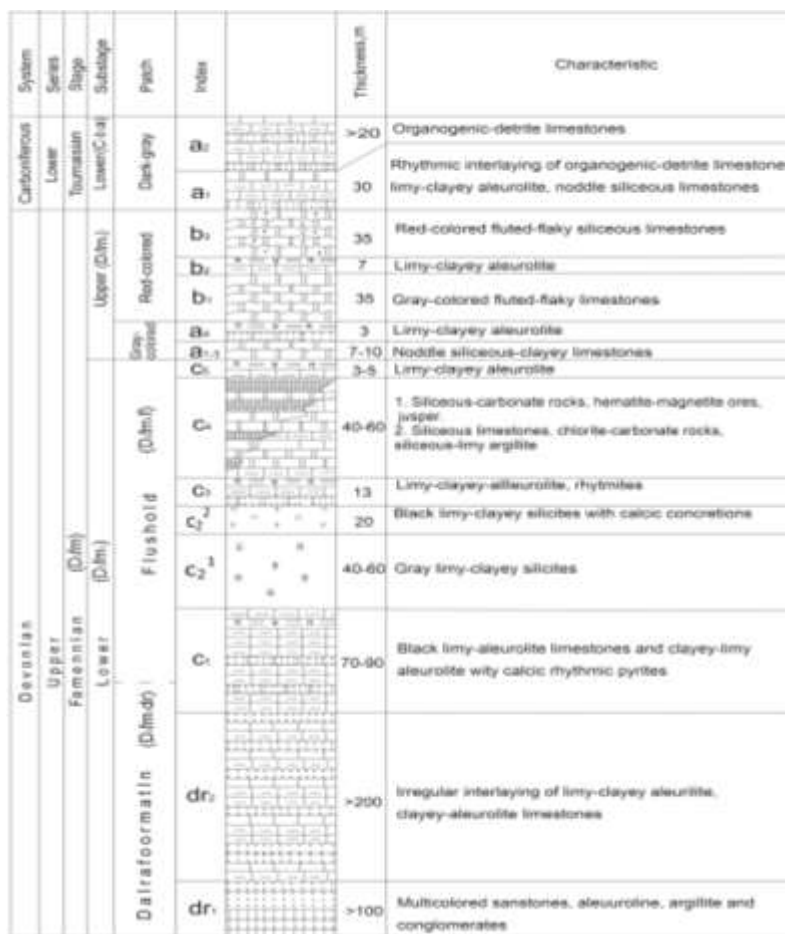
Figure 4 - Stratigraphic column of the Bestobe deposit [9]

Results

The Bestobe section is dominated by calcareous rocks, there are organogenic limestones; everywhere there are also horizons of lithocrystalline tuffs (up to 5 m thick) of liparite-dacitic composition, subvolcanic bodies of diabase porphyrites. The age of enclosing rocks, according to A.M. Sadykov is Upper Famennian [8]. In the ores of the deposit [9] there are about 60 minerals, of which the main ones are galena, sphalerite, pyrite, and barite.

The main reserves of barite-polymetallic ores of the deposit are confined to two synclinal structures located in the central part of the ore field (Figure 3).

The synclinal structures of the First section have been traced for more than 4 km, have the width of 150-250 m and the minimum depth of 170 m; the Second section of the deposit is up to 400 m wide and 350-400 m deep (Figure 5).

Morphologically, the ore bodies of the deposit are characterized by sheet-like and lenticular forms. They have the same occurrence elements as their enclosing rocks. In the First and Second sections, the ore bodies are elongated in the northeastern direction along the azimuth of about 45° and dip to the northwest at the angle of 30 to 90°. Their length is hundreds meters, the thickness is from a few to tens meters; in strike and dip they are unsteady. From the flanks to the central parts of the ore bodies, the thickness increases.

The internal structure of ore deposits is quite complex. Thus, alongside with an extremely uneven distribution of ore types, they also contain barren interlayers up to 5 m thick. The morphology of individual ore bodies is complicated by numerous late faults of various scales.

Lead-zinc-barite, lead-barite, barite and lead-zinc ores have been identified at the deposit. Lead-zinc-barite ores are developed in the lower parts of the ore bodies, lead-barite ores stand out as independent deposits in the central part and on the southwestern flank of the deposit, barite ores are widely developed in the near-surface part of the ore areas and lead-zinc ores form small lenticular bodies in the lower part of the ore horizon and in the upper layer of black clayey silicites. Thus, the deposit exhibits vertical zonality in the distribution of mineralization.
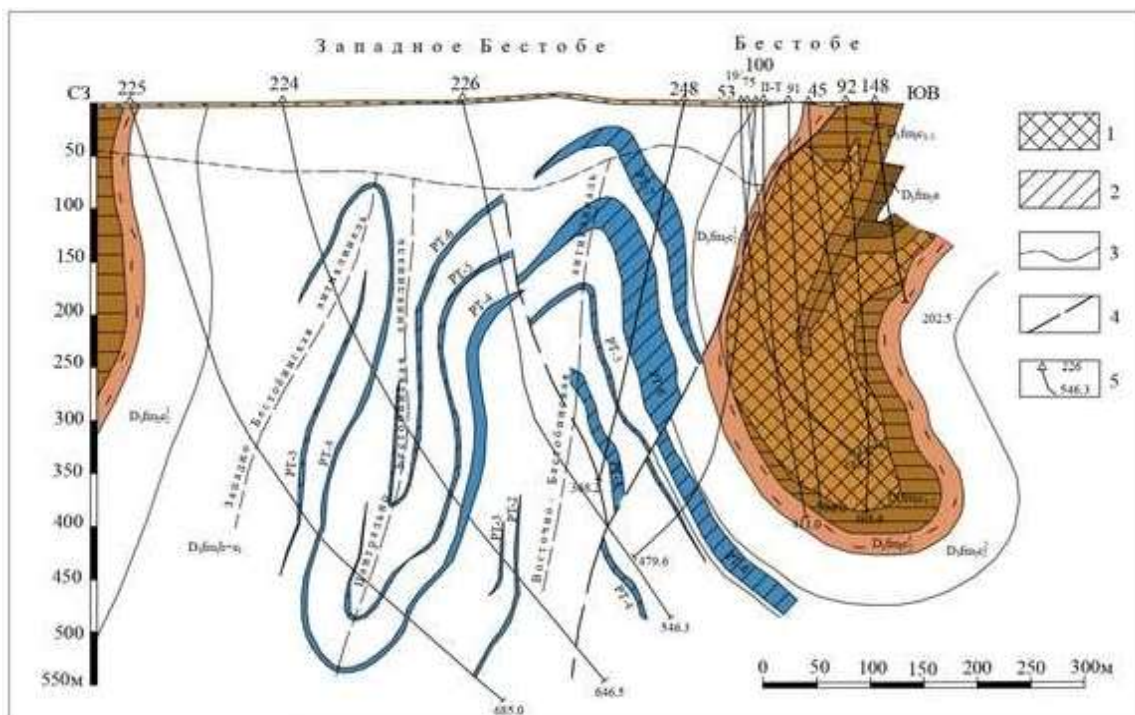
Figure 5 - Schematic geological section [7]
1 - barite-polymetallic ores; 2 – polymetallic ores; 3 – lower boundary of the weathering crust; 4 - tectonic faults;
5 – wells

In the distribution of elements in ore-bearing rocks, zoning is also observed (Table 1). It is characterized by different concentrations of elements above and below the ore bodies. Thus, the content of all the elements, except for copper, in the over-ore stratum is usually several times higher than in the under-ore one. Easily mobile elements in the under-ore zone are found in small quantities. In the over-ore stratum, the elements are dispersed over long distances from the ore bodies and form high concentrations, for example, arsenic.

Table 1 – Elements distribution zonality in ore-containing rocks of the Bestobe deposit

Zones	Number of samples	Distance from the ore body, m	The elemental composition of the zone		
			Basic	Rare	Very rare
IV above the ore	910	from 150 to 350	Hg	Ba, As	Ba, As
III above the ore	710	from 50 to 150	Ba, As, Hg	Pb, Zn, Cu, Sb	Tl, St
II above the ore	605	from 10 to 50	Pb, Ba, As, Hg, Ag, Cu, Zn, St	Sb, Cd, Tl	Mo, V, Ge et al.
Above the ore	373	up to 10	Pb, Ba, As, Hg, Ag, Cu, Zn, St, Cd, Ge, Sb, Tl	Ga, Mo, Bi, In	Cr, Co, Zr, Li et al.
Ore		Ore body	Pb, As, Hg, Ag, Cu, Zn, St, Cd, Ge, Sb, Tl	Ga, Mo, Bi, In	Cr, Co, Zr, Li et al.
I under the ore	393	up to 5-6	Ba, Pb, As, Hg, Ag, Cu, Zn, Sb, Cd		
II under the ore	252	from 5-6 to 20-30	Ba, Pb, Zn, Cu		
III under the ore	379	from 20-30 to 70-100	Ba, Cu		

The zonality in the distribution of elements around the ore bodies of the First and Second sections is generally the same. There are clearly distinguished the internal, intermediate and external zones. In the internal zones, elevated contents of those elements that are concentrated in the ore body are noted. In the intermediate zone, there are mostly common contents of lead, zinc, barium and arsenic, mercury. In the outer zone, significant concentrations of only volatile elements (mercury, sometimes arsenic) are noted. The most extensive halos are confined to the First section, where the enclosing rocks are intensely dislocated and where the thickest ore bodies have been identified. Such dimensions of the ore tail can be related to the superimposed dynamometamorphic flow.

When moving from one zone to another (in the direction from the ore bodies), the list of elements is reduced. So, if the number of elements in the halo in the first over-ore zone is 11, then in the second one it is 8, in the third one it is 3, and in the fourth one it is only one (mercury). The elemental composition of ores in the first over-ore zone is similar, i.e., this zone is a natural continuation of the ore body. There is noticed asymmetric distribution of moving elements relative to the ore bodies. If in the under-ore strata they (mercury, arsenic) form only internal zones, then in the over-ore stratum they form external ones.

The main components of the ores of the deposit (Table 1) are lead, zinc and barium, the content of which ranges from tenths to 98-99 %. Strontium is a constant impurity in barytes. Lead is mainly concentrated in galena, its insignificant amount is found in geocronite, boulangerite, jamsonite, bournonite, cerussite, anglesite, pyromorphite, and plumboiarosite. The highest lead content is found in the upper parts of the ore deposits, and the lowest content is in the lower ones.

The bulk of zinc is concentrated in the lower parts of the ore horizon in the form of sphalerite. Copper is a constant component of ores present as chalcopyrite, less commonly as fahlore, bournonite, enargite, chalcocite, and luconite. Silver is the most widespread impurity in ores. Its contents range from 3-109 g/t, the highest concentrations are found in galena (up to 500 g/t), fahlore and geocronite.

Cadmium is common in ores. Its high content was established in the significantly zinc varieties. In sphalerite, the content of cadmium is the highest; it is lower by 1-2 orders of magnitude in other sulfides. Mercury is constantly present in fahlore, sphalerite, as well as in the form of independent minerals: cinnabar and schwazite. Thallium was not detected in ores at the spectral analysis sensitivity of 0.0001 % [16]. But it is found in almost all the samples of globular pyrite, in galena and minerals of the jordanite-geocronite-schulcite series. Germanium occurs sporadically in zinc-lead-barite ores. Its own mineral, vanadium-arsenic germanite, was found at the deposit. In the ores there is almost absent bismuth, selenium and tellurium, which sharply distinguishes Bestobe, like other deposits of the Atasu type, from deposits of other genetic groups.

Conclusions

The analysis of the materials indicates that mineralization at the Bestobe deposit is a complex one, of the Atasu type. Its main value is polymetallic ores, the role of iron ore mineralization of the deposit is insignificant, manganese mineralization is practically absent.

Polymetallic ores are conditionally subdivided into lead-zinc-barite, lead-barite, barite and lead-zinc ones. According to the composition and content of lead minerals, the ores of the deposits are divided into three grades: sulfide (20 %), oxidized (60 %), and mixed (20–60 %). The main ore-forming minerals are galena, barite, sphalerite, the main mineral of the oxidation zone is cerussite.

Conflict of interests. On behalf of all authors, the correspondent author declares that there is no conflict of interests.

Бестөбе кен орнының геологиясы және минерагениясы (Орталық Қазақстан)

¹ Асқарова Н.С., ¹ Портнов В.С., ¹ Блялова Г.Г., ¹ Мадишева Р.К., ² Дьяконов В.В.

¹ Қарағанды техникалық университеті, Қарағанды, Қазақстан
² Серго Орджоникидзе атындағы Ресей мемлекеттік геологиялық барлау университеті, Мәскеу қ., Ресей

ТҮЙІНДЕМЕ

Полигендік стратиформды кен орындары барит және марганец қорлары, сондай-ақ қорғасын және мырыш қорлары бойынша әлемдегі ең ірі кенорындарына жатады. Қазақстан Республикасының минералдық-шикізат кешенінде олардың маңызы зор және дербес генетикалық Атасу типіне жатқызылған. Мақалада ірі рифтогендік құрылымдағы Жайылма грабен-синклиналь кен орындары Атасу типінің эталондық түрі ретінде қарастырылады. Жайылма синклинорийінің шығыс бөлігінде орналасқан Бестөбе стратиформды полиметалл кен орнының геологиялық құрылымы ұсынылған. Кен түзілімдерінің стратиграфиясы, кендену ерекшеліктері, кен денесінің морфологиясы және Бестөбе кен орнының кен сыйыстырушы жыныстарындағы элементтердің аймақтық таралу схемасы көрсетілген. Кен орнының ерекшелігі: қабатталған темір-марганец және қорғасын-мырыш кендері мен оларға үстемеленген мырыш-қорғасын-барит кендерінің бірігуі; қорғасын мен мырыштың жалпы қорындағы гидротермалды-шөгінді кендердің күрт бағыныңқы рөлі; қорғасын, мыс және күміс сульфо тұздарының салыстырмалы көптігі. Материалдарды талдау қорытындысы Бестөбе кен орнында кендену кешенді болып табылатынын көрсетеді. Оның басты құндылығы-полиметалл кендері. Кен орнының темір кенді кенденуінің рөлі шамалы. Марганецті кендену іс жүзінде жоқ. Полиметалл кендері шартты түрде қорғасын-мырыш-барит, қорғасын-барит, барит және қорғасын-мырыш болып бөлінеді. Бариттерде қоспада тұрақты стронций болады. Қорғасын негізінен галенитте шоғырланған, оның аз мөлшері геокронитте, буланжеритте, джемсонитте, бурнонитте, церусситте, англезитте, пироморфитте, плумбоярозитте болады. Мырыштың негізгі бөлігі сфалерит түрінде шоғырланған.

Түйін сөздер: Атасу типі, полиметалдар, Жайылма грабен-синклиналь, қорғасын-мырыш-барит кен орны.

Авторлар туралы ақпарат:

Асқарова Назым Сражадинқызы	*Қарағанды техникалық университетінің докторанты, «Геология және пайдалы қазбалар кен орындарын барлау» мамандығы бойынша техника және технология ғылымдарының магистрі, 100000, Қарағанды қ., Қазақстан Республикасы, e-mail: srajadin-nazym@mail.ru. ORCID: 0000-0002-2103-6198*
Портнов Василий Сергеевич	*Қарағанды техникалық университетінің «Геология және пайдалы қазбалар кен орындарын барлау» кафедрасының профессоры, техника ғылымдарының докторы, 100000, Қарағанды қ., Қазақстан Республикасы, e-mail: vs_portnov@mail.ru. ORCID: 0000-0002-4940-3156*
Блялова Гулим Галымжановна	*Қарағанды техникалық университетінің докторанты, «Геология және пайдалы қазбалар кен орындарын барлау» мамандығы бойынша техника ғылымдарының магистрі, 100000, Қарағанды қ., Қазақстан Республикасы, e-mail: krg_gulim@mail.ru. ORCID: 0000-0001-8801-8683*
Мадишева Рима Копбосынкызы	*PhD докторы, Қарағанды техникалық университетінің докторанты, «Геология және пайдалы қазбалар кен орындарын барлау» кафедрасының аға оқытушысы, 100000, Қарағанды қ., Қазақстан Республикасы, e-mail: rimma_kz@mail.ru. ORCID: 0000-0002-5726-9567*
Дьяконов Виктор Васильевич	*Геология-минералогия ғылымдарының докторы, профессор, Серго Орджоникидзе атындағы Ресей мемлекеттік геологиялық барлау университетінің «Жалпы геология және геологиялық карталау» кафедрасының меңгерушісі, 101000 Ж. Мәскеу, Ресей, e-mail: mdf.rudn@mail.ru*

Геология и минерагения месторождения Бестобе (Центральный Казахстан)

¹ Асқарова Н.С., ¹ Портнов В.С., ¹ Блялова Г.Г., ¹ Мадишева Р.К., ² Дьяконов В.В.

¹ Карагандинский технический университет, Караганда, Казахстан
² Российский государственный геологоразведочный университет имени Серго Орджоникидзе, г. Москва, Россия

АННОТАЦИЯ

Полигенные стратиформные месторождения являются крупнейшими в мире по запасам барита и марганца, также по запасам свинца и цинка. В минерально-сырьевом комплексе Республики Казахстан они имеют важнейшее значение и выделены в самостоятельный генетический Атасуйский тип. В статье в качестве эталонных для Атасуйского типа рассматриваются месторождения Жаильминской грабен-синклинали, в крупной рифтогенной структуры. Представлено геологическое строение стратиформного полиметаллического месторождения Бестобе, расположенное в восточной части Жаильминского синклинория. Показана стратиграфия рудных образований, особенности оруденения, морфология рудного тела и схема зональности распределения элементов в рудовмещающих породах месторождения Бестобе. Особенностью месторождения является: совмещение слоистых железомарганцевых и свинцово-цинковых руд и наложенного на них цинково-свинцово-баритового оруденения; резко подчиненная роль гидротермально-осадочных руд в общих запасах свинца и цинка; сравнительное обилие сульфосолей свинца, меди и серебра. Анализ материалов свидетельствует о том, что оруденение на месторождении Бестобе является комплексным. Главную его ценность составляют полиметаллические руды. Роль железорудного оруденения месторождения незначительна. Марганцевое оруденение, практически, отсутствует. Полиметаллические руды условно подразделяются на свинцово-цинково-баритовые, свинцово-баритовые, баритовые и свинцово-цинковые. В баритах постоянной примесью является стронций. Свинец сосредоточен, в основном, в галените, незначительное его количество находится в геокроните, буланжерите, джемсоните, бурноните, церуссите, англезите, пироморфите, плюмбоярозите. Основная масса цинка сконцентрирована в виде сфалерита.

Ключевые слова: Атасуйский тип, полиметаллы, Жаильминский грабен-синклиналь, свинцово-цинково-баритовые месторождения.

Информация об авторах:

Асқарова Назым Сражадинқызы — *Докторант Карагандинского технического университета, магистр техники и технологии специальности «Геология и разведка месторождений полезных ископаемых», 100000, г. Караганда, Республика Казахстан, e-mail: srajadin-nazym@mail.ru. ORCID: 0000-0002-2103-6198*

Портнов Василий Сергеевич — *Доктор технических наук, профессор кафедры «Геология и разведка МПИ» Карагандинского технического университета, 100000, г. Караганда, Республика Казахстан, e-mail: vs_portnov@mail.ru. ORCID: 0000-0002-4940-3156*

Блялова Гулим Галымжановна — *Докторант Карагандинского технического университета, магистр технических наук по специальности «Геология и разведка месторождений полезных ископаемых», 100000, г. Караганда, Республика Казахстан, krg_gulim@mail.ru. ORCID: 0000-0001-8801-8683*

Мадишева Рима Копбосынкызы — *Доктор PhD, старший преподаватель кафедры «Геология и разведка МПИ» Карагандинского технического университета, 100000, г. Караганда, Республика Казахстан, e-mail: rimma_kz@mail.ru. ORCID: 0000-0002-5726-9567*

Дьяконов Виктор Васильевич — *Доктор геолого-минералогических наук, профессор, Заведующий кафедрой общей геологии и геологического картирования Российского государственного геологоразведочного университета имени Серго Орджоникидзе, 101000 г. Москва, Россия, e-mail: mdf.rudn@mail.ru*

Reference

[1] Zhukovsky VI, Malchenko EG, Khamzin BS. Polimetallicheskiye i zhelezomargantsevyye mestorozhdeniya Tsentralnogo Kazakhstana (Atasuyskiy tip) [Polymetallic and ferromanganese deposits of Central Kazakhstan (Atasui type)]. Ore provinces of Central Asia. Almaty. 2008. 149-160. (in Russ.).

[2] Brusnitsyn AI, Kuleshov VN, Sadykov SA, Perova EN, Vereshchagin OS. Izotopnyy sostav (δ13C and δ13O) i genezis margantsenosnykh otlozheniy mestorozhdeniya Ushkatyn-III. Tsentralnyy Kazakhstan [Isotopic composition (δ13C and δ13O) and genesis of manganese-bearing deposits of the Ushkatyn-III deposit, Central Kazakhstan]. Lithology and Minerals 2020:6:522-548. https://doi.org/10.31857/S0024497X20060026 (in Russ.).

[3] Brusnitsyn AI, Perova EN, Vereshchagin OS, Britvin SN, Letnikova EF, Shkolnik SI & Ivanov AV. (2018). Barite-lead-zinc and iron-manganese deposits of the Zhairem ore cluster: geological excursion to Central Kazakhstan. Mineralogy. *4*(3), 82-92.

[4] Antonyuk RM, Ismailov HK. Promyshlennyye mestorozhdeniya metallicheskikh poleznykh iskopayemykh Tsentralnogo Kazakhstana. Geodinamicheskaya pozitsiya, stroyeniye, sostav rud [Industrial deposits of metallic minerals of Central Kazakhstan. Geodynamic position, structure, composition of ores]. Karaganda. 2019. 85. (in Russ.)

[5] Antonyuk RM, Ismailov HK, Klochkov MV, Kochergina AV, Kuznetsov KV. Zakonomernosti lokalizatsii mestorozhdeniy atasuyskogo tipa v riftogennykh strukturakh Tsentralnogo Kazakhstana pozdnedevonskogo–rannekamennougolnogo vozrasta [Regularities of localization of deposits of the Atasui type in rift structures of Central Kazakhstan of Late Devonian-Early Carboniferous age]. Geology and Protection of the Subsoil 2012;43(2):11-21. (in Russ.)

[6] Askarova NS, Roman AT, Portnov VS, Kopobayeva AN. Feature space of the Atasu type deposits (Central Kazakhstan). Naukovyi Visnyk Natsionalnoho Hirnychoho Universytetu 2021;5:5–10. https://doi.org/10.33271/nvngu/2021-5/005

[7] Baidalinov AT. Litologiya i rudonosnost nizhnefamenskikh otlozheniy Bestobinskogo rudnogo polya [Lithology and ore content of the Nizhnefamensk deposits of the Bestobinsky ore field]. Izvestiya NAS RK. Geological Series 2006;2:14-17 (in Russ.).

[8]   Shcherba GN. Nekotoryye osbennosti izucheniya mestorozhdeniy atasuyskogo tipa [Some features of the study of deposits of the Atasui type]. Izvestia of the Academy of Sciences of the Kazakh SSR. The series is geological. Alma-Ata. 1964. No. 5. 15-33. (in Russ.)

[9]   Mitryaeva NM. Mineralogiya baritovo-tsinkovo-svintsovykh rud mestorozhdeniy Atasuyskogo rayona [Mineralogy of barite-zinc-lead ores of deposits of Atasuysky district]. Publishing house "Science" of the Kazakh SSR. Alma-Ata. 1979, 225 (in Russ.).

[10] Lyubetsky VN, Lyubetskaya LD, Shabalina LV. Glubinnoye stroyeniye i etapy formirovaniya promyshlennykh stratiformnykh polimetallicheskikh rud Ataysuyskogo i Rudno-Altayskogo rudnykh rayonov [Deep structure and stages of formation of industrial stratiform polymetallic ores of the Ataysu and Rudno-Altay ore districts]. Izv. NAS RK. Geological series 2009;5:68-79 (in Russ.).

[11] Bespaev HA, Egembayev KM, Miroshnichenko LA, Kolesnikov VV, Akylbekov SA, Ganzhenko G.D. Mestorozhdeniya svintsa i tsinka Kazakhstana [Deposits of lead and zinc in Kazakhstan]. Almaty. 1997. 152. (in Russ.)

[12] Stroiteleva AV, Kaimirasova TG. Glubinnoye stroyeniye i metallogeniya Zhailminskoy sinklinali Tsentralnogo Kazakhstana [Deep structure and metallogeny of the Zailma syncline of Central Kazakhstan]. Alma-Ata: Nauka. 1982, 184. (in Russ.).

[13] Vasyukov YuA, Boldyrev VB. Gosudarstvennaya geologicheskaya karta Atasuyskogo rudnogo rayona [State geological map of the Atasuysky ore district]. M 1:50,000. Explanatory note. L. 1991. 214. (in Russ.)

[14] Abdulin AA, Kayupov AK, Li VG. et al. Metallogeniya Kazakhstana. Rudnyye formatsii. Mestorozhdeniya svintsa i tsinka [Metallogeny of Kazakhstan. Ore formations. Deposits of lead and zinc]. Alma-Ata, "Science" of the Kazakh SSR, 1978, 266 p. (in Russ.).

[15] Buzmakov EI, Shchibrik VI. Stratigrafiya i litologiya famenskikh i turneyskikh otlozheniy Atasuyskogo rudnogo rayona [Stratigraphy and lithology of Famennian and Tournaisian deposits of the Atasuysky ore region]. Soviet geology. 1976. No. 2. 61-79. (in Russ.).

[16] Shchibrik VI, Mitryaeva FF, Taranushich FF, et al. Barito-svintsovo-tsinkovoyye mestorozhdeniya Atasuyskogo rayona [Barite-lead-zinc deposits of Atasuysky district.]. Volcanogenic-sedimentary litho- and ore genesis. Alma-Ata. 1981. 96-106. (in Russ.)

Thermodynamic substantiation of compositions of silicon aluminium alloys with increased aluminium content in Fe-Si-Al system

Baisanov S., Tolokonnikova V.V., Narikbayeva G.I., Korsukova I.Ya.

Abishev Chemical-Metallurgical Institute, Karaganda, Republic of Kazakhstan

* Corresponding author email: met.rasplav@mail.ru

ABSTRACT

A priority direction of ferrous metallurgy development is to increase in output of the high quality metal and metal products of new assortment. One of the methods to improve a quality of steels is to involve of complex alloys based on aluminum, silicon, manganese, etc. for their output. They are necessary as deoxidizing agents and alloying additives. This paper considers the possibility of the thermodynamic substantiation of the aluminum solubility in the ferrosilicon-aluminum complex alloy (FeSiAl) on the basis of their phase diagrams using the osmotic coefficient of the Bjerrum-Guggenheim. Methodology used is based on the theoretical studies of the phase equilibria using the Bjerrum-Guggenheim concept. It includes a set of computer programs in C# language (C sharp) designed to evaluate a deviation scope of properties of a real system from the ideal one. Criterion for evaluation is an osmotic coefficient of the Bjerrum-Guggenheim. The pattern of change in an osmotic coefficient of the Bjerrum-Guggenheim on the ratio of activity of components in the ideal liquid and solid phases (positive Φi <1 or negative Φi >1) under the boundary forming conditions of crystallization regions of phases related to the melting ferrosilicon-aluminum processes is a direct proof of the possibility to use it as a metal reducing agent. The calculated mathematical dependences of the osmotic coefficient of the Bjerrum-Guggenheim permit us to determine the crystallization temperature of the ferrosilicon-aluminum alloy. The alloying process with rich aluminum content is observed at this temperature. The dependence diagrams of an osmotic coefficient of the Bjerrum-Guggenheim of a crystallizing component on the ratio of its activity in the liquid and solid phases demonstrated that a temperature rise leads to strong negative deviations in silicon properties, and thus to its good mixability in the melt with iron and aluminum. Compositions of silicon-aluminum alloys with high aluminum content in the ferrosilicon-aluminum complex alloy (FeSiAl) were determined on the basis of their phase diagrams using the osmotic coefficient of the Bjerrum-Guggenheim with iron content of 12-37%, aluminum 20-25% and silicon 68-38%. The received theoretical results permit to determine conditions which give the maximum possible aluminum assimilation with the ferrosilicon-aluminum melts supplied from the high-ash coal in the melting process of this metal in the ore-thermal furnaces. Thus it is a direct method to develop the output technology of the complex alloys.

Keywords: phase diagrams, Bjerrum-Guggenheim coefficient, crystallization regions of phases, silicon aluminium alloys, ferrosilicon aluminium, complex alloys.

Baisanov Sailaubai	*Information about authors:* *Doctor of technical sciences, professor, head of the laboratory of metallurgical melts of the Abishev Chemical-Metallurgical Institute, Karaganda, Kazakhstan. E-mail: splav_sailaubai@mail.ru, ORCID ID: 0000-0002-7328-2921*
Tolokonnikova Vera Vladimirovna	*Candidate of chemical sciences, leading researcher of the laboratory of metallurgical melts of the Abishev Chemical-Metallurgical Institute, Karaganda, Kazakhstan. E-mail: tolokon-splav@mail.ru, ORCID ID: 0000-0003-3386-0966*
Narikbayeva Gulnar Itemirovna	*Researcher of the laboratory of metallurgical melts of the Abishev Chemical-Metallurgical Institute, Karaganda, Kazakhstan. Email: narikbaeva63@mail.ru , ORCID ID: 0000-0002-1055-3448*
Korsukova Irina Yaroslavovna	*Researcher of the laboratory of metallurgical melts of the Abishev Chemical-Metallurgical Institute, Karaganda, Kazakhstan. Email: met.rasplav@mail.ru, ORCID ID: 0000-0003-2121-4270*

Introduction

Today the ferrosilicon-aluminum production with using the high-ash coal raw materials was only organized in Kazakhstan. The aluminum content is regulated by 5 - 15% in Kazakhstan. The basis to develop the technology was a detailed study of a reduction process of silicon and aluminum compounds with using the thermodynamic-diagram analysis of the Fe-Si-Al-C-O system.

The absence of the thermodynamic information for a wide range of composition and temperature makes it impossible to assess the real yield of the reaction products in the melting process of ferrosilicon aluminium. It should be pointed out that for Fe-Si-Al-C system melts the available quite

extensive experimental material on the thermodynamic parameters refers mainly to binary systems of Fe-C, Fe-Si and Si-Al, and also a small number of papers on the triple systems [[1], [2], [3]].

The analysis of the numerous phrase diagrams of various systems determined a common pattern in formation of crystallization regions as a correlation dependence of an osmotic coefficient of the crystallizing component on the ratio of its activity in the liquid and solid phases. The osmotic coefficient of Bjerrum-Guggenheim is able to be as a measure of deviation of the energetic properties of a real system from the ideal one described by Le Chatelier-Shreder equation.

The received data on crystallization regions of phases in the studied systems testify the presence of a regular change in the non-ideality coefficient Φ_i (Bjerrum-Guggenheim coefficient) along a line and crystallization surface of phases and a close connection of this value with the nature of the interparticle interaction of components in the melt and their state.

One of the methods of the technical solutions for melting of the complex alloys, in particular, ferrosilicon aluminium with a high aluminum content of up to 25%, is to conduct the thermodynamic studies of phase equilibria based on the Bjerrum-Guggenheim concept for a triple phase diagram of the Fe-Si-Al system, which will permit to calculate the rational compositions of alloys with the thermodynamic method and to determine areas of existence of an independent phase of aluminium.

Experimental part

The theoretical studies of the behavior of the osmotic coefficient of Bjerrum-Guggenheim of a dissolved substance (e.g. aluminum in iron) depending on the ratios of components in the melt can simultaneously have the positive and negative deviations from ideality. Depending on values of the osmotic coefficient of Bjerrum-Guggenheim in the thermodynamic calculations for various Fe:Al ratios, it will be possible to discuss in which areas of the melt the aluminum is absorbed very well, and in which it can be isolated as an independent phase.

The study of the phase diagrams of iron-based systems was performed according to the well-known classification of phase diagrams [[4], [5], [6], [7]] and taking into account the possibility of the analytical description of all types of their solid-liquid and solid-solid phase equilibrium diagrams

based on the nature of the change in the value of the Bjerrum-Guggenheim coefficient near the singular points.

The principle of our procedure is as follows: to take data on temperature and composition from a phase diagram and to find reference data on temperature and enthalpy of melting of a solvent and the dissolved substances for Le Chatelier-Shreder equation. Further our developed program is used: to process the initial data with finding the expressions of the osmotic coefficients of Bjerrum-Guggenheim for the liquid and solid phases, to plot the dependence diagrams of a osmotic coefficient of the crystallizing phases (Φ_i) on ratio of the component activities in the ideal liquid and solid phases and to find a mathematical expression of a correlation dependence. The mathematical expressions for the liquidus and solidus lines as a semi-empirical dependence of the modified equation of Le Chatelier-Shreder were obtained for the ideal system and the detected patterns on the monovariant phase equilibrium lines.

This paper focused on the binary systems of Fe - Al, Fe - Si and Si – Al [[7], [8]] characterized by the presence of the extensive areas of the limited solid ferrite and austenitic solutions and a whole cascade of the intermediate phases that are important for the production of ferrosilicon aluminium.

The binary phase diagrams of iron - aluminum (Fe-Al) and iron - silicon (Fe-Si) are previously described in full with the mathematical expressions from the position of the Bjerrum-Guggenheim concept [9]. Table 1 gives the coefficients of the dependence of the osmotic coefficient Φ_i' on the ratio of the activity of the liquid and solid phases (exponent of the Le Chatelier-Shreder equation) substituting in equations of (1) or (2), the correlation dependences will be calculated.

$$\Phi_i' = \left(\ln a_i^L / \ln a_i^S\right)/(\ln x_i^L / x_i^S) = A_i + B_i \cdot a_i^L / a_i^S, \quad (1)$$

$$\Phi_i'' = A_i + B_i \cdot a_i^L / a_i^S + \frac{C_i}{a_{\text{кр.}} - a_i^L / a_i^S}, \quad (2)$$

where $x_i^{L(S)}$ - concentration of a crystallizing component at a given temperature; $a_i^{L(S)}$ - activity of a crystallizing component for an ideal solution calculated by Le Chatelier-Shreder equation; A_i, B_i, C_i - constants determined by the nature of components and interparticle interaction;

$a_{crit.}$.- a value of the ratio of the component activities at T=T_{max} calculated by Le Chatelier-Shreder equation.

Based on these correlation dependences, the equation of crystallization of the first or second component will be calculated, depending on which component the solvent is. The mathematical dependence of the composition on temperature is expressed by equations of (3) or (4).

$$\ln x_i^L = \frac{\Delta H_{m,i}}{R}\left(\frac{1}{T_{m,i}} - \frac{1}{T}\right)\cdot / \Phi_i^{"}, \tag{3}$$

$$\ln x_i^S = \frac{\Delta H_{m,i}}{R}\left(\frac{1}{T_{m,i}} - \frac{1}{T}\right)\cdot\left(\frac{1}{\Phi_i^{"}} - \frac{1}{\Phi_i^{'}}\right), \tag{4}$$

where $\otimes H_{m,1(2)}$ is the enthalpy of melting of the 1st and 2nd components at melting point, J/mol; R is a universal gas constant, 8.3144 J/mol K; $T_{m,1(2)}$ and T - melting point of the 1st and 2nd components and crystallization of melts, К; Φ_i ' - the Bjerrum-Guggenheim coefficient for the 1st and 2nd components which permits to find a correlation dependence and to calculate a mathematical expression for the ratio of the activities of the i-component in the liquid and solid phases; Φ_i'' - the Bjerrum-Guggenheim coefficient for the 1st and 2nd components which permits to find a correlation dependence and calculate a mathematical expression for liquidus line of i-component.

These mathematical expressions (3, 4) are the semi-empirical dependencies as a modified Le Chatelier-Shreder equation.

So, referring to Table 1, the crystallization region of α-Fe (Fe-Si system) has two phase transitions, thus it is described by the equation from the melting point of iron 1811 K to the first phase transition:

for crystallization region of α–Fe (5):

$$\Phi_{Fe}^{"} = 1{,}87 - 1{,}47\cdot a_{Fe}^L / a_{Fe}^S, \tag{5}$$

for region of an ordered phase ofα₂–Fe (6):

$$\Phi_{Fe}^{"} = 0{,}9866 - 0{,}4218\cdot a_{Fe}^L / a_{Fe}^S, \tag{6}$$

for region of an ordered phase of α₁–Fe (7):

$$\Phi_{Fe}^{"} = 0{,}6349 + 1{,}5733\cdot a_{Fe}^L / a_{Fe}^S. \tag{7}$$

The crystallization region of α-Fe (Fe-Al system) is calculated by equation (8):

$$\Phi_{Fe}^{"} = 1{,}3606 - 1{,}3319\cdot a_{Fe}^L / a_{Fe}^S, \tag{8}$$

for region of an ordered phase of α₂–Fe (9):

$$\Phi_{Fe}^{"} = 0{,}5445 - 0{,}3883\cdot a_{Fe}^L / a_{Fe}^S. \tag{9}$$

The triple system of Fe-Si-Al is the basis of silicon aluminum alloys and the silicon crystallization region in it and the features of thermodynamics of melts in this area are essential for the melting process of ferrosilicon aluminum.

Combining of the calculation results of the osmotic coefficients of Φ_{si} for different sections of the Si-Fe-Al system (Figure 1) and isotherm Φ_{si} for the different temperatures (Figure 2) permits to identify the characteristics of the behavior of elements in the Fe- Si-Al system. The change in the crystallization beam of the alloys from the Si-Fe to Si-Al system shows (Figure 1) that only near with the Si-Fe system the melts, as noted above, have the component association and a huge negative deviation from ideality (Φ_{si} is much more than one), (Figure 2) [[9], [10], [11]].

In the Si-Al system, the initial additions of Al lead to a significant deviation of the energy characteristics of Si in comparison with values of an osmotic coefficient of the Si-Fe system. But the rate of this deviation with a temperature change is lower, and therefore if the starting is from $a_{Si.}$ = 0.8, the effect of Al will decrease (Figure 1).

The beam with a ratio of 0.19 Fe:0.81 Al (at.) (Figure 1) is characterized by a linear dependence of Φ_{si} caused with a weak development of association of components in the melt. But if the starting is from the ratio of 0.49 Fe:0.51 Al (at.), the bending of Φ_{si} for the beam can be observed.

As the temperature increases, the negative deviation of Si properties from ideality (figure 2) can be intensified and hence its better miscibility with iron and aluminum in the region of Fe : Al = 0.7 : 0.3% (at.), which corresponds to the compositions of ferrosilicon aluminum (FeSiA) alloys with 12-37% Fe and 20-25% Al in recalculation by weight concentrations [9]. The temperature reduction moves the studied area to the Fe-Si binary system. This indicates that at low temperatures Al dissolves better in Fe-Si-rich alloys, and as the temperature

increases, the alloying process with richer aluminum content is facilitated.

The received data on behavior of an osmotic coefficient of Bjerrum-Guggenheim (Φ_{si}) for systems of Si-Al and Si-Fe and also for the two median beams are approximated by the three-term expression (1), provided that the associated complexes are present in the melts (Table 1).

Isotherms of Φ_{si} (Figure 2) for the entire crystallization surface can be easily represented as:

$$\Phi_{gen.Si} = Z_{Fe} \cdot \Phi'_{Si-Fe} + Z_{Al} \cdot \Phi'_{Si-Al} + Z_{Fe}^2 \cdot Z_{Al} \cdot \Phi'_{Fe/Al} +$$
$$+ Z_{Fe} \cdot Z_{Al}^2 \cdot \Phi'_{Al/Fe}, \qquad (10)$$

where $Z_{Fe} = x_{Fe} / (x_{Fe} + x_{Al})$, (at.);
$$Z_{Al} = x_{Al} / (x_{Fe} + x_{Al});$$

$\Phi'_{Fe/Al}$ - generalized equation of Φ_{si}, determined by the Scheffé's method. By the solving of two linear equations with this value obtained after substitution in the general expression $\Phi_{gen.Si}$, the equation of Φ_{si} for the two beams of 0.491 Fe:0.501 Al and 0.19 Fe:0.81 Al (at.) and Zi values was calculated (Table 1).

Table 1 - Parameters of crystallization regions of phases in the phase diagram of the binary systems based on iron

System	Phase (Φ' or Φ")	Coefficients of equation of dependence of (1), (2)			Correlation coefficient	Variance ±⊗L,s
		A	B	C		
FeSi	δ-Fe(Φ')	13.38	-12.24	-	-0.9978	-
	δ-Fe(Φ")	1.87	-1.47	-	-0.9995	-
	α₂-Fe(Φ')	24.47	-25.42	-	-0.9907	-
	α₂-Fe(Φ")	0.99	-0.42	-	-0.9010	-
	α₁-Fe(Φ')	70.07	-81.53	-	0.9905	-
	α₁-Fe(Φ")	-0.63	1.57	-	-0.9801	-
FeSi-Fe	FeSi(Φ')	1.84	-1.59	-	-0.9920	-
FeSi-Si	FeSi(Φ')	1.55	-1.24	-	-0.9967	-
Si-Fe	Si(Φ')	-0.788	0.3504	-1.358	-	0.0018
Fe-Al α→α₂ (T calc. = 1584К)	α-Fe(Φ')	3.87	-3.17	-	-0.9974	-
	α-Fe(Φ")	0.399	0.05	-	0.9584	-
	α₂-Fe(Φ')	-1.03	2.50	-	0.9991	-
	α₂-Fe(Φ")	-0.57	1.17	-	0.9988	-
	ε-phase(Φ')	-118.99	154.37	-	0.9820	-
	ε- phase (Φ")	-3.27	4.48	-	0.9944	-
	ε- phase (Φ')	-118.99	154.37	-	0.9820	-
	ε- phase (Φ")	-3.27	4.48	-	0.9944	-
Fe₂Al₅-Fe	Fe₂Al₅(Φ')	5.99	-5.96	-	-0.9998	-
	Fe₂Al₅(Φ")	3.21	-3.17	-	-0.9988	-
Fe₂Al₅-Al	Fe₂Al₅(Φ')	1.28	-1.27	-	-0.9980	-
	Fe₂Al₅(Φ")	0.84	-0.83	-	-0.9880	-
Crystal. region FeAl₃	Fe₂Al₅(Φ')	0.76	-0.61	-	-0.9998	-
	Fe₂Al₅(Φ")	0.59	-0.57	-	-0.9978	-
SiAl	Si(Φ')	1.622	-0.58	0.001	-	0.0014
Si-0.491Fe: 0.509Al	Si(Φ')	0.7143	0.3297	-0.352	-	0.0021
Si-0.194Fe: 0.806Al	Si(Φ')	1.2279	-0.0445	-0.029	-	0.0016
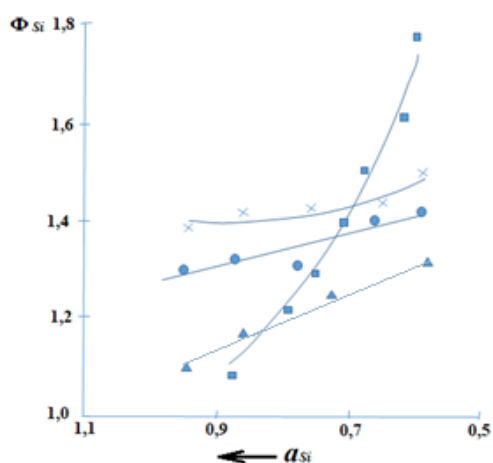
■ - Φ_{si}^{Si-Fe} , ▲ - Φ_{si}^{Si-Al} , ● − 0.49Fe:0.51Al, **x** − 0.19Fe:0.81Al

Figure 1 - Change of Φ_{si} along silicon crystallization line in binary systems of Si-Fe and Si-Al
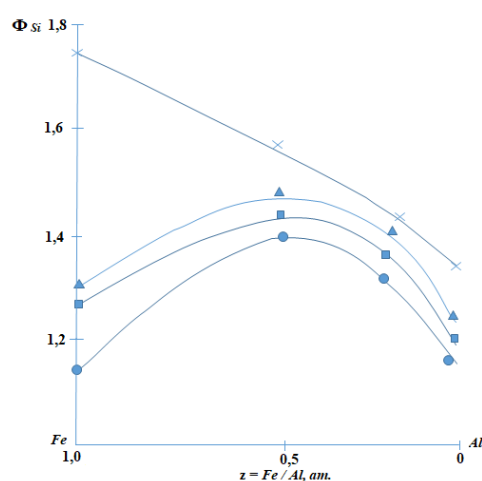
x − 1200⁰C, ▲ - 1250⁰C, ■ - 1300⁰C, ● - 1350⁰C

Figure 2 - Isotherms of Φ_{si} at different temperatures of Fe: Al = 0.7-0.3% (at.) which corresponds to compositions of Fe-Si-Al alloys with 12-37% Fe and 20-25% Al in recalculation

The obtained results for two binary systems of Si-Fe and Si-Al and two beams with Fe/Al composition ratio at the special temperatures and crystallization region demonstrated a good similarity of the calculated (solid lines) and experimental (points) composition data (Figure 2).

Conclusions

Based on the behavior of the osmotic coefficient of Bjerrum-Guggenheim in the melt of the Fe-Si-Al system using the thermodynamic method, the compositions of silicon-aluminum alloys with increased aluminum content were substantiated. The received mathematical dependences of the osmotic coefficient of Bjerrum-Guggenheim determined the crystallization temperature of the ferrosilicon-aluminium alloy, thus, the process of alloy formation with rich aluminum content was observed. Referring to the character of changes in the osmotic coefficient of Bjerrum-Guggenheim it was determined that the temperature increase leads to the strong negative deviations of silicon properties and thus to its better miscibility in the melt with iron and aluminum for the compositions of Fe: Al = 0.7 - 0.3 %. The optimum ratios of elements in the ferrosilicon aluminum complex alloy with the iron content of 12-37%, aluminum -20-25%, and silicon - 68-38% were defined. This composition characterizes the area of the alloy in which the aluminum melt will fully absorb.

Fe-Si-Al жүйесінің алюминий мөлшері жоғары кремний алюминий қорытпаларының құрамын термодинамикалық негіздеу

Байсанов С., Толоконникова В.В., Нарикбаева Г.И., Корсукова И.Я.

Ж. Әбішев атындағы химия-металлургиялық институт, Қарағанды, Қазақстан

ТҮЙІНДЕМЕ

Қара металлургияны дамытудың басым бағыты-жоғары сапалы металл өндірісін және металл бұйымдарының жаңа ассортиментін ұлғайту. Болаттардың сапасын жақсартуға қол жеткізудің бір әдісі - оларды өндіруге алюминий, кремний, марганец және т.б. негізіндегі күрделі қорытпаларды тарту, олар тотықсыздандырғыштар мен легірлеуші қоспалар ретінде қажет. Мақалада алюминийдің күрделі ферросиликоалюминий қорытпасында (FeSiAl) ерігіштігінің термодинамикалық негіздеу мүмкіндігі, олардың күй диаграммалары негізінде Бьеррум-Гуггенгейм осмостық коэффициенті арқылы талқыланады. Қолданылатын әдістеме Бьеррум-Гуггенгейм тұжырымдамасына негізделген фазалық тепе-теңдіктің теориялық зерттеулеріне негізделген және нақты жүйенің қасиеттерінің идеалдан ауытқу дәрежесін бағалауға арналған C# тіліндегі (Csharp) компьютерлік бағдарламалар жиынтығын қамтиды. Бағалау критерийі - Бьеррум-Гуггенгейм осмостық коэффициенті. Кристалдану өрістерінің пайда болуының шекаралық жағдайында идеалды сұйық және қатты фазалардағы компоненттердің белсенділігі (оң Фі <1 немесе теріс Фі >1) қатынасы бойынша Бьеррум-Гуггенгейм осмостық коэффициентінің өзгеру сипаты. ферросиликоалюминийді балқыту процестеріне байланысты фазалар оны металл тотықсыздандырғыш ретінде қолдану мүмкіндігінің тікелей дәлелі болып табылады. Бьеррум-Гуггенгейм осмостық коэффициентінің есептелген математикалық тәуелділіктері ферросиликоалюминий қорытпасының кристалдану температурасын анықтауға мүмкіндік берді, бұл кезде құрамында алюминий көп қоспалар бар. Кристалданатын компоненттің Бьеррум-Гуггенгейм осмотикалық коэффициентінің оның сұйық және қатты фазалардағы белсенділігінің арақатынасына тәуелділік графиктері температураның жоғарылауы кремнийдің қасиеттерінде күшті теріс ауытқуларға әкелетінін көрсетті, бұл оның жақсы араласуын білдіреді. Темір және алюминиймен балқытады. Күрделі ферросиликоалюминий қорытпасында (FeSiAl) алюминийдің құрамы жоғарылаған кремний-алюминий қорытпаларының құрамы олардың күйлік диаграммалары негізінде темір құрамы 12-37%, алюминий 20-25%, кремний 68-38% бар Бьеррум-Гуггенгейм осмостық коэффициенті арқылы құрылды күй диаграммалары негізінде орнатылған. Алынған теориялық нәтижелер бұл металды кенді-термиялық пештерде балқыту кезінде жоғары күлді көмірден келетін ферросиликоалюминий балқымаларымен алюминийдің максималды мүмкін ассимиляциясын қамтамасыз ететін жағдайларды анықтауға мүмкіндік береді, бұл-өндірістің дамуының тікелей жолы - күрделі қорытпаларды алу технологиясы.

Түйін сөздер: күй диаграммасы, Бьеррум-Гуггенгейм коэффициенті, фазалық кристалдану өрістері, кремний алюминий қорытпалары, ферросиликоалюминий, кешенді қорытпалар.

Авторлар туралы ақпарат:

Байсанов Сайлаубай
Техника ғылымдарының докторы, профессор, Ж. Әбішев атындағы химия-металлургия институтының металлургиялық балқымалар зертханасының меңгерушісі, Қарағанды, Қазақстан. E-mail: splav_sailaubai@mail.ru, ORCID ID: 0000-0002-7328-2921

Толоконникова Вера Владимировна
Химия ғылымдарының кандидаты, Ж. Әбішев атындағы химия-металлургия институты металлургиялық балқымалар зертханасының жетекші ғылыми қызметкері, Қарағанды, Қазақстан. E-mail: tolokon-splav@mail.ru, ORCID ID: 0000-0003-3386-0966

Нарикбаева Гульнар Итемировна
Ж. Әбішев атындағы химия-металлургия институты металлургиялық балқымалар зертханасының ғылыми қызметкері, Қарағанды, Қазақстан. Email: narikbaeva63@mail.ru, ORCID ID: 0000-0002-1055-3448

Корсукова Ирина Ярославовна
Ж. Әбішев атындағы химия-металлургия институтының металлургиялық балқымалар зертханасының ғылыми қызметкері, Қарағанды, Қазақстан. Email: met.rasplav@mail.ru, ORCID ID: 0000-0003-2121-4270

Термодинамическое обоснование составов кремнеалюминиевых сплавов с повышенным содержанием алюминия системы Fe-Si-Al

Байсанов С., Толоконникова В.В., Нарикбаева Г.И., Корсукова И.Я.

Химико-металлургический институт им. Ж. Абишева, Караганда, Казахстан

АННОТАЦИЯ

Приоритетным направлением развития чёрной металлургии является увеличение производства высококачественного металла и металлопродукции нового сортамента. Одним из путей достижения повышения качества сталей является вовлечение для их производства комплексных сплавов на основе алюминия, кремния, марганца и т.д., так необходимых в качестве раскислителей и легирующих добавок. В статье рассмотрена возможность термодинамического обоснования растворимости алюминия в комплексном сплаве ферросиликоалюминии (FeSiAl) на основе их диаграмм состояния через осмотический коэффициент Бьеррума-Гуггенгейма. Применяемая методология основана на теоретических исследованиях фазовых равновесий на основе концепции Бьеррума-Гуггенгейма и включает комплекс компьютерных программ на языке C# (Csharp), предназначенных для оценки степени отклонения свойств реальной системы от идеальной. Критерием оценки является осмотический коэффициент Бьерумма-Гугенгейма. Характер изменения осмотического коэффициента Бьеррума-Гуггенгейма от отношения активности компонентов в идеальной жидкой и твердой фазах (положительный Фі <1 или отрицательный Фі

>1) при граничных условиях формирования полей кристаллизации фаз, относящихся к процессам выплавки ферросиликоалюминия является прямым доказательством возможности применения его в качестве металлического восстановителя. Расчитанные математические зависимости осмотического коэффициента Бъеррума-Гуггенгейма позволили определить температуру кристаллизации сплава ферросиликоалюминия, при которой происходит процесс сплавообразования с более богатым содержанием алюминия. Графики зависимости осмотического коэффициента Бьеррума-Гуггенгейма кристаллизующегося компонента от отношения его активности в жидкой и твердой фазах показали, что рост температуры приводит к сильным отрицательным отклонениям свойств кремния, а значит лучшей смешиваемости его в расплаве с железом и алюминием. Установлены составы кремнеалюминиевых сплавов с повышенным содержанием алюминия в комплексном сплаве ферросиликоалюминий (FeSiAl) на основе их диаграмм состояния через осмотический коэффициент Бьеррума-Гуггенгейма с содержанием железа 12-37 %, алюминия 20-25 %, кремния 68-38 %. Полученные теоретические результаты позволяют определить условия, обеспечивающие максимально возможное усвоение алюминия расплавами ферросиликоалюминия, поступающего из высокозольного угля в процессе плавки этого металла в руднотермических печах, а это прямой путь к разработке технологии получения комплексных сплавов.

Ключевые слова: диаграмма состояния, коэффициент Бьеррума-Гуггенгейма, поля кристаллизации фаз, кремнийалюминиевые сплавы, ферросиликоалюминий, комплексные сплавы.

Информация об авторах:

Байсанов Сайлаубай	*Доктор технических наук, профессор, заведующий лабораторией металлургических расплавов Химико-металлургического института им. Ж. Абишева, Караганда, Казахстан. E-mail: splav_sailaubai@mP°il.ru, ORCID ID: 0000-0002-7328-2921*
Толоконникова Вера Владимировна	*Кандидат химических наук, ведущий научный сотрудник лаборатории металлургических расплавов Химико-металлургического института им. Ж. Абишева, Караганда, Казахстан. E-mail: tolokon-splav@mail.ru, ORCID ID: 0000-0003-3386-0966*
Нарикбаева Гульнар Итемировна	*Научный сотрудник лаборатории металлургических расплавов Химико-металлургического института им. Ж. Абишева, Караганда, Казахстан. Email: narikbaeva63@mail.ru, ORCID ID: 0000-0002-1055-3448*
Корсукова Ирина Ярославовна	*Научный сотрудник лаборатории металлургических расплавов Химико-металлургического института им. Ж. Абишева, Караганда, Казахстан. Email: met.rasplav@mail.ru, ORCID ID: 0000-0003-2121-4270*

References

[1] Ghos G. The phase equilibria and thermodynamic properties of the ternary Al-Fe-Si system were analyzed and   a *complete*. Ternary Alloys: A Comprehensive Compendium *of* Evaluated Constitutional Data and Phase Diagrams, G. Petzow and G. Effenberg, eds., VCH Publishers, New York, NY. 1992. 5. 394–438.

[2] Zi-Kui Liu, Austin Chang Y. Thermodynamic Assessment of the Al-Fe-Si System. Metall. Trans 1999;30:1081-1095. https://doi.org/10.1007/s11661-999-0160-3

[3] Issagulov AZ, Chekimbayev AZ, Makayev TS, Babenko AA. Studying the Fe-Al-Si system in relation to ferrosilicon-aluminum alloy crystallization. Metalurgija 2020;59(1):81-84.

[4] Zaharov AM. Diagrammy sostoyaniya dvojnyh i trojnyh sistem [Phase diagrams of binary and ternary systems]. Moscow: Metallurgy. 1978, 295. (in Russ.).

[5] Hansen M, Anderko K. Struktura dvojnyh splavov [Structure of double alloys]. Moscow: Metallurgy. 1962, 1488. (in Russ.).

[6] Zaharov MA. Raschet osnovnyh tipov diagramm sostoyaniya binarnyh rastvorov v ramkah obobshchennoj reshetochnoj modeli [Calculation of key types of phase diagrams of binary solutions under the generalized lattice model]. Vestnik Novgorodskogo gosudarstvennogo universiteta = Bulletin of Novgorod State University 2016;98(7):22-26. (in Russ.).

[7] Voronin GF. Novye vozmozhnosti termodinamicheskogo rascheta i postroeniya diagramm fazovyh sostoyanij geterogennyh sistem [New possibilities of thermodynamic calculation and construction of phase diagrams of heterogeneous systems]. Zhurnal fizicheskoi himii = Russian Journal of Physical Chemistry 2003;77(10):1874-1883. (in Russ.).

[8] Bajsanov S, Tolokonnikova VV, Narikbaeva GI, Korsukova IYa. Metody issledovaniya linij geterogennyh fazovyh ravnovesij na diagramme sostoyaniya cherez osmoticheskij koeffitsient B'erruma-Guggengejma [Research methods of the lines of heterogeneous phase equilibria on phase diagram using the osmotic coefficient of Bjerrum-Guggenheim]. Karaganda: Ekozhan. 2020, 73. (in Russ.).

[9] Shahnazarov KYu. Priznaki promezhutochnyh faz v sistemah Al-Si, Fe-C, Al-Cu [Signs of intermediate phases in systems of Al-Si, Fe-C and Al-Cu]. Vestnik MGTU im. G.I. Nosova = Bulletin of Moscow State Technical University named after G.I. Nosov 2016;14(3):71-77. (in Russ.).

[10] Baisanov SO, Tolokonnikova VV, Narikbayeva GI, Korsukova IYa, Zhuchkov VI. Thermodynamic assessment of smelting of manganese and chromium ferroalloys based on the analysis of their state diagrams. Izvestiya NAN RK. Seriya «Khimii i tekhnologii» = Izvestia of the National Academy of Sciences of the Republic of Kazakhstan. The series "Chemistry and technology" 2018;5:47-57. https://doi.org/10.32014/2018.2518-1491.7

[11] Baisanov S, Tolokonnikova V, Narikbayeva G, Korsukova I, Mukhambetgaliyev Ye. Mathematical method of phase equilibrium of binary system Cr-Si based on Bjerrum - Guggenheim concept. Metalurgija 2020;59(1):97-100.

Crossref

(cc) creative commons

The problem of optimizing pumping units for oil transportation

[1] Bekibayev T.T., [1*] Ramazanova G.I., [2] Pakhomov M.A.

[1]*Satbayev University, Almaty, Kazakhstan*
[2] *Kutateladze Institute of Thermophysics, Siberian Branch of the Russian Academy of Science, Novosibirsk, Russia*

* Corresponding author email: gaukhar.ri@gmail.com, g.ramazanova@satbayev.university

ABSTRACT

During pipeline transportation of oil through main oil pipelines, the greater part of the energy consumed is spent on the operation of main and booster pumping units at oil pumping stations. In this regard, the determination of the optimal operating modes of pumping units is an urgent problem for energy saving. The article is devoted to the optimization of the operation of pumping units for energy saving of oil pipeline transport. The operation of pumping units is regulated using removable rotors with different diameters of impellers or a frequency-controlled drive. An optimization criterion has been formulated to minimize the operating costs of pumping units. A technique for determining the energy consumption of pumping units with different diameters of impellers and a frequency-controlled drive is presented. An algorithm for finding the optimal operating mode of pumping units is presented, which was built using the definitions of graph theory and dynamic programming.

Keywords: optimization criterion, energy-saving, oil transportation, graph theory, dynamic programming.

Bekibayev Timur Talgatovich	*Master of engineering and technology, head of section. Non-commercial joint-stock company "Satbayev University", Research and Production Laboratory "Energy Modeling", Almaty, the Republic of Kazakhstan. E-mail: timur_bekibaev@mail.ru, https://orcid.org/0000-0001-7030-0015*
Ramazanova Gaukhar Izbasarovna	*Candidate of physical and mathematical sciences, Leading Researcher. Non-commercial joint-stock company "Satbayev University", Research and Production Laboratory "Energy Modeling", Almaty, the Republic of Kazakhstan. E-mail: gaukhar.ri@gmail.com, g.ramazanova@satbayev.university, https://orcid.org/0000-0002-8689-9293*
Pakhomov Maksim Aleksandrovich	*Doctor of Physical and Mathematical Sciences, Professor, Leading Researcher, Kutateladze Institute of Thermophysics, Siberian Branch of the Russian Academy of Science, Novosibirsk, Russia. h-index: 15; Scopus ID: 6602734341. E-mail: pakhomov@ngs.ru*

Introduction

The main consumers of electricity when pumping oil through main oil pipelines are pumping units (PU) at oil pumping stations (OPS). Problems of optimizing operating modes of pumping units are considered in [[1], [2], [3], [4], [5], [6], [7]].

Several oil pumping stations can be located in the oil pipeline section. Regulating the operation of main pumping units (MPU) is controlled by variable frequency drives (VFD) or removable rotors. Such control conditions of MPU in the MOP section lead to difficulties in determining the objective function [8].

Algorithm development for optimizing calculations is the main problem for determining energy-saving pumping modes. In this paper, a general optimality criterion is formulated when controlling MPU with VFD and removable rotors, an algorithm for calculating the energy-saving pumping mode without intermediate heating of oil is developed.

A problem statement

The optimal combination of operating pumps is being sought. At the same time, some pumps can operate with VFD.

The optimization criterion is defined as:

$$\sum_{i=1}^{n}\left(z_i \sum_{j=1}^{m_i} c_{ij} N_{ij}^{PU}(\boldsymbol{k}_{ij}) \right) \rightarrow \min \quad (1)$$

where n is the number of OPS in the section, m_i is the number of pumps in the i-th OPS, z_i is the cost of electricity in the i-th OPS tg/(kW·h); c_{ij} is the

integer variable that takes the value 1, if the pump is in operation, and 0 otherwise; N_{ij}^{PU} is the power consumption of the j-th PU of the i-th OPS (kW); k_{ij} is the ratio of the rotor speed to the nominal speed for the given pump.

The criterion (1) is considered together with the conditions of safe pumping: satisfaction of the setpoint chart; safe operation of pumps; prevention of gravity flow of oil; accounting for pipeline defects.

For any value of k_{ij}, it is true:

$$k_{ij}^{\min} \le k_{ij} \le 1 \qquad (2)$$

where $k_{ij}^{\min}$ is the lower limit of the rotation speed for any pump.

The number of simultaneously operating pumps with VFD is limited by the number of drives p in OPS. The number of pumps with VFD cannot be greater than the number of drives themselves. Therefore, for each i-th OPS, it is necessary to set a limit on the number of simultaneously operating pumps with VFD:

$$\sum_{j=1}^{m_i} c_{ij}[1 - k_{ij}] \le \quad _i \qquad (3)$$

where operator $[\ ]$ means rounding operation to a bigger side.

The pressure drop through a group of pumps ΔP^{gr} is determined by the formula:

$$\Delta \ ^{gr}(Q,k) = \begin{cases} 0, & c_{oper} = 0 \\ \rho g H\left(\dfrac{Q}{c_{oper}}, k\right), & c_{oper} > 0 \end{cases} \qquad (4)$$

where c_{oper} is the number of operating pumps in the group, ρ is the oil density, $H(Q,k)$ is the head dependence on the flow rate for any pump in the group.

Let's build a concrete view for the dependencies $H(Q,k)$ and $P^{PU}(Q,k)$.

To recalculate characteristics of the pump with VFD, the well-known similarity formulas are used [11]:

$$Q^{VFD}/Q = k, \ H^{VFD}/H = k^2, \ N^{VFD}/N = k \quad (5)$$

where Q, H, N and $Q^{VFD}, H^{VFD} \ N^{VFD}$ are the flow rate, head and power of the pump without VFD and with VFD, respectively.

The curves of head and efficiency of pumps can be approximated by polynomials of the third degree [9]:

$$\begin{aligned} H(Q) &= C_0^H + C_1^H Q + C_2^H Q^2 + C_3^H Q, \\ \eta(Q) &= C_0^\eta + C_1^\eta Q + C_2^\eta Q^2 + C_3^\eta Q \end{aligned} \qquad (6)$$

where $C_0^H, C_1^H, C_2^H, C_3^H$ and $C_0^\eta, C_1^\eta, C_2^\eta, C_3^\eta$ are the coefficients of approximation of head and pump efficiency, respectively.

The characteristic of pump head when working with VFD:

$$H(Q,k) = C_0^H k^2 + C_1^H k Q + C_2^H Q + \frac{C_3^H Q^3}{k} \quad (7)$$

The characteristic of pump efficiency when working with VFD can be written in the form [11]:

$$\eta(Q,k) = C_0^\eta + \frac{C_1^\eta Q}{k} + \frac{C_2^\eta Q^2}{k^2} + \frac{C_3^\eta Q^3}{k} \qquad (8)$$

Thus, pump power has the form:

$$N(Q,k) = \frac{C_0^H k^5 Q + C_1^H k^4 Q^2 + C_2^H k^3 Q^3 + C_3^H k^2 Q^4}{C_0^\eta k^3 + C_1^\eta k^2 Q + C_2^\eta k Q^2 + C_3^\eta Q^3} \rho g \quad (9)$$

Dependence (9), the efficiency of the clutch η_m and the efficiency of the electric motor η_{el} uniquely determine the power consumption of the entire pumping unit:

$$\begin{aligned} N^{PU}(Q,k) &= \frac{N(Q,k)}{\eta_m \eta_{el}} \quad \frac{N(Q,k)}{\eta_m} + \\ &+ \frac{1 - \eta_{el\,nom}}{2\eta_{el\,nom}}\left(N_{el\,nom} \quad \frac{N^2(Q,k)}{\eta_m^2 N_{el\,nom}} \right. \end{aligned} \qquad (10)$$

where $N_{el\,nom}$, $\eta_{el\,nom}$ are the nominal values of power and efficiency of the electric motor, $k_3 = N/(\eta_m N_{el\,nom})$ is the load factor of the electric motor.

The pressure balance equation [9] can be written in the form of pressure:

$$P_{init} + \sum_{i=1}^{n} \sum_{j=1}^{m_i^{gr}} \Delta P_{ij}^{gr} = \sum_{i=1}^{n} \Delta P_i^{PR} + \sum_{i=1}^{n} \Delta P_i^{ac} + \Delta P^p + \Delta P_{res} \quad (11)$$

where P_{init} is the initial pressure; m_i^{gr} is the number of pumping groups in OPS; ΔP_{ij}^{gr} is the pressure increase generated by the j-th pump group of the i-th OPS; ΔP_i^{pl} is the pressure loss after the pressure regulator (PR); ΔP_i^{ac} is the pressure loss in the pipeline taking into account hydrostatic pressure drop between the i-th and (i+1)-th OPS at the flow rate Q; ΔP^p is the amount of back pressure created by gate valve at the inlet of the final OPS; P_{res} is the residual pressure.

The values of pressure drops through OPS and pressure losses through the PR are the optimization problem solution.

It is necessary to determine the limitation imposed on the optimization problem solution by pressure at the inlet and outlet of OPS. The pressure at the inlet of the k-th oil pumping station is equal to P_k^{in}, and at the outlet of OPS before the PR is P_k^{out1} and after the PR is P_k^{out2}.

Then, based on (11), we can write:

$$P_k^{in} = P_{init} + \sum_{i=1}^{k-1}\sum_{j=1}^{m_i^{gr}} \Delta P_{ij}^{gr} - \sum_{i=1}^{k-1}\Delta P_i^{PR} - \sum_{i=1}^{k-1}\Delta P_i^{ac} \geq P_k^{in\,min} \quad (12)$$

$$P_k^{out1} = P_k^{in} + \sum_{j=1}^{m_k^{gr}} \Delta P_{kj}^{gr} \leq P_k^{out1\,max}$$

$$(13)$$

$$P_k^{out2} = P_k^{out1} - \Delta P_k^{PR} \leq P_k^{out2\,max}$$

where $P_k^{in\,min}$ is the minimum allowable pressure at the inlet of the k-th OPS, $P_k^{out1\,max}$ and $P_k^{out2\,max}$ are the maximum allowable pressure before and after the PR at the outlet of the k-th OPS.

A necessary and sufficient condition for the forced oil flow in the i-th pipeline section with a saddle point:

$$^{out2} - max\_\Delta P_i^{ac} > 0 \quad (14)$$

Let be $P_*^{def\,max}$ is the maximum allowable pressure in the place of the pipe defect, which does not cause its damage/deformation.

Then the necessary condition for taking into account each j-th defect is as follows:

$$P(X) \leq P_j^{def\,max} \quad (15)$$

Each pump has an operating range with permissible flow rates Q^{min}, Q^{max}, which in the VFD mode depend on the rotor speed:

$$Q^{min}(\mathbf{k}) \leq Q \leq Q^{max}(\mathbf{k}) \quad (16)$$

The condition for the cavitation-free operation of each l-th group of pumps and the k-th OPS has the form:

$$P_{kl}^{in\,gr} = P_k^{in} + \sum_{j=1}^{l-1}\Delta P_{kj}^{gr} \geq P_{kl}^{min\,ingr} \quad (17)$$

In the operation of the pumps, overloading of the electric motor is also not allowed:

$$N^{PU}(Q,\mathbf{k}) \leq k^{over}\ N^{nom} \quad (18)$$

where $k^{over} = 1.1$ is the overload coefficient of the electric motor.

The optimal solution search algorithm

The search algorithm is a nonlinear problem programming, objective function (1) and constraints (2, 3, 12-18) are non-linear functions.

In the optimization theory, the Lagrange method is widely used for nonlinear programming problems. In the considered problem, constraints imposed on variables are inequalities, therefore, to modify the method, the Karush-Kuhn-Tucker conditions must be satisfied [10]. Constraint functions are not continuously differentiable, which contradicts the mandatory conditions of the Lagrange method.

We have proposed an approach based on the ideas of dynamic programming. The search problem for the energy-saving mode can be divided into many overlapping subtasks with finding the optimal substructure. Using the problem solution for n pumps, we can efficiently find solutions for n+1 pumps.

The graph of the state of the operation of PU is built. Each node of the graph contains data on the number of used PU and their parameters, pressure drop in the PR. Graph nodes are connected based on the pressure characteristics of pumps and the rotational speeds of their rotors. The subtask solution transition to the general problem solution is found and the correctness of the approach is proved.

The object of each subtask is the cost dependence function of consumed electricity $S(P)$ from the generated differential pressure of the pump.

Naturally, that $P \geq 0$. In the search for the solution, instead of the continuous function $S(P)$, its discrete version is used. The pressure value is presented discretely with a fairly small step $\varepsilon_p = 0.01$ bar.

The problem solution is stored in the discrete array $Info(P)$, which, for each value P, contains a list of necessary pumps to create this pressure drop. This array has rotational speed, used rotors, as well as pressure loss values after the PR. Array parameters for the particular P are determined by unknowns c_{ij} and $\mathbf{k}_{ij}$ of pumps in condition (1).

The cost function $S(P)$ and the array of solutions $Info(P)$ for the pump without VFD are written as:

$$S(P) = \begin{cases} +\infty, & P \neq P_{pump} \\ zN^{PU}(Q), & P = P_{pump} \end{cases}$$

$$Info(P) = \begin{cases} \varnothing, & P \neq P_{pump} \\ (pump\,number), & P = P_{pump} \end{cases} \quad (19)$$

Where z is the cost of electricity tg/(kW·h), N^{PU} is the consumed power of PU (kW), Q is the flow rate, which passes through the pump (m³/h), P_{pump} is the pressure drop generated by the pump, which is found as:

$$P_{pump} = [\rho g H(Q)]$$

where $[\ ]$ is the rounding to the nearest rational number with a step ε_p.

Similarly, $S(P)$ and $Info(P)$ are defined for the pump with VFD:

$$S(P) = \begin{cases} +\infty, & P \notin [P^{min}, P^{max}] \\ zN^{PU}(Q, \mathbf{k}), & P \in [P^{min}, P^{max}] \end{cases}$$

$$Info(P) = \begin{cases} , & P \notin [P^{min}, P^{max}] \\ (pump\,number) + k, & P \in [P^{min}, P^{max}] \end{cases} \quad (20)$$

where p^{min} and p^{max} are the minimum and maximum pressure drops.

If pumps are operating simultaneously in parallel, then their cost function is defined as:

$$S_r(P) = \begin{cases} +\infty, & P \neq P_{pump} \\ z\sum_{i=1}^{r} N_i^{PU}\left(\dfrac{Q}{r}\right), & P = P_{pump} \end{cases} \quad (21)$$

where P_{pump} is the pressure drop created by pumps operating in parallel.

For pumps operating in parallel in the VFD mode, the function $S_r(P)$ and array $Info_r(P)$ will take the form similar to expressions (21).

In order to take into account the operating area condition of the pump (18), it is necessary to change the cost function according to the following principle:

$$S(P) = \begin{cases} S(P), & Q^{min}(\mathbf{k}) \leq Q \leq Q^{max}(\ ) \\ +\infty, & otherwise \end{cases} \quad (22)$$

Similarly, the cost function is adjusted if it is necessary to take into account the operating condition of the pump motor without overload (20):

$$S(P) = \begin{cases} S(P), & N^{PU}(Q, \mathbf{k}) \leq k^{over} * N^{nom} \\ +\infty, & otherwise \end{cases} \quad (23)$$

Definition 1.

The union of two functions S^A and S^B denotes such the function $S(P)$, that has the value for each P:

$$S(P) = S^A(P) \bigcup S^B(P) \quad \min(S^A(P), S^B(P)) \quad (24)$$

Similarly, the union of two arrays $Info^A$ and $Info^B$ denotes such the array $Info(P)$ that has the value for each P:

$$Info(P) = Info^A(P) \cup Info^B(P) = \\ = \begin{cases} Info^A(P), & S^A(P) \leq S^B(P) \\ Info^B(P), & S^A(P) > S^B(P) \end{cases}$$

If the pump has several replaceable rotors, then its cost function is determined by the expression:

$$S(P) = \bigcup_{i=1}^{n} S^{rotor\,i}(P) \quad (25)$$

where n is the number of replaceable rotors, $S^{rotor\,i}$ is the cost function of the pump, when working with the rotor i.

Similarly, its array of solutions $Info(P)$ is determined.

For each pressure value that a group of parallel operating pumps can create, it is possible to find a combination of pumps at which there will be a minimum of costs. Obviously, the answer and solution to this problem for a group of r pumps will be "unions":

$$S^{gr} = \bigcup S_1 \cup ... \cup \bigcup S_{r_-} \cup S$$
$$Info^{gr} = \bigcup Info_1 \cup ... \cup \bigcup Info_{r_-} \cup Info \qquad (26)$$

where $\bigcup S_i$, $\bigcup Info_i$ are the "unions" of the function $S(P)$ and array $Info(P)$, respectively, for all samples of i pumps from the r group.

Definition 2.

The imposition of the function S^B on the function S^A denotes the function $S(P)$ that has the value (similarly, for $Info(P)$) for each P:

$$S(P) = S^A(P) \leftarrow (S\quad) =$$
$$= \min(S^A(P), S^A(P - P^*) + S^B(P\quad)) \qquad (27)$$

where the variable value P^* at the specific value P is defined as:

$$P^* = \arg\min(S^A(P - P^*) + S\quad(P^*))$$
$$\quad^* \in [0, P] \qquad (28)$$

Definition 3.

Let's call the cost function $S(P)$ optimal for any set of pumps if, for any value of its argument P, it contains the minimum cost that is necessary to create pressures with the value P using some pumps from the required set.

The optimal cost function $S_{in}^{st}(P)$ and its array of solutions $Info_{out}^{st}(P)$ at the outlet from stations will be the "imposition" of cost functions and arrays of solutions of all pump groups available in the station to the optimal function $S_{in}^{st}(P)$ and its array $Info_{out}^{st}(P)$ at the inlet of the station:

$$S_{out}^{st}(P) = S_{in}^{st}(P) \leftarrow (S_1^{gr}) \leftarrow (S^{gr}) \leftarrow ... \leftarrow (S_m^{gr})$$
$$Info_{out}^{st}(P) = Info_{in}^{st}(P) \leftarrow (Info_1^{gr}) \leftarrow \qquad (29)$$
$$\leftarrow (Info_2^{gr}) \leftarrow ... \leftarrow (Info_m^{gr})$$

The limitation on the minimum head at the inlet to the pump or to the group of pumps (18) is taken into account by "imposing" (30) group functions strictly in the order in which groups are located on OPS, as well as in the "imposing" operation by changing the condition (28) for each i-th group for:

$$P^* \in [P - P_i^{\min in\,gr}, P] \qquad (30)$$

If OPS has several pump layouts, then its overall cost function at the outlet of the station is defined as:

$$S_{out}^{st}(P) = \bigcup_{i=1}^{n} S_{out}^{st,\,layout\,i}(P) \qquad (31)$$

Where n is the number of pump layouts at OPS, $S_{out}^{st,\,layout\,i}$ is the cost function at the outlet from OPS in the scheme i.

Similarly, its array of solutions $Info(P)$ is determined.

If the number of VFD is less than the number of pumps at OPS, then the cost function and the array of solutions for OPS will have an additional argument v for pumps operating with VFD. The value v should not exceed the number of drives p on OPS.

Then, to take into account the limitation of the form (3), the "imposition" of the cost function for the groups of pumps has the form (similarly, for $Info^{st}(P, v)$):

$$S^{st}(P, v) = S^{st}(P,\quad) \leftarrow (S^{gr}) =$$
$$= \min(S^{st}(P, v), S^{st}(P - P^*,\quad - N(P^*)) + S^{gr}(P^*)) \qquad (32)$$

where $N(P^*)$ is the number of pumps in a group operating with VFD to create pressure P^*.

The number of operating pumps in a group can be determined from the solution array of the group $Info^{gr}(P^*)$. Whether they operate in the mode with VFD is determined by the criterion $k \neq 1$ for each value $Info^{gr}(P^*)$.

The value of the variable P^* at specific values P and v is defined as:

$$P^* = \arg\min(S^{st}(P - P^*, v - N(P^*)) + S^{gr}(P^*)) \quad (33)$$
$$^* \in [0, P]$$

When "imposing" by formulas (32) and (33) for each v the cost function will retain its own optimality. After "imposing" the cost functions of all pump groups and their arrays of solutions, it is necessary to switch to the form with one pressure argument by the following "combining":

$$S^{st}(P) = \bigcup_{v=0}^{p} S^{st}(P, v) \qquad (34)$$

Definition 4.

By pruning the function $^{old}(P)$ by pressures P^A and P^B $P^A < P^B)$ is the function $S^{new}(\ )$ that has the value for each P:

$$S^{new}(P) \quad CUT(S^{old}(P), P^A, P^B) =$$
$$= \begin{cases} +\infty, & P \notin [P^A, P\ ] \\ S^{old}(P), & P \in [P^A, P^B] \end{cases} \qquad (35)$$

Similarly, for an array of solutions:

$$Info^{new}(P) = CUT(Info^{old}(P), P^A, P^B) =$$
$$= \begin{cases} \text{"no pumps"}, & P \notin [P^A, P^B] \\ Info^{old}(P), & P \in [P^A, P^B] \end{cases}$$

Taking into account that pressure drop in the section between two OPS at the fixed value Q does not depend on pressure at the outlet of the initial OPS, it is possible to determine minimum allowable pressure at the outlet of OPS so that the pressure condition at the inlet to the next station is fulfilled (12). Obviously, the value of such pressure for the k-th OPS should be no less $^{in\min}_{+1} + \Delta P_k^{ac}$, i.e. the pressure condition at the inlet in the station is determined through the condition at the outlet from the previous station.

Taking into account the condition of non-gravity flow (14), the final condition for minimum allowable pressure at the outlet from the station ($P_{out}^{\min,k}$) has the form:

$$P_k^{out2} \geq P_{out}^{\min,k} = \max(P_{k+1}^{in\min} + \Delta P_k^{ac}, \max\_\Delta P_i^{ac}) \quad (36)$$

Taking into account pressure drop in the section and pressure conditions at the points of the pipe defect (16), it is possible to calculate in advance maximum pressure at the outlet of OPS $P^{pipe\max}$, at which conditions (15) will be fulfilled. Then the final condition for maximum allowable pressure at the outlet of OPS (denote $P_{out}^{\max,k}$) has the form:

$$P_k^{out2} \leq P_{out}^{\max,k} \quad \min(P_k^{out2\max}, P_k^{pipe\max}) \quad (37)$$

If you do not take into account the operation of the PR at stations, i.e. $\Delta P^{PR} = 0$, then it is obvious that all pressure conditions are taken into account in functions $S(P)$ and the array $Info(P)$ by the next "pruning" (similarly, for $Info(P)$):

$$S(P) = CUT(S(P), P_{out}^{\min}, P_{out}^{\max}) \qquad (38)$$

If we take into account the possible benefit of the PR in solving the optimal problem, then before "pruning" (35) to take into account the condition (16) for outlet pressure up to the PR, it is necessary to change $S(P)$ and $Info(P)$ as follows:

$$S(P = \begin{cases} S(P'), & S(P) > S(P') \\ S(P), & \text{otherwise} \end{cases}$$
$$Info(P) = \qquad\qquad (39)$$
$$= \begin{cases} Info(P') + \text{"lowering in the PR by"} + (P' - P), & S(P) > S(P') \\ Info(P), & \text{otherwise} \end{cases}$$

where values P' for a specific value P are defined as:

$$P' = \arg\min(S(P))$$
$$P' \in [P, P_k^{out1\max}] \qquad (40)$$

In other words, these operations mean that if higher pressures were obtained at a lower cost, then with the help of the PR with the same costs, lower pressures can be obtained.

Definition 5.

The shift of the function $S^{old}(P)$ by an amount ΔP is the function $S^{new}(\ )$ that has the value for each P:

$$S^{new}(P) = \text{SHIFT}(S^{old}(P), \Delta P) = S^{old}(P - \Delta P) \quad (41)$$

Then the transition to the next station (similarly, for $Info(P)$) has the form:

$$S_{in}^{next\,st}(P) = \text{SHIFT}(S_{out}^{st}(P), P^{ac}) \qquad (42)$$

where the function $S_{out}^{st}(P)$ should be "pruned", $_{in}^{next\,st} P)$ is the cost function at the inlet of the next station.

Above-listed operations must be done for all OPS in the order of their location on the MOP section except for the last OPS. The calculation algorithm has the form:

$k = 1$

For $i = 1$ to m^k calculate $S_i^{gr,k}$ by formulas (21)-(28);

$$S_{out}^{st,k}(P) = S_{in}^{st,k}(P) \leftarrow (S_1^{gr,k}) \leftarrow (S^{gr,k}) \leftarrow$$

$$\leftarrow \cdots \leftarrow (S_{m^k}^{gr,k});$$

Calculation ΔP_k^{ac}

$$S_{out}^{st,k}(P) = CUT(S_{out}^{st,k}(P), P^{\min}, P^{\max});$$ (43)

$$S_{in}^{st,k+1}(P) \quad SHIFT(S_{out}^{st,k}(P), \Delta P_k^{ac});$$

$k = k + 1$.

If, $k \neq n+1$ then go to step 1, otherwise exit the loop.

The function is used as the initial cost function:

$$S_{in}^{st,1}(\ ) = \begin{cases} +\infty, & P \neq P_{init} \\ 0, & P = P_{init} \end{cases}$$ (44)

The initial function $S_{in}^{st,1}(\ )$ is the simplest and contains an obvious zero cost to create static head from the reservoir. This function is optimal because there is no a cheaper option for creating pressure P_{init}. Therefore, the further "imposition" of the cost function of pumps or pump groups to it preserves its optimality.

So, the minimum amount of costs for performance Q will be the value of functions $S_{in}^{st,n+1}(P^{answ})$. The optimal combination of operating pumps and their operating modes will be stored in the cell of the array $Info_{in}^{st,n+1}(P^{answ})$.

In the present algorithm, the presence of VFD is no longer a problem: VFD only expands the domain of definition of the cost function $S(P)$ and does not affect the complexity of this algorithm in any way. In contrast to genetic algorithms, the approach described above makes it possible to obtain guaranteed the most optimal result.

The algorithm for calculating energy consumption was used to carry out thermal-hydraulic calculations and showed its effectiveness in determining the rational operating modes of pumping units [[11], [12], [13]].

Conclusions

The establishment of energy-saving operating modes of pumping units is important for the efficiency of oil transportation through main oil pipelines. A method has been developed for determining the energy consumption of pumping units with different diameters of impellers and a frequency-controlled drive. The algorithm for calculating the methodology is built using graph theory and dynamic programming. The advantage of the proposed algorithm in comparison with the simple enumeration algorithm and the genetic algorithm in determining the optimal operating conditions of pumping units has been proved.

Conflict of interests. On behalf of all authors, the corresponding author states that there is no conflict of interest.

Мұнай тасымалдау үшін сорғы қондырғыларын оңтайландыру проблемасы

[1] Бекібаев Т.Т., [1] Рамазанова Г.І., [2] Пахомов М.А.

[1] Сәтбаев университеті, Алматы, Қазақстан
[2] Кутателадзе атындағы Теплофизика институты, Ресей Ғылым академиясының Сібір бөлімшесі, Новосибирск, Ресей

ТҮЙІНДЕМЕ

Магистралды мұнай құбырлары арқылы мұнайды тасымалдау кезінде тұтынылатын энергияның басым бөлігі мұнай айдау станцияларындағы магистральдық және тірек сорғы қондырғыларының жұмысына жұмсалады. Осыған байланысты мұнай құбырларындағы сорғы қондырғыларының оңтайлы жұмыс режимдерін анықтау энергия үнемдеудің өзекті мәселесі болып табылады. Мақала құбырмен мұнай тасымалдаудың энергиясын үнемдеу үшін сорғы қондырғыларының жұмысын оңтайландыру мәселесіне арналған. Сорғылардың жұмысы доңғалақтарының диаметрі әртүрлі ауыстырылмалы роторлар немесе жиілікпен басқарылатын жетек көмегімен реттеледі. Сорғы қондырғыларын пайдалану шығындарын барынша азайту үшін оңтайландыру критерийі тұжырымдалды. Доңғалақтарының диаметрі әртүрлі және жиілікпен басқарылатын жетекті сорғы қондырғыларының энергия шығынын анықтау әдістемесі ұсынылды. Сорғы қондырғыларының оңтайлы жұмыс режимін іздеу алгоритмі графтар теориясы мен динамикалық бағдарламалау анықтамаларын пайдалана отырып жасалды.

Түйін сөздер: оңтайландыру критериі, энергияны үнемдеу, мұнай тасымалдау, графтар теориясы, динамикалық бағдарламалау.

Авторлар туралы ақпарат:

Бекібаев Тимур Талғатұлы

Техника и технология магистрі, бөлім бастығы, Сәтбаев университеті, «Энергетикадағы модельдеу» ғылыми-өндірістік зертханасы, Алматы қ., Қазақстан Республикасы. Электрондық пошта: timur_bekibaev@mail.ru, https://orcid.org/0000-0001-7030-0015

Рамазанова Гаухар Ізбасарқызы

Физика-математика ғылымдарының кандидаты, жетекші ғылыми қызметкер, Сәтбаев университеті, «Энергетикадағы модельдеу» ғылыми-өндірістік зертханасы, Алматы қ., Қазақстан Республикасы. Электрондық пошта: gaukhar.ri@gmail.com, g.ramazanova@satbayev.university, https://orcid.org/0000-0002-8689-9293

Пахомов Максим Александрович

Физика-математика ғылымдарының докторы, Ресей ғылым академиясының профессоры, жетекші ғылыми қызметкер, С.С. Кутателадзе атындағы Теплофизика институты, Ресей Ғылым академиясының Сібір бөлімшесі, Новосибирск қ., Ресей. h-индекс: 15; Scopus ID: https://www.scopus.com/authid/detail.uri?authorId=6602734341. Электрондық пошта: pakhomov@ngs.ru

Проблема оптимизации насосных агрегатов для транспортировки нефти

[1] Бекибаев Т.Т., [1] Рамазанова Г.И., [2] Пахомов М.А.

[1] *Satbayev University, Алматы, Казахстан*
[2] *Институт теплофизики им. С.С. Кутателадзе, Сибирское отделение РАН, Новосибирск, Россия*

АННОТАЦИЯ

При транспортировке нефти по магистральным нефтепроводам большая часть расходуемой энергии уходит на работу магистральных и подпорных насосоных агрегатов на нефтеперекачивающих станциях. В этой связи определение оптимальных режимов работы насосных агрегатов, эксплуатирующихся на нефтепроводах, является актуальной проблемой для энергосбережения. Статья посвящена оптимизации работы насосных агрегатов для энергосбережения трубопроводного транспорта нефти. Работа насосных агрегатов регулируется с использованием сменных роторов с различными диаметрами рабочих колес или частотно-регулируемым приводом. Сформулирован критерий оптимизации для минимизации эксплуатационных затрат насосных агрегатов. Представлена методика определения энергопотребления насосных агрегатов с различными диаметрами рабочих колес и частотно-регулируемым приводом. Алгоритм поиска оптимального режима работы насосных агрегатов построен с использованием определений теории графов и динамического программирования.

Ключевые слова: критерий оптимизации, энергосбережение, транспортировка нефти, теория графов, динамическое программирование.

Информация об авторах:

Бекибаев Тимур Талгатович

Магистр техники и технологии, руководитель отдела, Некоммерческое акционерное общество «Satbayev University», научно-производственная лаборатория «Моделирование в энергетике», г. Алматы, Республика Казахстан. E-mail: timur_bekibaev@mail.ru, https://orcid.org/0000-0001-7030-0015

Рамазанова Гаухар Избасаровна

Кандидат физ.-мат. наук, ведущий научный сотрудник, Некоммерческое акционерное общество «Satbayev University», научно-производственная лаборатория «Моделирование в энергетике», г. Алматы, Республика Казахстан. E-mail: gaukhar.ri@gmail.com,

	g.ramazanova@satbayev.university, *https://orcid.org/0000-0002-8689-9293*
Пахомов Максим Александрович	*Доктор физико-математических наук, профессор РАН, ведущий научный сотрудник, Институт теплофизики им. С.С. Кутателадзе, Сибирское отделение РАН, г. Новосибирск, Россия. h-индекс: 15; Scopus ID: https://www.scopus.com/authid/detail.uri?authorId=6602734341. E-mail: pakhomov@ngs.ru*

References

1. Jefferson JT. Dynamic Mathematical Programming for Power Cost Optimization. IBM Liquid Pipe Lines Computer Workshop. Chicago, Illinois, 1960.
2. Jefferson JT. Shell Pipe Line calls it Dynamic Programing. The Oil and Gas Journal. 1961;59:102-107.
3. Golosovker VI. Opredeleniye ekonomicheskoy effektivnosti meropriyatiy po uvelicheniyu proizvoditel'nosti nefteprovoda [Determining the economic efficiency of measures to increase the productivity of the oil pipeline]. Transport i khranenie nefti i nefteproduktov = Transport and storage of oil and petroleum products. 1969;11:24-26. (In Russ).
4. Meerov MV, Fridman VG, Shchepetkov LG. Zadacha optimal'nogo upravleniya nefteprovodom [The optimal control problem for oil pipelines]. M.: Moscow Institute of Petrochemical and Gas Industry named after I.M. Gubkina, 1971. 37. (In Russ.).
5. Vyazunov EV, Schepetkov LG, Golosovker VI. Optimal'noye upravleniye nef-teprovodom i otsenka yego effektivnosti [Optimal pipeline management and assessment of its effectiveness]. Neftyanoe khozyaistvo = Oil industry. 1974;5:55-57. (In Russ.).
6. Tumansky AP. Optimizatsiya rezhimov perekachki po magistral'nym truboprovodam s perekachivayushchimi stantsiyami, oborudovannymi chastotno-reguliruyemym privodom [The optimization of pumping modes through main pipelines with pumping stations equipped with a variable-frequency drive]. Transport i khranenie nefti = Transport and storage of oil products. 2005;8:11-14. (In Russ).
7. Akhmadullin KR. Metody rascheta i regulirovaniya rezhimov raboty nasosnykh stantsiy magistral'nykh nefteproduktoprovodov [Methods for calculating and regulating operating modes of pumping stations of main oil product pipelines]. Neftyanoe khozyaistvo = Oil industry. 2005;3:100-103. (In Russ.).
8. Shabanov VA, Bondarenko OV. Tselevyye funktsii i kriterii optimizatsii perekachki nefti po nefteprovodam pri chastotno-reguliruyemom elektroprivode magistral'nykh nasosov [Target functions and optimization criteria for pumping oil through oil pipelines with a frequency-controlled electric drive of main pumps]. Neftegazovoye delo = Oil and Gas Business. 2012;4:10-17. (In Russ.).
9. Tugunov PI, Novoselov VF, Korshak AA, Shammazov AM. Tipovyye raschoty pri proyektirovanii i ekspluatatsii neftebaz i nefteprovodov [Typical calculations when designing and operating oil depots and pipelines]. Ufa, 2002. 658. (In Russ.).
10. Headley J. Nelineynoye i dinamicheskoye programmirovaniye [Nonlinear and dynamic programming]. M.: Mir, 1967. 506. (In Russ.).
11. Bekibayev TT, Zhapbasbayev UK, Ramazanova GI, Bossinov DZh. Oil pipeline hydraulic resistance coefficient identification. Cogent Engineering. 2021. 8 (1950303). https://doi.org/10.1080/23311916.2021.1950303
12. Zhapbasbayev UK, Ramazanova GI, Bossinov DZh, Kenzhaliyev B.K. Flow and heat exchange calculation of waxy oil in the industrial pipeline. Case Stud. Thermal Eng. 2021. 26 (101007). https://doi.org/10.1016/j.csite.2021.101007
13. Bekibayev TT, Zhapbasbayev UK. and et al. Simulation of oil pipeline shutdown and restart modes. Kompleksnoe Ispol'zovanie Mineral'nogo Syr'a = Complex Use of Mineral Resource. 2021;316(1):15-23. https://doi.org/10.31643/2021/6445.02

On the applicability of hardening mechanisms to low-carbon and low-alloy steels

[1*] Jaxymbetova M.A., [1] Kanayev A.T., [2] Akhmedyanov A.U., [2] Kirgizbayeva K.Zh.

[1] *S. Seifullin Kazakh Agro Technical University, Nur-Sultan, Kazakhstan*
[2] *L.N. Gumilyov Eurasian National University, Nur-Sultan, Kazakhstan*

* Corresponding author email: dzhaksymbetov@list.ru

ABSTRACT

On the basis of experimental studies, the approximate contribution of various hardening mechanisms to the yield point of low-carbon and low-alloy steels is estimated. It has been established that for hot-rolled steels (St.3sp and St5ps), solid-solution and grain-boundary hardening (54.0% and 29.0, %) make the greatest contribution to the yield point. The predominant strengthening mechanism of low-alloy steel 10HNDP is solid solution, a high proportion of which in this steel is explained by the resistance to moving dislocations from the side of dissolved atoms of Ni, Cu, P, and Cr in α-Fe. In low-alloy steel 16G2AF, along with these hardening components, the role of precipitation hardening is noticeable (20.0%). It is shown that thermomechanical treatment of steel grade St.5ps leads to an increase in the value of dislocation hardening up to 27.0% due to an increase in the density of dislocations and the retention of most of the dislocations in the rolled stock during accelerated cooling of hot-deformed austenite. It is noted that solid solution hardening with alloying with cheap alloying elements (Mn, Si), as well as dislocation and dispersion hardening through the use of thermomechanical treatment in combination with the addition of carbide and nitride-forming elements V (C, N).

Keywords: hardening mechanisms, yield stress, thermomechanical treatment, accelerated cooling, dislocation density, phase components.

Jaxymbetova Makpal Adlikanovna	*Doctoral student of the Department of Standardization, Metrology and Certification, S. Seifullin Kazakh Agro Technical University, Nur-Sultan, Kazakhstan. E-mail: dzhaksymbetov@list.ru, ORCID ID: 0000-0002-3345-4071*
Kanayev Amangeldy Tokeshovich	*Doctor of Technical sciences, Professor of the Department of Standardization, Metrology and Certification, S. Seifullin Kazakh Agro Technical University, Nur-Sultan, Kazakhstan. E-mail: aman-kanaev2012@yandex.ru, ORCID ID: 0000-0002-2530-038X*
Akhmedyanov Abdulla Ugubayevich	*Candidate of Technical Sciences, Associate Professor of the Department of Standardization, Certification and Metrology, L.N. Gumilyov Eurasian National University, Nur-Sultan, Kazakhstan. E-mail: abdulla261@yandex.ru, ORCID ID: 0000-0002-6156-9335*
Kirgizbayeva Kamilya Zhuzbayevna	*Candidate of Technical Sciences, Associate Professor of the Department of Standardization, Certification and Metrology, L.N. Gumilyov Eurasian National University, Nur-Sultan, Kazakhstan. E-mail: abdulla261@yandex.ru, ORCID ID: 0000-0001-8715-9513*

Information about authors:

Introduction

The structural strength of low-carbon and low-alloy steels with a ferrito-perlite structure can be characterised by the yield strength of steel and the temperature of transition from viscous to fragile. Therefore, knowledge of individual hardening mechanisms allows for an indicative quantitative assessment of the steel yield strength and compare the calculated values of the yield strength with experimental ones. The purpose of this article is to quantify the yield strength of low-carbon and low-alloy steels widely used in construction and engineering in terms of structure parameters after various technological treatments.

Experimental part

Initial data for quantifying steel strength are data on its chemical composition, distribution of elements between phases and quantitative parameters of the structure (grain size, ratio of

phase and structural components, their size and distribution, nature of the dislocation structure, volume fraction and size of dispersed particles). Such a calculation is based on the quantitative ratios established for each strengthening mechanism. Note that the above calculations seem to be indicative semi-quantitative, since there are a number of assumptions and simplifications in the theory of the strengthening mechanisms themselves. In addition, the complex distribution of dislocations in real steels and alloys is difficult to be strictly quantified. However, such calculations are necessary to identify the role of individual strengthening mechanisms in the formation of individual steel properties. The solution of such problems allows you to approach the solution of the main problem of physical and applied materials science - the quantitative relationship between the structure and properties of steels and alloys.

The main characteristics of steels to determine their structural strength are strength and propensity for brittle destruction [1]. Steel strength is estimated by the lower yield strength by the known Hall-Petch ratio, which for stretching conditions is as follows:

$$\sigma_y = \sigma_i + k_h \cdot d^{-1/2} \qquad (1)$$

Where σ_i is the friction voltage of the lattice when dislocations move inside the grains;

k_h - coefficient characterising the contribution of grains to hardening;

d – is the diameter of the grain.

With sufficient accuracy, this ratio is applicable to ferrite steels with grain size from 0.3 to 400 µm; it follows that the lower yield strength of the material increases with the decrease in grain size [2]. The tendency of steel to fragile destruction is assessed by the temperature of transition from viscous to fragile, which is defined as the ratio of viscous destruction area to the initial design section. The lower the transition temperature from

viscous to fragile, the more reliable the material is, so they tend to use a material whose transition temperature is lower than the operating temperature [3].

It is believed that the contribution of certain hardening factors to the total strengthening additive σi in the Hall-Petch strengthening can be represented as a sum:

$$\sigma_i = \sigma_o + \sigma_{S.S} + \sigma_p + \sigma_d + \sigma_{p.h} \qquad (2)$$

The lower limit of steel yield followed from equations (1) and (2) is characterized by the lattice friction stress- α-Fe σ_o, solid solution strengthening $\Delta\sigma_{S.S}$, hardening due to pearlite formation σ_p, strain hardening σ_d, dispersion hardening $\sigma_{p.h}$ and strengthening due to grain boundaries $\sigma_{gb} \cdot d^{-1/2}$. The share of the contribution of individual hardening factors to the total lower yield stress of steel is not the same and depends on the type of alloying elements and the degree of alloying, its presence and dispersion of the hardening phases, the use of heat treatment, and other reasons.

This paper proposes an analysis of the effectiveness of various mechanisms of hardening of low-carbon and low-alloy steels of grades St3sp, St5ps, 10KhNDP, 16G2AF. They are used in construction and differ not only in chemical composition, but also in the applied heat treatment. The magnitude of the individual hardening factors, as well as their contribution to the total lower yield stress of these steels, are determined by the well-known empirical formulas of Table 1 [[3], [4]]. The coefficients required for the calculation are taken from these literature sources. The values of the lower yield stress of the studied steels calculated in this way were compared with the data according to GOST-380, GOST 19282, GOST 5781, GOST 10884.

Table 1 - Hardening coefficients and calculation formulas for quantitative evaluation

№	Hardening factors	Calculation formula of hardening
1	Lattice friction stress α-Fe	$\sigma_o = 2 \cdot G \cdot 10^{-4}$
2	Solid solution alloying	$\Delta\sigma_{ss} = \sum_{i=1}^{n} k_1 \cdot c_1$
3	Hardening due to the formation of perlite	$\Delta\sigma_p = 2{,}4\% \cdot \Pi$
4	Deformation hardening	$\Delta\sigma_d = 0{,}5 \cdot G \cdot b \cdot \rho^{1/2}$
5	Dispersion hardening	$\Delta\sigma_{p.h} = (9{,}8 \cdot 10)/\lambda \cdot ln(2\lambda)$
6	Intergranular (substructural) hardening	$\Delta\sigma_{gb} = k_h \cdot d^{-1/2}$ $\Delta\sigma = k_s \cdot I^{-m}$

Determination of structural parameters (perlite content in steel, diameter of ferrite grains, size and volume fraction of carbonitride phase, etc.) for quantitative assessment of the lower yield limit was carried out by quantitative metallography methods on the NeoPhot 21 research microscope and the UEMV-100V electron microscope. The average length of a straight section crossing the grain in the microgrind plane was used as the diameter of ferrite (d) grain. The volume fraction of dispersed particles (1) and their diameter (D) in low-alloy steel 16G2AF were determined by electron microscopy, and the interparticle distance (λ) was determined by a known ratio:

$$\lambda = D \cdot (P/6f)^{1/2}$$

The proportion of the perlite component is determined by the Rosiwal method. According to it, the area of the structural component is calculated by the lengths of the straight section falling on each of the structural components in accordance with the evaluation criterion. Strengthening of thermomechanically hardened steels St.5ps is determined by X-ray structural analysis by the shape of diffraction lines. The density of dislocations is quantified by translucent electron microscopy of thin foils.

Discussion of the results

The lattice friction stress - α-Fe (Peierls-Nabaro stress) is estimated by the formula:

$$\sigma_o = 2 \cdot 10^{-4} \cdot G$$

где G – iron shear modulus (G = 84000 Mpa).

However, this estimate depends largely on the content of impurities in the metal [3]. For high purity iron [<10^{-7} (C+N)], the experimental values obtained (σ_o=18-21 МПа) almost coincide with the theoretically calculated (σ_o = 17M Па). α-Fe-based steels take the value of σ_o = 30 MPa in calculations.

Other additions of hardenings (Δσ$_{s. s}$, σ$_p$, σ$_d$, σ$_{p.h}$, σ$_{gb}$) taking into account known assumptions, quantified for the steels under study, are given in Table 1 [[3], [4]]. For the convenience of comparing and analysing the effectiveness of various hardening mechanisms, the results of calculations are presented in the form of pie and column charts, histograms (Fig. 1-5). In carbon steels St3sp, St5ps (hot-rolled state), the main components of quenching are solid-solid and grain-boundary hardening, which account for St3sp steel 54% and 29%, respectively (Fig. 1). They are equal in absolute value: 140.5 MPa and 89.9 MPa.

Table 2 - Initial data for the quantitative assessment of the lower yield strength of the studied steels

№	Characteristics of steel	Steel grade				
		St3sp	St5sp (hot rolled)	St5sp (heat-treated)	16G2AF	10KHNDP
1	The content of alloying elements in a-Fe,%					
	Mn	0.52	0.65	0.65	1.5	0.45
	Si	0.21	0.11	0.11	0.45	0.27
	P	0.04	0.04	0.04	0.035	0.095
	V	-	-	-	0.11	-
	Ni	-	-	-	-	0.45
	Cr	-	-	-	-	0,65
	Cu	-	-	-	-	0.40
	(C+N)	0.015	0.015	0.015	0.015	0.015
2	Hardening phase	-	-	-	V(CN)	-
3	Perlite fraction, %	22	35	26	17	14.3
4	Grain size, d мм	0.056	0.051	0.033	0.014	0.028
5	Volume fraction of dispersed particles (f), %	-	-	-	0.096	-
6	Size of dispersed particles (D) нм	-	-	-	30	-
7	Interparticle distance (X) нм	-	-	-	765	-
8	Dislocation density (ρ), см$^{-2}$	10^3	10^8	10^{10}	10^8	10^8

Note: Experimental determination of dislocation density and volume fraction of phase components is a difficult task, so the data are taken from reliable literary sources.
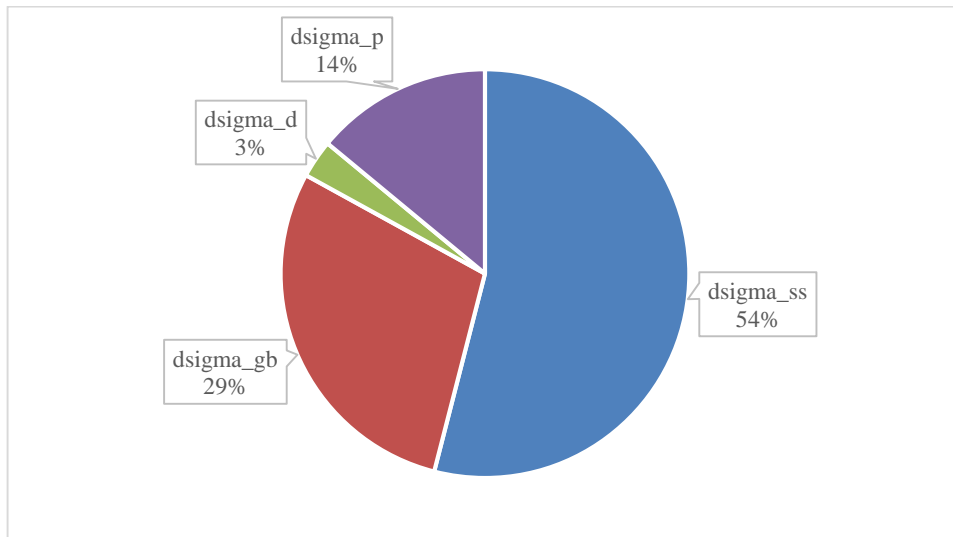
Figure 1 - Pie chart of hardening components for St3sp
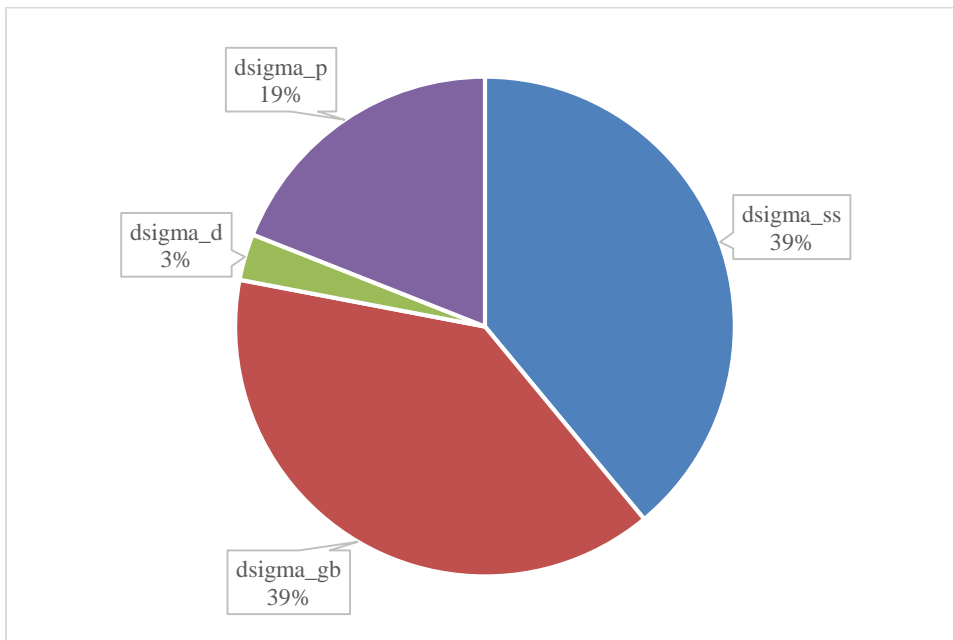
Figure 2 - Pie chart of St5ps hardening components (hot-rolled)
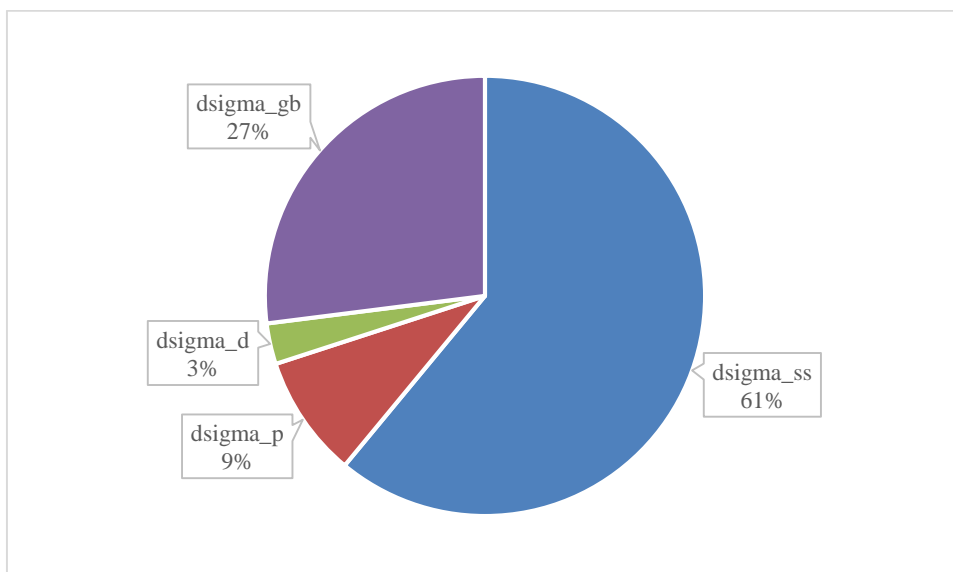
Figure 3 - Pie chart of the distribution of hardening components for 10KHNDP
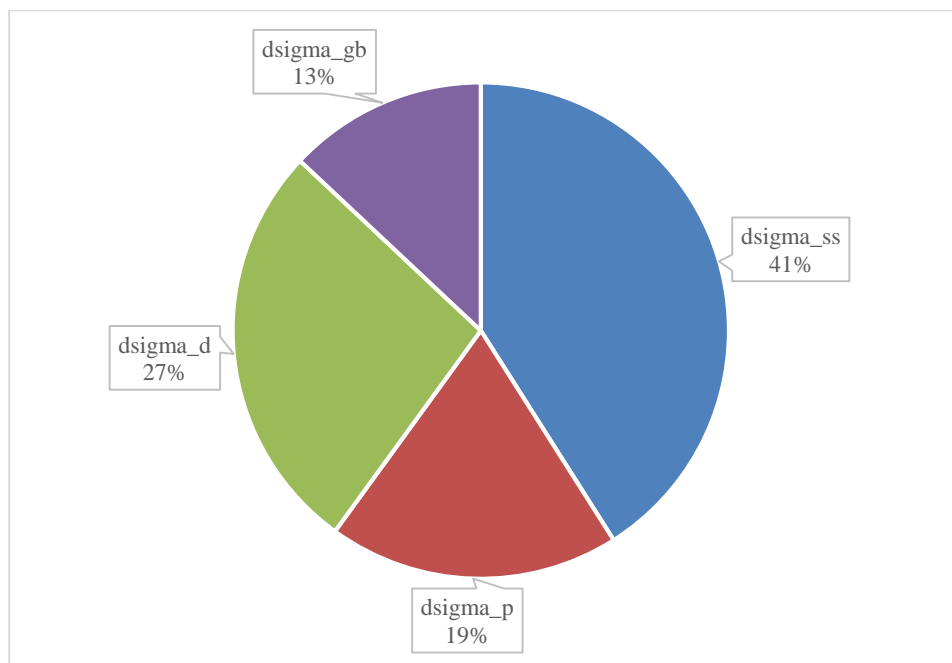
Figure 4 - Pie chart of St5ps hardening components (heat-strengthened)
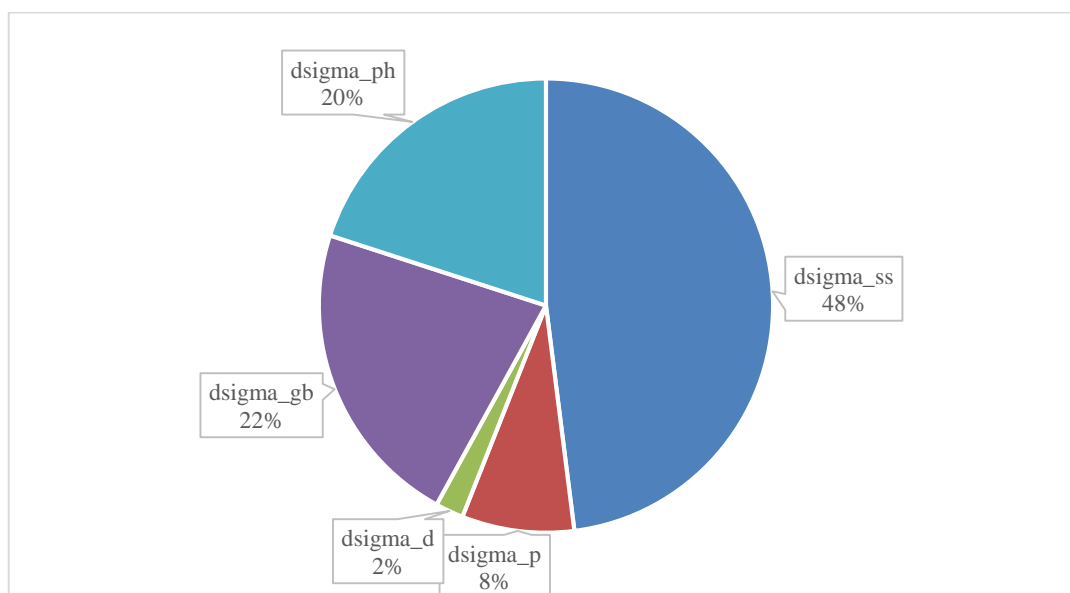
Figure 5 - Pie chart of hardening components for 16G2AF steel

When St5ps steel is subjected to thermomechanical treatment, deformation (location) hardening makes a significant contribution to the overall hardening. If the share of deformation hardening of St5ps steel cooled in calm air from the end temperature of rolling 1050 °C (hot-rolled state) is 3% in this steel, then in thermomechanically treated steel according to the intermittent hardening scheme followed by high-temperature mode (in a thermally hardened state), the proportion of deformation hardening increases to 27%, $\Delta\sigma d$ = 104 MPa (absolute value). This is due to the fact that during thermomechanical processing, recrystallisation processes are suppressed by sharp cooling and therefore a significant part of the dislocations arising from hot rolling of austenite are recorded.

Thus, the dislocation structure of hot-deformed austenite is inherited by the formed martensite in the process of phase austenitic-martensitic transformation [5].

The formation of martensite crystals is achieved simultaneously with the grinding of austenite grain during thermomechanical processing.

The predominant mechanism of hardening low-alloy steel 10CNP is solid solution (Fig. 3). The high proportion of solid-solid hardening in 10CNP steel is due to the resistance of moving dislocations on the

part of dissolved atoms Ni, Cu, P and Cr in α-Fe, provided that the hardening of the solid solution is caused by a difference in atomic diameters in the lattice, alloying element and their elastic modules. Ferrite hardening coefficients of these elements:

$$K_{Ni}^{F} = 30; \; K_{Cu}^{F} = 40; \; K_{P}^{F} = 690; \; K_{Cr}^{F} = 30.$$

Indicating the effectiveness of this hardening mechanism and its applicability, it should be emphasised that there is probably some optimal degree of alloying of α-Fe, since saturation of α-Fe with substitution atoms causes only dangerous elastic deformation of the lattice and reduction of the impact toughness of the alloy [6].

In low-alloy steel 16G2AF, the role of dispersion hardening is noticeable, equal to 20% (Figure 5), Δ σp.h = 94.0 MPa. From Table 2, this steel forms a carbonitride phase V(C, N), which strengthens ferrite by the Orovan mechanism, will form dispersed carbonitride. It is assumed that the carbonitride phase V(C, N) is incoherent with the lattice (α-Fe) and, as a result, the dislocations envelope non-coherent discharges V(C, N).

However, there are statements [[7], [8]] believe that in low-alloy steels small carbonitride particles released directly from the lattice may be coherently linked to it [9].

The influence of disperse phases on grain size is reflected in the efficiency and prospects of dispersion hardening [10]. Table 2 shows that a smaller grain d=0.014 mm is formed in 16G2AF steel, in the structure of which there is a carbonitride phase V(C, N), which has an embryo effect in the formation of new austenite grains during the transition through critical points Ac1 and Ac3 [11]. In addition, the carbonitride phase inhibits the growth of austenite grain when further heated to the dissolution temperature of these phases in austenite. Undissolved carbides and nitrides, as well as those released from austenite before the beginning of γ→α transformation, serve as embryo centres for the formation of new ferrite grains [12]. All this leads to a noticeable grinding of ferrite grain in low-alloy steels with dispersed strengthening phases. Thus, dispersed particles of the carbonitride phase V (C, N) in steel cause additional grain boundary strengthening [13]. For the first time, this feature of hardening of carbonitride phases by dispersed particles is specified in article [14].

Ferrite is the main phase and structural component in low-carbon and low-alloy steels. Its share in these steels reaches 90÷95% [15]. When applying the load, deformation begins to manifest itself in ferrite, this is due to the fact that perlite is a "barrier" for such deformation. A certain contribution to the overall hardening (in the yield strength) is made by hardening from pearlite components [16]. From the above figures 1-4 it can be seen that the share of hardening from perlite formation is about 10-20%, according to the absolute estimate of Δσp = 75MPa for hot-rolled steels St3sp and St5ps [17].

Comparison of the calculated values of the steel yield strength with its value in the relevant GOSTs shows a satisfactory difference: for 16G2AF steel after normalisation, this difference is 17.8% (GOST 19282) and for St.5ps. (hot-rolled state) the difference is 12.0% (GOST 5781). After VTMO, the difference between the calculated value of the yield strength and the value according to GOST 10884 is 13.4%. These data indicate the applicability of quantification of the steel yield strength by the parameters of the formed structure after certain treatments and provide reliable information on existing hardening mechanisms [18].

It should be noted that non-metallic inclusions can affect the mechanical properties of steels [19]. However, their volume fraction in the studied steels does not exceed 0.1%, they do not have a strengthening effect and, therefore, in this work the behaviour of non-metallic inclusions was not taken into account [20].

Conclusion

The contribution of different hardening mechanisms to reducing the yield strength of low-carbon and low-alloy steels varies. For hot-rolled steels, the greatest contribution is made by solid-soluble and intergrain hardening (54% and 29% St3sp, 61% and 27% 10CNP), and 16G2AF steel, along with these hardening components, has a noticeable role of dispersion hardening (22%).

Thermomechanical treatment of St5ps leads to an increase in the value of dislocation hardening to 27% due to an increase in the density of dislocations and the preservation of most of the dislocation with accelerated cooling of hot-deformed austenite.

As effective and promising ways to increase the strength of low-alloy steels, it is necessary to consider solid-solution hardening with alloying with cheap alloying elements (Mn, Si), as well as dislocation and dispersion hardening by applying thermomechanical processing in combination with micro-alloying additives of carbide and nitride-

forming elements (V, A). A comparison of the calculated values of the yield strength of steel with its value in the corresponding GOST-ah shows a satisfactory difference, which indicates the applicability of a quantitative assessment of the yield strength of steel according to the parameters of the formed structure after certain treatments and provides reliable information about the existing hardening mechanisms.

Analysis of the data of quantitative assessment of the yield strength of carbon and low-alloy steels by structure parameters shows that the main mechanisms of their hardening are solid-solution hardening by alloying with relatively cheap alloying elements (Mn, Si), as well as dislocation and dispersion hardening using hardening heat treatment and micro-alloying of steel with carbide and nitride-forming elements V (C, N).

Conflict of interests. On behalf of all authors, the correspondent author declares that there is no conflict of interests.

Көміртегі аз және легирленген болатқа қатаю механизмдерінің қолданылуы

[1*] Джаксымбетова М.А., [1] Канаев А.Т., [2] Ахмедьянов А.У., [2] Киргизбаева К.Ж.

[1] *С. Сейфуллин атындағы Қазақ Агротехникалық Университеті, Нур-Султан, Қазақстан*
[2] *Л.Н Гумилев атындағы Еуразия Ұлттық Университеті, Нур-Султан, Қазақстан*

ТҮЙІНДЕМЕ

Эксперименттік зерттеулер негізінде әр түрлі қатаю механизмдерінің көміртегі аз және легирленген болаттардың түсу нүктесіне шамамен үлесі бағаланады. Ыстық илектелген болаттар үшін (Ст3сп және Ст5пс) қатты ерітінді мен дән шекарасының беріктігі (54,0% және 29,0, %) шығыс нүктесіне үлкен үлес қосатыны анықталды. 10ХНДП аз легирленген болаттың басым күшейту механизмі-бұл қатты ерітінді, оның болаттағы үлесі α-Fe-де Ni, Cu, P және Cr атомдарының еріген жылжымалы дислокациясына төзімділігімен түсіндіріледі. Төмен легирленген 16Г2АФ болатта осы қатайтатын компоненттермен бірге жауын-шашынның қатаюының рөлі байқалады (20,0%). Ст5пс болат сыныбының термомеханикалық өңдеуі дислокация тығыздығының жоғарылауы мен дислокацияның көп бөлігін прокат өнімдерінде ұстау есебінен дислокацияның қатаю мәнінің 27,0% дейін өсуіне әкелетіні көрсетілген ыстық деформацияланған аустенит. Арзан легирлеуші элементтермен (Mn, Si) легирлеумен қатты ерітіндінің қатаюы, сондай-ақ V (C, N) карбиді мен нитрид түзуші элементтерді қосумен термомеханикалық өңдеуді қолдану арқылы дислокация мен дисперсияның қатаюы байқалады.

Түйін сөздер: қатаю механизмдері, түсу кернеуі, термомеханикалық өңдеу, тездетілген салқындату, дислокация тығыздығы, фазалық компоненттер.

Авторлар туралы ақпарат:

Джаксымбетова Макпал Адликановна	*«Стандарттау, метрология және сертификаттау» кафедрасының докторанты, С.Сейфуллин атындағы Қазақ агротехникалық университеті, Нұр-Сұлтан, Қазақстан. E-mai: dzhaksymbetov@list.ru, ORCID ID: 0000-0002-3345-4071*
Канаев Амангельды Токешович	*Техника ғылымдарының докторы, «Стандарттау, метрология және сертификаттау» кафедрасының профессоры, С.Сейфуллин атындағы Қазақ агротехникалық университеті, Нұр-Сұлтан, Қазақстан. E-mail: aman-kanaev2012@yandex.ru, ORCID ID: 0000-0002-2530-038X*
Ахмедьянов Абдулла Угубаевич	*Техника ғылымдарының кандидаты, «Стандарттау, сертикаттау және метрология» кафедрасыны доценті, Л.Н. Гумилев атындағы Еуразия Ұлттық Университеті, Нұр-Сұлтан, Қазақстан. E-mail: abdulla261@yandex.ru, ORCID ID: 0000-0002-6156-9335*
Киргизбаева Камиля Жузбаевна	*Техника ғылымдарының кандидаты, «Стандарттау, сертикаттау және метрология» кафедрасыны доценті, Л.Н. Гумилев атындағы Еуразия Ұлттық Университеті, Нұр-Сұлтан, Қазақстан. E-mail: abdulla261@yandex.ru, ORCID ID: 0000-0001-8715-9513*

О применимости механизмов упрочнения к малоуглеродистым и низколегированным сталям

[1*] Джаксымбетова М. А., [1] Канаев А. Т., [2] Ахмедьянов А. У., [2] Киргизбаева К.Ж.

[1] Казахский агротехнический университет имени С.Сейфуллина, Нур-Султан, Казахстан
[2] Евразийский национальный университет имени Л.Н.Гумилева, Нур-Султан, Казахстан

АННОТАЦИЯ

На основе экспериментальных исследований оценен ориентировочный вклад различных механизмов упрочнения в предел текучести малоуглеродистых и низколегированных сталей. Установлено, что для горячекатаных сталей (Ст.3 сп и Ст5пс) наибольший вклад в предел текучести дают твердо-растворное и зерно-граничное упрочнения (54,0% и 29,0, %). Преобладающим механизмом упрочнения низколегированной стали 10ХНДП является твердорастворный, высокая доля которого в этой стали объясняется сопротивлением движущимся дислокациям со стороны растворенных атомов Ni, Cu, P и Cr в α-Fe. В низколегированной стали 16Г2АФ наряду с этими слагаемыми упрочнения заметна роль дисперсионного упрочнения (20,0%). Показано, что термомеханическая обработка стали марки Ст.5пс приводит к росту величины дислокационного упрочнения до 27,0 % за счет роста плотности дислокаций и сохранения большей части дислокаций в прокате при ускоренном охлаждении горячедеформированного аустенита. Отмечено, что в качестве эффективных и перспективных способов повышения прочности низколегированных сталей является твердорастворное упрочнение с легированием дешевыми легирующими элементами (Mn, Si), а также дислокационное и дисперсионное упрочнение путем применения термомеханической обработки в сочетании с добавками карбидо- и нитридообразующих элементов V (C, N).

Ключевые слова: механизмы упрочнения, предел текучести, термомеханическая обработка, ускоренное охлаждение, плотность дислокаций, фазовые составляющие.

Информация об авторах:

Джаксымбетова Макпал Адликановна	*Докторант кафедры «Стандартизация, метрология и сертификация», Казахский агротехнический университет имени С.Сейфуллина, Нур-Султан, Казахстан. E-mail: dzhaksymbetov@list.ru, ORCID ID: 0000-0002-3345-4071*
Канаев Амангельды Токешович	*Доктор технических наук, профессор кафедры «Стандартизация, метрология и сертификация», Казахский агротехнический университет имени С.Сейфуллина, Нур-Султан, Казахстан. E-mail: aman-kanaev2012@yandex.ru, ORCID ID: 0000-0002-2530-038X*
Ахмедьянов Абдулла Угубаевич	*Кандидат технических наук, доцент кафедры «Стандартизация, сертификация и метрология», Евразийский национальный университет имени Л.Н.Гумилева, Нур-Султан, Казахстан. E-mail: abdulla261@yandex.ru, ORCID ID: 0000-0002-6156-9335*
Киргизбаева Камиля Жузбаевна	*Кандидат технических наук, доцент кафедры «Стандартизация, сертификация и метрология», Евразийский национальный университет имени Л.Н.Гумилева, Нур-Султан, Казахстан. E-mail: abdulla261@yandex.ru, ORCID ID: 0000-0001-8715-9513*

References

[1] Pikering FB. Fizicheskoe metallovedenie I razrabotka stalei [Physical metallurgy and steel development]. Moscow: Metallurgiya. 1992;83. (in Russ.).
[2] Tylckin MA, Bolshakov V., Odesscky PD. Strycture and Properties of Building Steel. Moscow: Metallurgiya. 1993;286.
[3] Tushinskiy LI, Mochalina NS, Plokhov AV, Kuzmin NG. Svoistva stali posle reguliruemogo termoplasticheskogo uprochneniya pri formirovanii struktury na makro-, mexo- I nanourovnyakh [Properties of steel after controlled thermoplastic hardening during structure formation at macro-, meso- and nanolevels]. Izvestiya vysshikh uchebnykh zavedeniy. Chernaya metallurgiya = Proceedings of higher educational institutions. Ferrous metallurgy. 2010;4:37-40. (in Russ.).
[4] Kanayev AT. Povyshenie kachestva sortovogo prokata sovmesshennoi deformatsionno – termicheskoi obrabotkoi [Improving the quality of long products by combined degormation – heat treatment]. Astana: Izdatelstvo Arman-TV. 2009;180. (in Russ.).
[5] Khirsh P. Raspredelenie dislokatsiy I mekhanizm uprochneniya metallov [Distribution of dislokations and the mechanism of hardening of metals]. Moscow: Metallurgiya. 1987;194. (in Russ.).
[6] Tushinskiy L.I. Problemy sovremennogo materialovedeniya XXI veka [Problems of modern materials science of the XXI centery]. Fundamentalnye I prikladnye problem chernoi metallurgii. Sbornik nauchnykh trudov = Fundamental and applied problems of ferrous metallurgy. Collection of scientific papers. 2004;7:23-49. (in Russ.).
[7] Sidorenko OG, Fedorova IP, Sukhiv AP et al. Formirovanie struktury armaturnogo prokata, termicheski uprochnennogo sposobom prervannoi I preryvistoi zakalki [Formation of the structure of reinforcing bars, thermally hardened by interrupted and intermittent hardening]. Stal = Steel. 2012;1:61-64. (in Russ.).

[8]   Goldshtein MI, Litvinov VS, Bronfin BM. Metal-physika of high-strength allpys. Moscow: Metallurgiya. 1986;312.

[9]   Grachev SV, Goldshtein MI, Veksler UV. Spetsialnye stali (Special steels). Moscow: Metallurgiya. 1995;407.

[10] Rybin VV. Formirovanie struktury I svoistv nizkouglerodistoy stali pri retmomekhanicheskoy obrabotke s uskorennym okhlazhdeniem [Formation of the structure and properties of low-carbon and low-alloy steel during thermomechanical processing with accelerated cooling]. Voprosy metallovedeniya = Metallurgy issues. 2007;4:329-340. (in Russ.).

[11] Kamenetskaya DS, Piletskaya IB, Shiryayev VI. Zhelezo vysokoy stepeni chistoty [High purity iron]. Moscow: Metallurgiya. 1988;248. (in Russ.).

[12] Bolshakov VI, Starodubov KF, Tylkin MA. Termicheskaya obrabotka stali povyshennoy prochnosti [Heat treatment of high strength steel]. Moscow: Metallurgiya. 1977;200. (in Russ.).

[13] Tushinskiy LI. Strukturnaya teoriya konstruktivnoy prochnosti materialov [Struktural theory of structural strength of materials]. Novosibirsk: NGTU. 2004;400. (in Russ.).

[14] Bernshtein ML, Zaimovskiy VA, Kaputkina LM. Termomekhanicheskaya obrabotka stali [Thermomechanical treatment of steel]. Moscow: Metallurgiya. 1993;479. (in Russ.).

[15] Panin VYe, Dudarev YeF, Bushnev LS. Struktura I mekhanicheskie svoistva tverdykh rastvorov zamesheniya [Strukture and mechanical properties of substitutional solid solutions]. Moscow: Metallurgiya. 1991;206. (in Russ.).

[16] Martin J. Mikromekhanizmy dispersionnogo tverdeniya splavov [Mikromechnisms of precipitation hardening of alloys]. Moscow: Metallurgiya. 1983;168. (in Russ.).

[17] Kelli A, Niklson R. Dispersionnoe tverdenie [Dispersion hardening]. Moscow: Metallurgiya. 1966;300. (in Russ.).

[18] Blanter MYe. Teoriya termicheskoy obrabotki [Heat treatment theory]. Moscow: Metallurgiya. 1984;327. (in Russ.).

[19] Novikov II. Teoriya termicheskoy obrabotki metallov [Theory of heat treatment of metals]. Moscow: Metallurgiya. 1986;479. (in Russ.).

[20] Kelli A. Vysokoprochnye materialy [High strength materials]. Moscow: Mir. 1976;262. (in Russ.).

Surface-strength approach for concrete monitoring using sensors and shock-pulse method

[1,2] Utepov Ye.B., [3] Aniskin A., [2] Lukpanov R.E., [1,2] Tulebekova A.S., [1,2*] Zharassov Sh.Zh.

[1] CSI Research & Lab, LLP, Nur-Sultan, Kazakhstan
[2] L.N. Gumilyov Eurasian National University, Nur-Sultan, Kazakhstan
[3] University North, Varaždin, Croatia

Corresponding author email: zhshzh95@gmail.com

ABSTRACT

There are many methods used for temperature-strength control of reinforced concrete structures globally. Their majority is associated with the significant challenges of being time-consuming, costly and prone to errors. Therefore, this study investigated the potential applicability of the surface-strength approach of specimens using non-destructive testing methods to derive temperature-strength relationships as an alternative approach to the currently widely used methods. The studies were carried out by comparing the surface strength of small laboratory specimens (SS) and large specimens (LS), imitating building structures, obtained by the shock-pulse method and the strength obtained by the destructive method; and the obtained calibration dependencies were adapted to the results of specimens' thermal control. The temperature-strength dependence was corrected by comparing the strength and temperature parameters of SS and LS. The obtained nomograms make it possible to correct changes in the temperature regime of hydration of structures curing in real climatic conditions. The final adaptation of the temperature-strength dependence to the real erected structures showed a significant potential of this method in the construction industry. The difference between the actual strength of the drilled cores and the predicted strength of concrete at 28 days was only 1.02%.

Keywords: Concrete maturity, surface strength, shock-pulse method, operational control, sensor.

Information about authors:

Utepov Yelbek Bakhitovich	*PhD, Acting Professor of the Department of Structural Engineering, L.N. Gumilyov Eurasian National University, Nur-Sultan, Kazakhstan. ORCID ID: 0000-0001-6723-175X, Email: utepov-elbek@mail.ru*
Aniskin Alexey	*C.t.s., Assistant Professor of the Department of Civil Engineering, University North, Varaždin, Croatia. Email: aaniskin@unin.hr*
Lukpanov Rauan Ermagambetovich	*PhD, Professor, Director of the Research and Production center "ENU LAB", L.N. Gumilyov Eurasian National University, Nur-Sultan, Kazakhstan. ORCID ID: 0000-0003-0085-9934, Email:rauan_1982@list.ru*
Tulebekova Assel Serikovna	*PhD, Associate Professor of the Department of Structural Engineering, L.N. Gumilyov Eurasian National University, Nur-Sultan, Kazakhstan. ORCID ID: 0000-0001-8553-3081, Email: krasavka5@mail.ru*
Zharassov Shyngys Zharassovich	*PhD. Student, Department of Structural Engineering, L.N. Gumilyov Eurasian National University, Nur-Sultan, Kazakhstan. ORCID ID: 0000-0002-0468-8362, E-mail: zhshzh95@gmail.com*

Introduction

The concrete strength is the main characteristic that establishes the ability of a concrete or reinforced concrete structure (hereinafter – RCS) to bear the design loads [[1], [2], [3], [4], [5]]. Among the non-destructive methods of concrete strength control in the CIS countries, the most widespread is the shock-pulse method, implemented by a special device IPS MG4 [[6], [7], [8], [9]].

In contrast to the destruction of standard specimens [[10], [11], [12], [13], [14]] is faster, less labour-intensive, and relatively inexpensive. In contrast to CIS countries, these methods are regulated by state standards of several countries: the USA [15], Canada [16], the Netherlands [17], Germany [18], South America [19], Russia [[20], [21], [22], [23]]. According to these standards' requirements, concrete strength estimates can be performed according to the following basic

methods: temperature graphs, concrete maturity, and analytical functions. Standards [[15], [16], [18], [24]] specify that there are four steps in the use of the method of calculating the current strength of concrete by its maturity:

i. Establishing the maturity-strength relationship in the laboratory;

ii. Embedding maturity sensors inside the formwork at the construction site;

iii. Sensor reading of concrete maturity at the construction site;

iv. Data analysis.

The method for concrete strength estimation by maturity is based on the "maturity index" concept. The maturity index is calculated using one of two measures: the temperature-time factor (TTF) or an equivalent age at 20 °C; due to the complexity of the calculation, the equivalent age is used infrequently compared to the TTF. The maturity method called "Weighted Maturity" [17] takes into account the "C" parameter specific to cement and is used depending on cement strength, although it also allows the use of additives. Previous studies have mainly focused on modifying maturity methods in the data analysis phase. This study investigates the potential applicability of the surface-strength approach of specimens using non-destructive testing methods to derive temperature-strength relationships. The general objective of this study is to express the maturity function based on the relationship between the curing temperature, time, and the surface strength of concrete [25]. In the future, this relationship can be used for prompt strength control using temperature sensors embedded in the concrete body [[2], [24], [26], [27], [28], [29]].

Experimental technique

The studies were conducted in two stages: at the first stage, the temperature-strength dependence of small cylindrical specimens (hereinafter – SS) was investigated; at the second stage, the same studies were conducted for large specimens (hereinafter – LS). The comparison of the results of studies of SS and LS shows the acceptability of strength control of RCS by measuring the thermal regime in the process of hydration. The important indicator of the study is the estimation of obtained temperature-strength dependence of SS adapted for real structures. Therefore, LS of imitating real RCS were used in the studies. The studies were carried out in the following sequence.

Stage 1 – Study of the SS (Figure 1a):

i.   Preparation of 30 cylindrical SS with a height and diameter of 15 cm;

ii.   Determination of the surface strength of SSs by the non-destructive shock-pulse method of control [[18], [19]], with measurements every 24 hours until the 28-day of curing of the specimens.

iii.   Determination of the cylindrical strength of SS by destructive compression method [20] at curing ages of 1, 3, 7, 14, 28 days (six SSs for each age);

iv.   Plotting the calibration dependence between the surface and cylindrical strength;

v.   Measurement of concrete curing temperature in two SS for 28 days with 0.5-hour interval;

vi.   Determination of the temperature-strength (surface) dependence according to ASTM [12].

Stage 2 – Study of the LS (Figure 1b):

i.   Preparation of two LSs of cubic form with the size of 50x50x50 cm;

ii.   Measurement of concrete curing temperature in two LS for 28 days with 0.5-hour interval;

iii.   Determination of the temperature-strength (surface) dependence according to ASTM [12];

iv.   Determination of the functional dependencies of SS and LS enabling correction of temperature-strength (surface) dependence;

v.   Determination of the temperature-strength (cylindrical) dependence, taking into account the corrections.

All SS and LS were made with the same concrete mix B25 M350. The strength tests of the specimens by the non-destructive control method are performed using a shock-pulse device IPS MG4.

a   b

Figure 1 – Experimental studies of specimens: a – SSs, b – LSs

This is an express method and being an indirect assessment of the strength characteristics of structures, it requires a calibration dependence on the destructive method [19] performed on a testing press (in this case, the Pilot Compact 500 kN automatic press was used).

A handmade measuring device consisting of the following components was used to measure the temperature mode of concrete curing:

i. Four DS18B20 type temperature sensors;

ii. Two lithium-ion batteries with a nominal voltage of 3.7V and a capacity of 3000mAh;

iii. Atmega328p microcontroller (this microprocessor is an 8-bit AVR microcontroller with 32KB of programmable Flash memory, it is relatively inexpensive compared to other energy-efficient microcontrollers but also has a compact TQFP32 package).

iv. 8GB memory card to store up to 28 days of recordings;

v. DS3231 timing module to periodically wake up the device and poll the connected sensors.

The processing of the temperature-strength dependence for predicting the concrete structure's strength was carried out in two stages. The first stage involved correcting the temperature-strength (surface) dependence of the LS to the temperature mode of the LS and the corresponding surface strength of the SS. This is because SS and LS were directly subjected to both temperature and surface strength control (unlike the strength by the destructive method), and the variables of the obtained dependences had a frequent periodicity of measurements (the measurement of surface strength every 24 hours, temperature - every 30 minutes). The second stage involved the correction of the obtained temperature-strength (surface) dependence for the transition from the surface strength to the cylindrical one, meaning from the indirect method to the direct destructive method. For the controlled assessment of the obtained temperature-strength dependence after 28 days, cores were taken from the LS to determine the actual strength. The obtained results of the actual strength were compared with the predicted strength obtained by the temperature-strength relationship.

Results and Discussion

2.1 Strength tests on specimens

Figure 2a shows the dependence of measured non-destructive and destructive strengths on the age of concrete specimens (SS and LS). Before the tests, local measurement sites were prepared. The results of the non-destructive testing of the LSs are also shown in Figure 2a. Strength measurements were also performed on the side faces of the specimens. A total of 4 test measurements were made for each specimen, i.e., one test measurement was made from each of the side faces. Also, as in the case of SS, the control measurement included 15 particular strength measurements. The dependencies presented in Figure 2a are described by logarithmic functions having a close relationship with the specific values, whose coefficients of determination are more significant than 92%. Figure 2b shows a comparison of particular values of strength characteristics of LS and SS obtained by a non-destructive method. Figure 2c shows the calibration dependence or comparison of particular values of SS strength characteristics obtained by non-destructive and destructive methods.

According to the results of comparative analysis, the best convergence of values of strength is observed between the destructive and non-destructive methods of SS (the difference of particular values does not exceed 23%, on average 10%). It can be expressed by the corrective function, obtained from the correlation dependence between the surface and the cylindrical strength of SS (Eq. 1):

$$\sigma_d^{SS} = 1.1192\sigma_{nd}^{SS}, \qquad (1)$$

The convergence of values between the non-destructive method of SS and LS also has a close relationship (the differences of particular values do not exceed 25%, on average 15%). It can be expressed by the following corrective function (Eq. 2):

$$\sigma_{nd}^{LS} = 0.8945\sigma_{nd}^{SS}, \qquad (2)$$

y = 5.3091ln(x) + 15.677
R² = 0.9296

y = 5.7574ln(x) + 11.844
R² = 0.985.

y = 6.3143ln(x) + 9,3363
R² = 0.9773

a

b

c
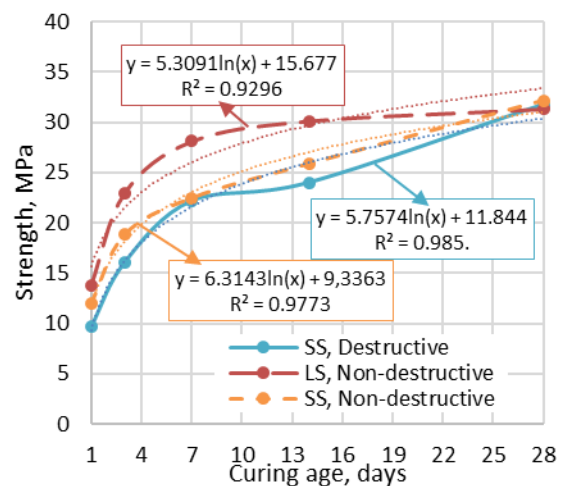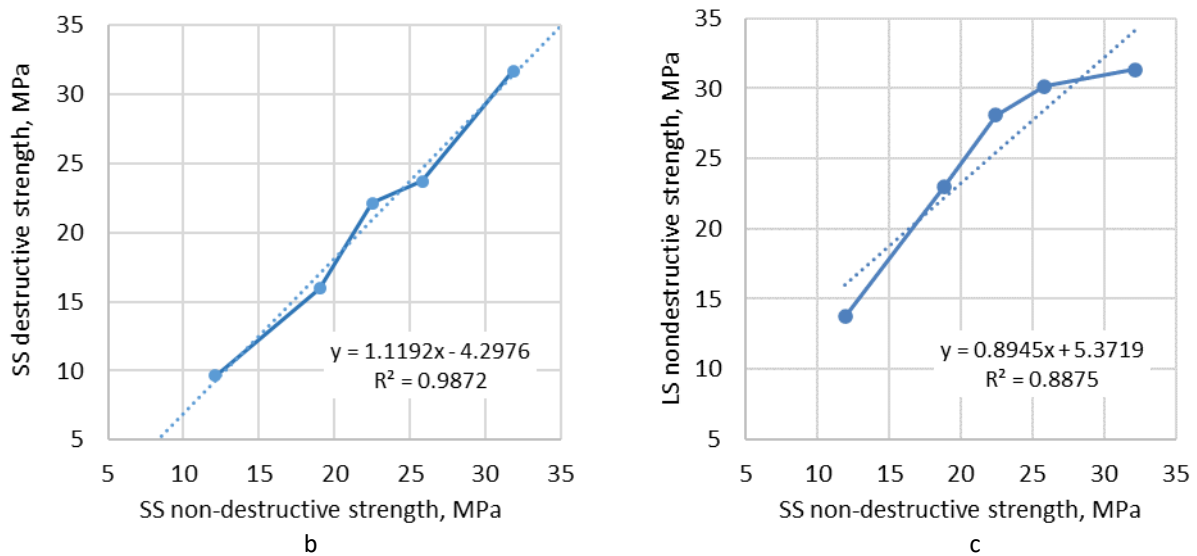
Figure 2 – Results of strength measurements of SS and LS: a – Dependence of strength by age, b – Correlation between the surface and cylindrical strength of SS, c – Correlation between the surface strengths of SS and LS
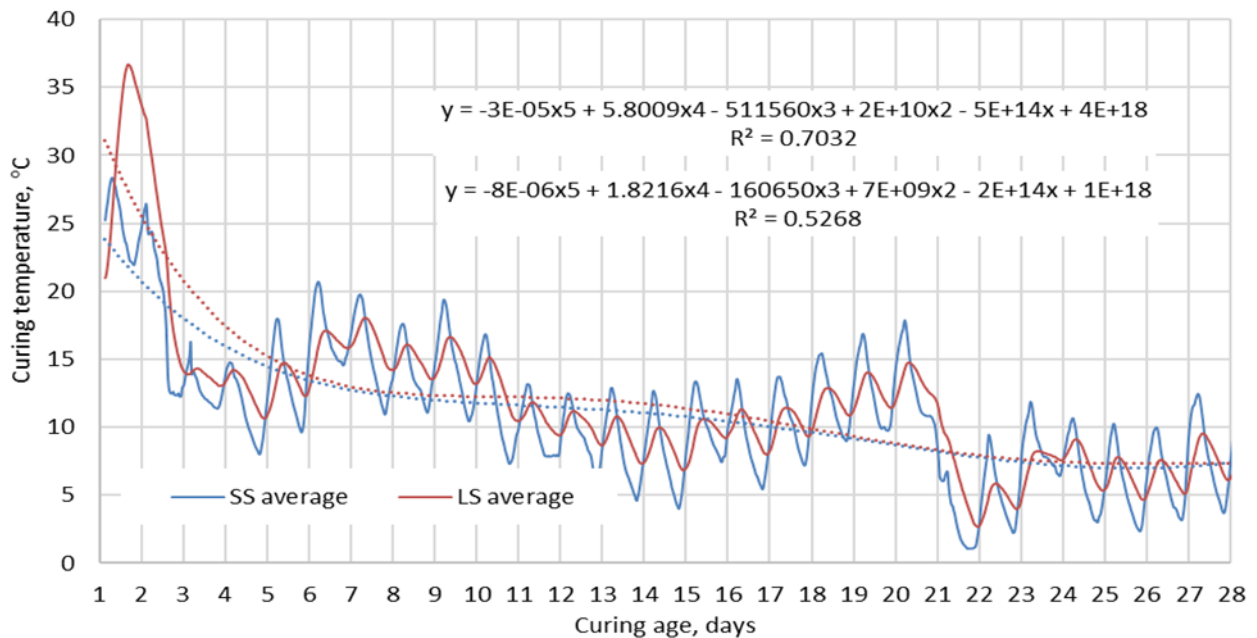
Figure 3 – Comparison of SS and LS temperature histories

According to the statistical analysis, particular values of strength measurements have close relations within the limits of control measurements, as well as control measurements among themselves: coefficient of variation of all related particular values on the average makes 0.02, lies in a range from 0.01 to 0.05; coefficient of reliability herewith makes 1.23 on the average, lies in a range from 1.01 to 2.46. It is necessary to note that extreme values of the range

are out of general statistics and represent a single case, but they meet the requirements of statistical tests for exclusion of accidental errors and are within the acceptable 95% confidence level.

2.2. Thermal control of specimens

The data obtained for temperature changes by age showed a close relationship between SS and LS (Figure 3).

According to the obtained temperature regimes, the greatest thermal response of LS concrete was observed in the early period of its curing, after 13.5 hours of its pouring, with a temperature of 36.5 °C. The minimum LS temperature was observed after 22 days, amounting to 2.25 °C. A similar pattern of thermal fluctuation was observed in SS, where the maximum temperature of 28.27 °C corresponds to the curing age of 4.5 hours, the minimum temperature of 1.02 °C - after the same 22 days. The

thermal fluctuation in both cases has a common pattern in the setting and curing of concrete.

In both cases, the maximum exothermic process occurs at the initial stage of concrete curing (due to three-calcium aluminate hydration). The difference in temperature at the initial stage of the hydration process may be explained by the massiveness of LS in relation to SS. The more massive the structure, the less convection surface heat removal; consequently, more time is needed to achieve thermal balance with the environment, as evidenced by the large amplitude of thermal cyclicity of the SS concerning the LS. Generally, the particular values of temperatures have high convergence (which can be observed when superimposing the dependencies on each other (Figure 4), numerically described by the dependency y=1.049x, which indicates deviations of particular values of SS from LS, on average, by 5%.
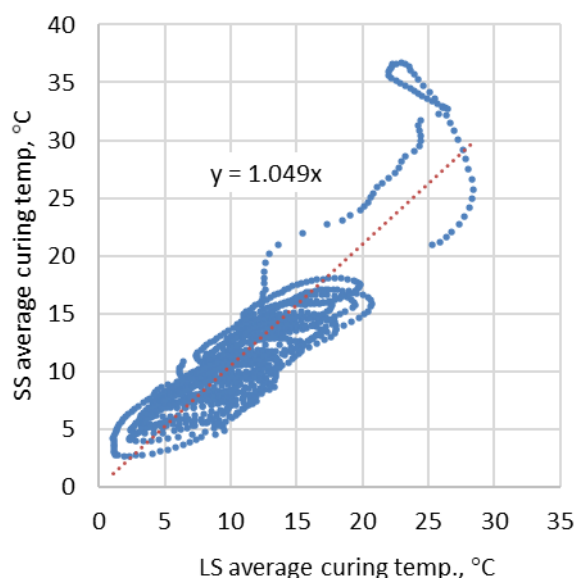

Figure 4 – Correlation of SS and LS temperature histories

It is necessary to correct the values of surface strength of large specimens from the available database of their temperature measurements as a result of the hydration process (Figure 5a). For the transition to the cylindrical strength of the LS concrete, we use the previously obtained function of the calibration dependence between the strength of non-destructive control and the cylindrical strength of the SS. Figure 5b shows the predicted dependence between LS's surface and cylindrical strength. The obtained dependence makes it possible to carry out indirect non-destructive strength control of reinforced concrete structures with the same mixture of concrete and kept in the

same climatic conditions. The specimens were subjected to destructive strength tests. According to the results, the following was obtained: the average core strength was 32.9 MPa, with a quadratic deviation of 0.29 and a coefficient of variation of 0.01. Comparing the strength of the cores with the predicted strength calculated from the previously obtained dependence, it was found that the average actual core strength has a high convergence with the expected strength of 33.24 MPa. The error of the indirect method was: 1.02 %. In general, the studies to assess the strength characteristics of structures based on measurements of temperature conditions of concrete curing in the process of its hydration refers to indirect methods of strength control, so it requires a qualitative analysis of the data to be compared and considering regional characteristics of construction. According to the standard method [15], the transition to strength indexes of concrete is made by measuring the temperature regime and the control measurement of the cylindrical strength of concrete in different periods of its curing. The resulting pattern of temperature-strength dependence is subsequently adapted for strength control of real building structures. In the present study, in contrast to the standard method, it was decided to carry out strength control using the data on the surface strength of concrete by the shock-pulse method.

In the case of this study, the error of the obtained temperature-strength dependence, in comparison with the actual strength of four control tests of the strength (destructive method) of drilled cores, was 1.02%. It should be noted that comparisons with the actual strength of large specimens were made only after 28 days, which may not be sufficient for a complete conclusion about the reliability of this method. Also, the next study program will include an assessment of the influence of the temperature and humidity regime of the environment on the thermal changes in the concrete during the design period of hydration (up to 28 days).

In this case, the ambient temperature range will be within +5°C to +25°C, as exceeding this temperature range is not acceptable for curing the concrete without the use of additional measures. The obtained nomograms will make it possible to correct changes in the temperature regime of hydration of structures curing in real climatic conditions.

a

b
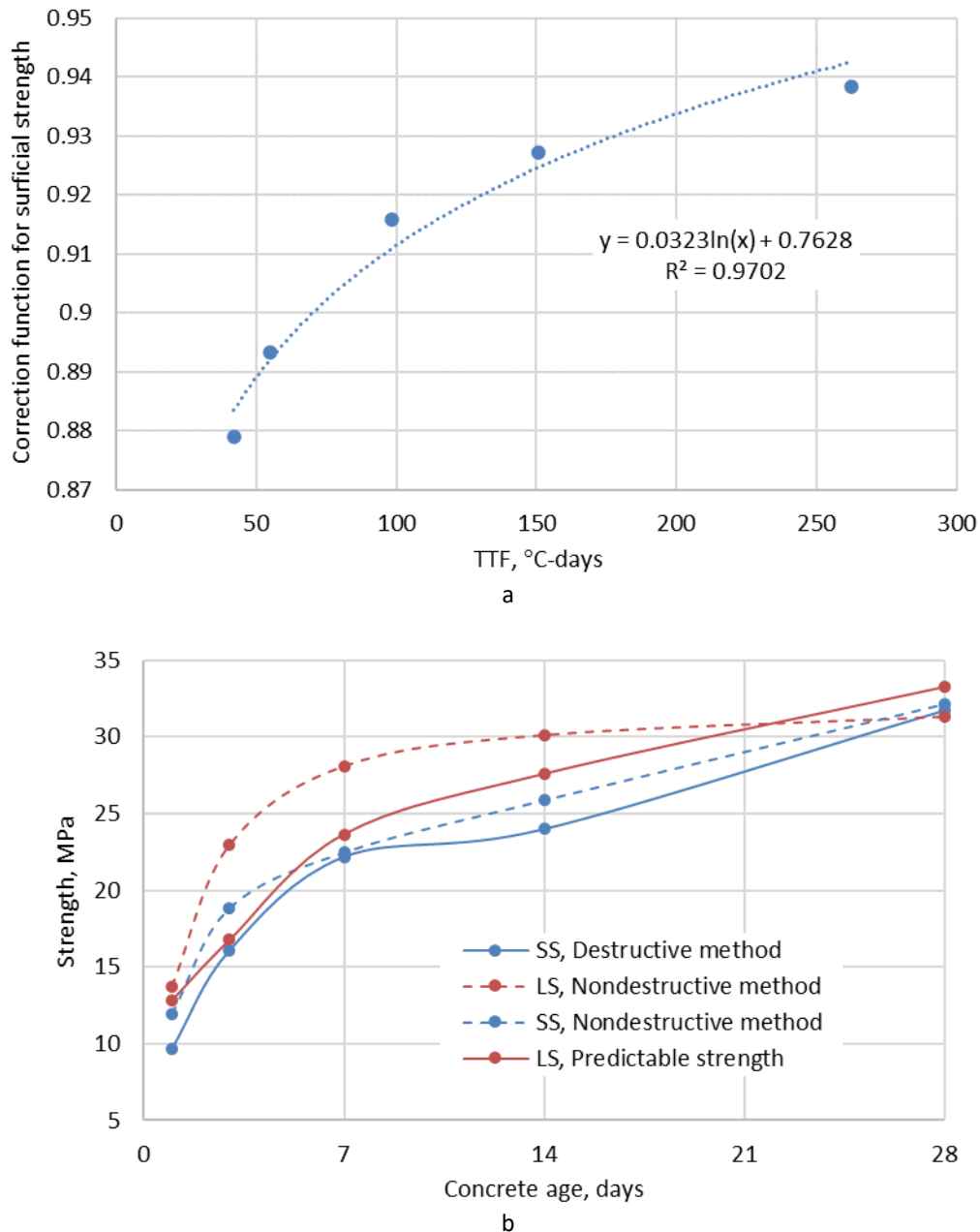
Figure 5 – Correction of the results of the temperature-strength dependence of LS: a – Correction function for surface strength, b – Corrected LS cylinder strength

Conclusion

A set of tests and strength measurements of small specimens (laboratory) and large specimens (imitating the relative massiveness of reinforced concrete structures in relation to the laboratory specimens), non-destructive and destructive tests were conducted. The following conclusions can be made based on the results of the studies; Firstly, the obtained particular strength values have a close relationship within the limits of the control measurements, have a high degree of reliability, as evidenced by high statistical indices and a large number of measurements: the coefficients of variation do not exceed 2%. Secondly, the average strength data of small and large specimens showed a remarkable convergence of the results, which is a positive indicator for further data reduction in the temperature-strength analysis and the error of indirect strength control. Thirdly, the temperature control results revealed the influence of the massiveness of large specimens on the amplitude of thermal cycling. Fourthly, the temperature-strength functional dependence was obtained, making it possible to perform strength control of reinforced concrete structures made of the same concrete mixture composition and kept under the same climatic conditions. The control method refers to the

indirect one and has a high correlation with the actual strength of concrete. On the 28th day, the strength error made up 1.02% of the actual cylindrical strength of the collected core.

Conflict of interest. On behalf of all the authors, the correspondent author states that there is no conflict of interest.

Датчиктер мен соққы-импульстік әдісті қолдана отырып, бетонның беткі беріктігі бойынша мониторингі

[1,2] Утепов Е.Б., [3] Анискин А., [2] Лукпанов Р.Е., [1,2] Тулебекова А.С., [1,2] Жарасов Ш.Ж.

[1] CSI Research&Lab, ЖШС, Нұр-Сұлтан, Қазақстан
[2] Л.Н. Гумилев атындағы Еуразия ұлттық университеті, Нұр-Сұлтан, Қазақстан
[3] Солтүстік Университеті, Вараждин, Хорватия

ТҮЙІНДЕМЕ

Әлемде темір-бетон конструкцияларын температуралық-беріктік мониторингі және бақылау үшін пайдаланылатын көптеген әдістер бар. Алайда, бұл әдістер мен процедуралар маңызды мәселелермен байланысты, өйткені олар көп уақытты, шығындарды талап етеді және қателіктерге бейім. Сондықтан, бұл зерттеу қазіргі уақытта кеңінен қолданылатын әдістерге балама тәсіл ретінде температура мен беріктік арасындағы тәуелділікті алу үшін бұзылмайтын бақылау әдістерін қолдана отырып, үлгілердің беттік беріктігін анықтау әдісінің ықтимал қолданылуын зерттеді. Зерттеулер соққы-импульстік әдіспен алынған құрылыс конструкцияларын имитациялайтын шағын зертханалық үлгілердің (SS) және үлкен үлгілердің (LS) беткі беріктігін және бұзу әдісімен алынған беріктігін салыстыру арқылы жүргізілді. Алынған калибрлеу тәуелділіктері үлгілердің жылу бақылауының нәтижелеріне бейімделді. Температура-беріктік тәуелділігі SS және LS беріктігі мен температуралық параметрлерінің нәтижелерін салыстыру арқылы түзетілді. Нақты салынған конструкцияларға температуралық-беріктік тәуелділігінің түпкілікті бейімделуі құрылыс саласындағы осы әдістің елеулі әлеуетін көрсетті, мұнда бұрғыланған керндердің нақты беріктігі мен бетонның 28 күндік болжамды беріктігі арасындағы айырмашылық бар болғаны 1,02% - ды құрады. Алынған номограммалар нақты климаттық жағдайларда қататын құрылымдарды гидратациялаудың температуралық режиміндегі мүмкін болатын өзгерістерді түзетуге мүмкіндік береді.

Түйін сөздер: бетонның жетілуі, бетінің беріктігі, импульстік соққы әдісі, операциялық бақылау, сенсор.

Авторлар туралы ақпарат:

Утепов Елбек Бахитович
PhD, «Ғимараттар және имараттарды жобалау» кафедрасының профессор м.а., Л.Н. Гумилев атындағы Еуразия ұлттық университеті, Нұр-Сұлтан, Қазақстан. ORCID ID: 0000-0001-6723-175X, Email: utepov-elbek@mail.ru

Анискин Алексей
Т.ғ.к., «Құрылыс» кафедрасының Ассистент профессоры, Солтүстік Университеті, Вараждин, Хорватия. Email: aaniskin@unin.hr

Лукпанов Рауан Ермагамбетович
PhD, Доцент, "ENU LAB" ғылыми-өндірістік орталығының директоры, Л.Н. Гумилев атындағы ЕҰУ, Нұр-Сұлтан, Қазақстан. ORCID ID: 0000-0003-0085-9934, Email: rauan_1982@list.ru

Тулебекова Асель Сериковна
PhD, «Ғимараттар және имараттарды жобалау» кафедрасының доценті, Л.Н. Гумилев атындағы Еуразия ұлттық университеті, Нұр-Сұлтан, Қазақстан. ORCID ID: 0000-0001-8553-3081, Email: krasavka5@mail.ru

Жарасов Шынгыс Жарасович
PhD докторанты, «Ғимараттар және имараттарды жобалау» кафедрасы, Л.Н. Гумилев атындағы Еуразия ұлттық университеті, Нұр-Сұлтан, Қазақстан. ORCID ID: 0000-0002-0468-8362, E-mail: zhshzh95@gmail.com

Мониторинг бетона по поверхностной прочности с применением датчиков и ударно-импульсного метода

[1,2] Утепов Е.Б., [3] Анискин А., [2] Лукпанов Р.Е., [1,2] Тулебекова А.С., [1,2] Жарасов Ш.Ж.

[1] CSI Research & Lab, ТОО, Нур-Султан, Казахстан
[2] Евразийский национальный университет им. Л.Н. Гумилева, Нур-Султан, Казахстан
[3] University North, Вараждин, Хорватия

АННОТАЦИЯ

В мире существует множество методов, используемых для температурно-прочностного мониторинга и контроля железобетонных конструкций. Однако эти методы и процедуры связаны со значительными проблемами, поскольку требуют много времени, затрат и подвержены ошибкам. Поэтому в данном исследовании изучалась потенциальная применимость метода определения поверхностной прочности образцов с использованием методов неразрушающего контроля для получения зависимостей между температурой и прочностью в качестве альтернативного подхода к широко используемым в настоящее время методам. Исследования проводились путем сравнения поверхностной прочности малых лабораторных образцов (SS) и больших образцов (LS), имитирующих строительные конструкции, полученных ударно-импульсным методом, и прочности, полученной разрушающим методом. Полученные калибровочные зависимости были адаптированы к результатам теплового контроля образцов. Зависимость температура-прочность корректировалась путем сравнения результатов прочностных и температурных параметров SS и LS. Окончательная адаптация температурно-прочностной зависимости к реальным возведенным конструкциям показала значительный потенциал данного метода в строительной отрасли, где разница между фактической прочностью выбуренных кернов и прогнозной прочностью бетона в возрасте 28 дней составила всего 1,02%. Полученные номограммы позволят корректировать возможные изменения температурного режима гидратации конструкций, твердеющих в реальных климатических условиях.

Ключевые слова: зрелость бетона, поверхностная прочность, ударно-импульсный метод, оперативный контроль, датчик.

Информация об авторах:

Утепов Елбек Бахитович
PhD, и.о. профессор кафедры «Проектирование зданий и сооружений», Евразийский национальный университет им. Л.Н. Гумилева, Нур-Султан, Казахстан. ORCID ID: 0000-0001-6723-175X, Email: utepov-elbek@mail.ru

Анискин Алексей
К.т.н., Ассистент Профессор кафедры «Строительство», Университет Север, Вараждин, Хорватия. Email: aaniskin@unin.hr

Лукпанов Рауан Ермагамбетович
PhD, Профессор, Директор научно-производственного центра «ENU LAB», ЕНУ им. Л.Н.Гумилева, Нур-Султан, Казахстан. ORCID ID: 0000-0003-0085-9934, Email: rauan_1982@list.ru

Тулебекова Асель Сериковна
PhD, Доцент кафедры «Проектирование зданий и сооружений», ЕНУ им. Л.Н.Гумилева, Нур-Султан, Казахстан. ORCID ID: 0000-0001-8553-3081, Email: krasavka5@mail.ru

Жарасов Шынгыс Жарасович
Докторант PhD, Кафедра «Проектирование зданий и сооружений», ЕНУ им. Л.Н.Гумилева, Нур-Султан, Казахстан. ORCID ID: 0000-0002-0468-8362, E-mail: zhshzh95@gmail.com

References

[1] Dobshits L. M. & B. A.V., The question of determining the strength of concrete structures Quality Innovation Education. 2017;9:38-41.

[2] Utepov Y, Aniskin A, Ibrashov A, Tulebekova A. Maturity sensors placement based on the temperature transitional boundaries. Magazine of Civil Engineering. 2019;90:93-103. https://doi.org/10.18720/MCE.90.9

[3] Ulybin A. V, On the choice of concrete strength inspection methods of ready-built structures. Magazine of civil engineering, 22 (2011) 10–15. https://doi.org/10.5862/MCE.22.1

[4] Shoukry S N, William G W, Downie B, Riad M Y. Effect of moisture and temperature on the mechanical properties of concrete. Construction and Building Materials, 2011; 25: 688–696.

[5] Utepov Y, Akhmetov D, Akhmatshaeva I, Root Y. Study of the influence of fine fillers from technogenic waste and chemical additives on the properties of self-compacting concrete. Kompleksnoe ispol'zovanie mineral'nogo syr'â/Complex Use of Mineral Resources/Mineraldik shikisattardy Keshendi Paidalanu, 311 2019; 311: 64–73. https://doi.org/10.31643/2019/6445.39.

[6] Sharipova I A, Dorofeeva O S. Concrete strength control by the shock-pulse method. Proc. II All-Russian Conf. with Int. Particip. Kumertau. 2019, 179-184.

[7] Arundas P H, U. K. Dewangan. Compressive Strength of Concrete based on Ultrasonic and Impact Echo Test. Indian Journal of Science and Technology, 2016;9. https://doi.org/10.17485/ijst/2016/v9i23/94124.

[8]   Martin J, Forde M C. Influence of concrete properties on impulse hammer spectrum and compression wave velocity. Construction and Building Materials, 1995;9:245-255.https://doi.org/10.1016/0950-0618(95)00027-D.

[9]   Poorarbabi A, Ghasemi M, Azhdary Moghaddam M. Concrete compressive strength prediction using non-destructive tests through response surface methodology. Ain Shams Engineering Journal, 2020;11:939–949. https://doi.org/10.1016/j.asej.2020.02.009.

[10]   Hong S, Yoon S, Kim J, Lee C, Kim S, Lee Y. Evaluation of Condition of Concrete Structures Using Ultrasonic Pulse Velocity Method. Applied Sciences, 2020;10:706. https://doi.org/10.3390/app10020706.

[11]   Kibar H, Ozturk T, Determination of concrete quality with destructive and non-destructive methods. Computers and Concrete, 2015;15: 473–484. https://doi.org/10.12989/cac.2015.15.3.473.

[12]   Karahan Ş, Büyüksaraç A, Işık E. The Relationship Between Concrete Strengths Obtained by Destructive and Non-destructive Methods. Iranian Journal of Science and Technology, Transactions of Civil Engineering, 2020;44:91–105. https://doi.org/10.1007/s40996-019-00334-3.

[13]   Dihanbaev B I, Dikhanbaev A B. The development of the thermal schemes joint processing of sulphide of lead concentrates, and waste slags by the method of extreme power saving. Kompleksnoe ispol'zovanie mineral'nogo syr'â/Complex Use of Mineral Resources/Mineraldik shikisattardy Keshendi Paidalanu, 2019;308:51-61. https://doi.org/10.31643/2019/6445.06.

[14]   Bekbayeva L, Negim E-S, Yeligbayeva G, Ganjian E. The effect of blend copolymers on physico-mechanical properties of mortar. Kompleksnoe ispol'zovanie mineral'nogo syr'â/Complex Use of Mineral Resources/Mineraldik shikisattardy Keshendi Paidalanu, 2019;311:5-11. https://doi.org/10.31643/2019/6445.32.

[15]   Interstate standard ASTM C1074-17. Method, Standard Practice for Estimating Concrete Strength by the Maturity. 2017. https://www.astm.org/c1074-17.html

[16]   Interstate standard CSA A23.1/A23.2. Concrete Materials and Methods of Concrete Construction/Test Methods and Standard Practice for Concrete. 2014. https://civilnode.com/download-standard/10644237618004/csa-a23119a23219-concrete-materials-and-methods-of-concrete-constructiontest-methods-and-standard-practices-for-concrete

[17]   Interstate standard NEN 5970. Determination of strength of fresh concrete with the method of weighted maturity. 2001. https://standards.globalspec.com/std/10294720/NEN%205970

[18]   Interstate standard DIN 1045-3. Concrete, reinforced and prestressed concrete structures - Part 3: Execution of structures - application rules for DIN EN 13670. 2013. https://standards.globalspec.com/std/1494526/din-1045-3

[19]   Interstate standard NCH 170. Hormigon– Requisitos generals (Concrete– General requirements). 2016. https://ru.scribd.com/document/455151872/NCH170-2016

[20]   Interstate standard ST–NP SRO SSK–04–2013, Temperature and strength control of concrete during the construction of monolithic structures in winter. 2013. https://docs.cntd.ru/document/1200143622

[21]   Interstate standard GOST 10180. Concretes. Methods for strength determination using reference specimens. 2012. https://docs.cntd.ru/document/1200100908

[22]   Interstate standard GOST 18105. Concretes. Rules for control and assessment of strength, 2018. https://docs.cntd.ru/document/1200164028

[23]   Interstate standard GOST 22690. Concretes. Determination of strength by mechanical methods of non-destructive testing. 2015. https://docs.cntd.ru/document/1200124396

[24]   Lukpanov R E, Dyussembinov D S, Utepov Y B, Bazarbayev D O, Tsygulyov D V, Yenkebayev S B, Shakhmov Z A. Homogeneous pore distribution in foam concrete by two-stage foaming. Magazine of Civil Engineering, 2021;3: 10313. https://doi.org/10.34910/MCE.103.13.

[25]   Soutsos M, Kanavaris F. The modified nurse-saul (MNS) maturity function for improved strength estimates at elevated curing temperatures. Case Studies in Construction Materials, 2018;9 e00206. https://doi.org/10.1016/j.cscm.2018.e00206.

[26]   Aniskin A, Tulebekova A S. A unified approach for temperature and strength control of concrete. Bulletin of L.N. Gumilyov Eurasian National University., 2021;135:71–81. https://doi.org/10/gn32rk.

[27]   Utepov Y, Aniskin A, Tulebekova A, Aldungarova A, Zharassov S, Sarsembayeva A. Complex Maturity Method for Estimating the Concrete Strength Based on Curing Temperature, Ambient Temperature and Relative Humidity. Applied Sciences, 2021;11:7712. https://doi.org/10.3390/app11167712.

[28]   Utepov Y, Aniskin A, Tulebekova A, Zharassov S, Aldungarova A. RSSI Performance of Maturity Sensor Based on LoRaWAN Network. Trudy Universiteta, 2021: 232–240. https://doi.org/10/gnx9jh.

[29]   Utepov Y, Tulebekova A, Akhazhanov S, Zharassov S, Bazarbayev D. Prototyping of a concrete maturity sensor with a hermetically sealed housing made of two-component plastic. Bulletin of the Karaganda University. "Physics" Series, 2021;103: 60–70. https://doi.org/10/gn32tt.

Deposition of carbonitride titanium coatings by magnetron sputtering and its effect on tribo-mechanical properties

Mamayeva A.A., Kenzhegulov A.K.[*], Panichkin A.V., Kshibekova B.B., Bakhytuly N.

"Institute of Metallurgy and Ore Beneficiation" JSC, Satbayev University, Almaty, Kazakhstan

* Corresponding author email: a.kenzhegulov@satbayev.university

ABSTRACT

Metal parts in machinery often fail as a result of damage caused by wear and tear, resulting in the loss of functionality of the products. Thin film solid nitride coatings are used to improve the wear resistance and service life of parts and are considered to be effective. The article presents a brief overview of modern literature in the field of obtaining wear resistant coatings of titanium carbonitride by using magnetron sputtering. The review presents a detailed assessment of the scientific results obtained depending on the deposition parameters and the conditions for obtaining coatings. The results of the coefficient of friction, wear rate of the coating and counterbody, nanohardness and adhesion force of coatings obtained by magnetron sputtering and its modifications are shown. The influence of alloying elements on the mechanical and tribological properties of titanium carbonitride coatings is considered. Recent advances in the production of titanium carbonitride coatings with improved wear characteristics are discussed.

Keywords: titanium carbonitride, magnetron sputtering, coating, wear resistance, coefficient of friction.

	Information about authors:
Mamaeva Axaule Alipovna	*Associate professor, Candidate of Physical and Mathematical sciences, Head of laboratory "Metal science" of the JSC "Institute of Metallurgy and Ore Beneficiation", Almaty, Kazakhstan. ORCID ID: 0000-0002-9659-8152. Email: a.mamayeva@satbayev.university*
Kenzhegulov Aidar Karaulovich	*PhD, Researcher, JSC "Institute of Metallurgy and Ore Beneficiation", Almaty, Kazakhstan. ORCID ID: 0000-0001-7001-2654. Email: a.kenzhegulov@satbayev.university*
Panichkin Aleksandr Vladimirovich	*Candidate of Technical sciences, Head of the National Scientific Collective Use Laboratory of JSC "Institute of Metallurgy and Ore Beneficiation", Almaty, Kazakhstan. ORCID ID: 0000-0002-2403-8949. Email: a.panichkin@satbayev.university*
Kshibekova Balzhan Bulotovna	*Researcher, JSC "Institute of Metallurgy and Ore Beneficiation", Almaty, Kazakhstan. ORCID ID: 0000-0002-5944-7865. Email: b.kshibekova@satbayev.university*
Bakhytuly Nauryzbek	*Junior Researcher, JSC "Institute of Metallurgy and Ore Beneficiation", Almaty, Kazakhstan. ORCID ID: 0000-0003-3087-0616. Email: n.bakhytuly@satbayev.university*

Introduction

Hard and ultra-hard protective coatings are increasingly being used in various technical fields, including the automotive, aerospace, and manufacturing industries. Today, the use of wear resistant coatings in harsh working conditions is becoming more and more important [[1], [2], [3]]. For this reason, a number of studies have been devoted to the problems of creating thin hard coatings and their application in the production of machine parts and tools [[4], [5], [6], [7]]. Transition metal nitrides are widely used as functional coatings, which is justified by a set of their properties, such as good conductivity, hardness, high melting point, chemical resistance, and wear resistance [[8], [9]].

Titanium carbonitride (TiCN) coating is one of the most attractive among them. The tribological properties of such coatings have been studied in the following works [[10], [11]].

Such coatings have found application in cutting tools, in the details of the instrument, and mechanical engineering to increase the duration of their service life. They are biocompatible [[12], [13]], which, combined with their relatively high ductility and hardness, makes this material promising for medical applications.

Currently, a wide range of developed and tested techniques is used to form TiCN coatings. These include physical vapor deposition (PVD), chemical vapor deposition (CVD), spray techniques, and others. Each of these methods has advantages and disadvantages. Disadvantages common to many

methods include poor adhesion of the coatings to the substrate, the inability to regulate their elemental composition, and the limited choice of substrate material [14]. Physical deposition methods are devoid of some disadvantages. Thus, the widespread use of PVD technologies for industrial applications is associated with the possibility of obtaining hard and durable coatings that can be applied to organic or inorganic substrates [15]. For example, magnetron sputtering (MS), cathodic arc, and pulsed laser spraying methods can be used to apply TiCN coatings with high tribotechnical properties to parts that are exposed to aggressive environments or extreme operating conditions.

The MS method allows the deposition of hard TiCN coatings with a low level of impurities at a controlled rate [16]. Depending on the sputtering conditions, this method makes it possible to obtain coatings of various morphologies and structures.

Since the chemical composition and structure of coatings are interrelated with their mechanical properties and, in particular, tribological characteristics, it is important to know how the parameters of magnetron sputtering affect them. Therefore, the purpose of this review is to show a rief, modern scientific and technical literature analysis on the preparation of wear resistant coatings based on TiCN, obtained using MS under different conditions of their deposition.

Research on obtaining titanium carbonitride coatings

Magnetron sputtering is a vacuum coating process using a specially formed magnetic field applied to a target. A typical MS scheme for TiCN coating deposition is shown in Figure 1. A typical deposition system includes a vacuum chamber, magnetron, cooling system, power supply, evacuation pumps, and other additional instrumentation for measurement.
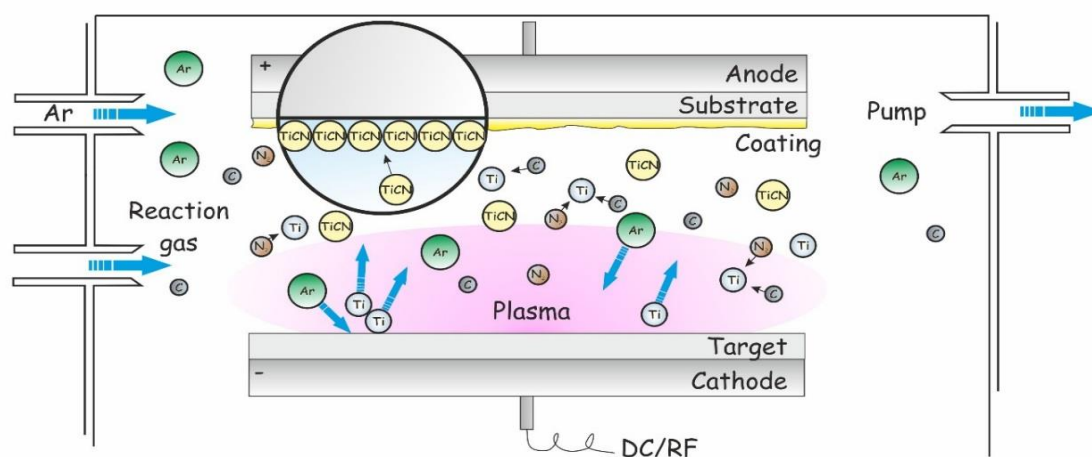
Figure 1 - Typical MS scheme and coating deposition process

TiCN coatings are obtained by MS at direct current (DCMS) [[17], [18], [19], [20], [21], [22], [23]] and radio frequency (RFMS) [[15], [25], [26], [27]] under balanced and unbalanced magnetron operating conditions [[28][29]]. The deposition process of TiCN hard coatings is directly influenced by parameters such as working atmosphere pressure, composition and ratio of reaction gases, current power supplied to the magnetron, bias potential and substrate temperature, target composition, and more. Let us consider the influence of these parameters on the structure, composition, and properties of TiCN coatings.

Numerous studies [[11], [30]] are aimed at obtaining and improving tribological properties of TiCN nanocomposite coatings. The formation of nanocrystals in the amorphous matrix of the deposited compound is an effective way to improve the tribological properties of TiN and TiC coatings, which leads to increased hardness and reduced friction [[31], [32]].

The carbon content of TiCN coatings significantly affects the final coating properties. From the results of the following studies, it has been determined that the presence of amorphous carbon and carbon sp2 in composite films significantly reduces the coefficient of friction (CoF) and wear rate (WR) [[17], [22]], increasing carbon content gives results similar to decreasing substrate displacement stress [20] and reduces corrosion resistance [21]. In the paper [20],

detailed X-ray diffraction studies of TiCN coatings are given depending on the carbon content. The following conclusions were drawn from the results: 1) the adatomic mobility decreased with increasing carbon content in the coating; 2) the measured lattice parameter is in agreement with published literature data for stoichiometric TiN coatings; 3) the observed micro deformation as a function of carbon content in the coating, increased with increasing carbon content. The results of electrochemical experiments described in [21] showed that the corrosion resistance of TiCN coatings decreases with an increase in the carbon content in them. The authors explain this by an increase in the density of defects in such coatings, despite their high hardness and adhesion to substrates. The film structure was directly affected by its thickness, and the residual stress values were higher for thinner coatings (1 μm).

When TiCN coatings are deposited, a titanium target or a combined target is used. In the latter case, the target can be made from titanium and carbon powders in different ratios or by assembling the target from individual segments, disks. For example, in [22], TiN/(a-C) composite coatings were deposited with different ratios of graphite to Ti (G/Ti) in a single target on steel at 200 °C. The G/Ti ratio in the target was 0.5, 1.0, 2.0. The obtained coatings showed an orientation (222) and a columnar structure at a lower G/Ti ratio. The tribological properties of the coatings were tested on a ball-on-disc tribometer under dry conditions, at 60 % relative humidity, using a hardened steel ball HRC62 as a counterbody at a normal load of 1.0 N. The results showed that the presence of amorphous carbon in composite films significantly reduces the CoF and WR [22]. The authors of [17] conducted a similar study where TiCN nanocomposite coatings were obtained by DC from a combined Ti/C target at different nitrogen flow rates. When nitrogen flow is increased from 0 to 30 sccm at an operating pressure of 0.3 Pa, both the crystallinity and the carbon sp2 content of the coatings are increased. CoF and WR can be significantly reduced by increasing the carbon sp2 content. Figure 2 shows the CoF and WR of the coatings obtained at different nitrogen flow rates. Based on the results of [17] it can be said that at a nitrogen flow rate of 30 sccm the TiCN coating can provide a combination of high hardness, toughness, and wear resistance.

Among the works studied, the relatively lowest coefficient of friction of the TiCN coating with low WR (~10^{-6} mm³/Nm) was achieved in our

experimental work [23]. Sample rotation speed, 1 cm/s; load, 1 N; wear track radius, 7 mm; friction path, 100 m; data collection speed: 50 Hz, a Si_3N_4 ball with a diameter of 6 mm was used as a counter body.
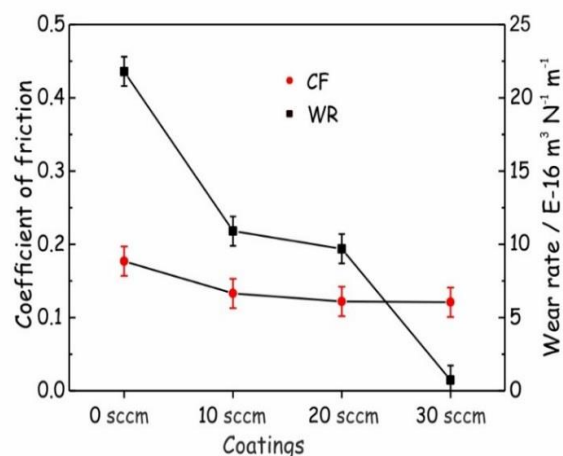
Figure 2 - Results of CoF and WR of coating obtained at different nitrogen flow rates [17]

The magnetron sputtering deposition condition at a substrate bias -70 V made it possible to obtain a coating with a CoF of 0.06 (figure 3). This was due to the formation of third bodies in contact and the subsequent formation of a lubricating transition layer. Also, it should be noted that during the test, no sharp jumps in CoF were observed, which indicates a high adhesion of the coating to the substrate [24].
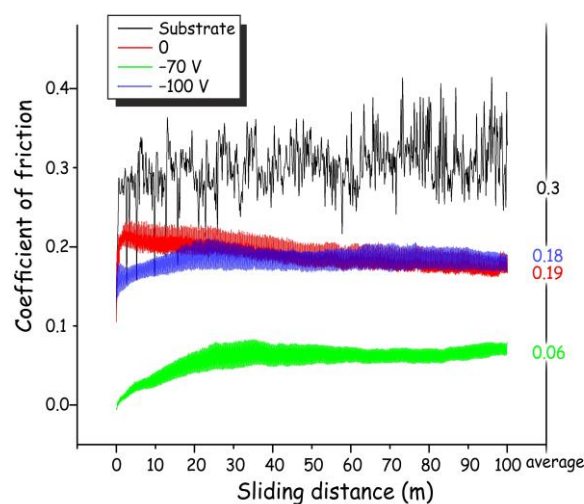
Figure 3 - CoF for titanium VT6 substrate and TiCN coatings [23]

The sputtering of a pure titanium layer is considered necessary by some researchers to improve the adhesion properties between the carbonitride coating and the substrate. According to

the authors [[15], [17], [33], [34]] this helps to increase the nucleation density and reduce the surface roughness of the coating.

In the works considered above the coatings were deposited by MS method at direct current. The authors of works [[15], [25]] have shown, that the coatings deposited in conditions of RFMS are not inferior in tribomechanical properties to the coatings received at direct current. Saoula N. and colleagues [15] investigated the effect of substrate potential displacement on the structure and properties of TiCN coatings. TiCN coatings were grown on silicon and steel substrates by RFMS method by sputtering a pure titanium target in Ar-CH₄-N₂ gas mixture.

The tribotechnical properties of the coatings were investigated by testing them together with an alumina ball in the air. The experimental results showed a decrease in the deposition rate from 31 to 9 nm/min with an increase in the bias voltage of the substrate from Us = 0 to -100 V, respectively. The coating deposited at 0 V was amorphous, while the coatings deposited when a bias voltage was applied to the substrate had a facecentered cubic structure with a predominant growth orientation (111). The results also show that TiCN coatings deposited at a substrate voltage of -70 V had a maximum hardness of 39 GPa and showed better wear resistance at a minimum WR and lower CoF of 0.13, this tendency showed also in [23].

As the bias voltage was increased from 0 to -70 V, the hardness increased from 16 to 39 GPa, and then slightly decreased to 38 GPa, while it was further increased to -100 V, as shown in Figure 4. In [24], the mechanical properties of TiN, TiC, and TiCN coatings deposited by the RFMS method were compared. Plasma power during deposition was maintained at 200 W. The hardness of TiN, TiC, and TiCN coatings was evaluated using the nanoindentation test. All thin film samples showed increased hardness with an increase in the applied negative bias voltage to -75 V. The increase in hardness was explained by a change in surface morphology. The hardness of the TiN, TiCN and TiC films ranged from 4.9 to 34.1 GPa, from 16 to 39 GPa, and from 9.8 to 26.97 GPa, respectively.

The tribological properties of coatings depend significantly on the test conditions. Wang Q. and others [35] showed significant dependence of WR and CoF on friction speed and load value on the results of tests of TiCN coatings on WC-based hard alloy substrates on a ball-on-disk tribometer. The measurements were performed concerning balls

made of SiC, SUJ2 and SUS440C steels at normal load from 3 to 12 N and sliding speed from 0.1 to 0.4 m/s.
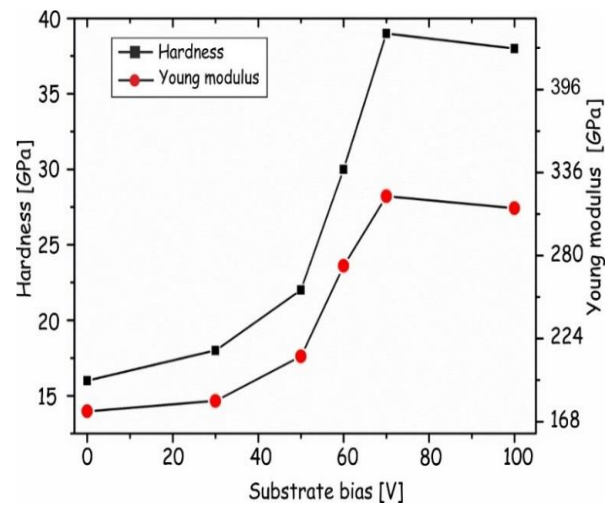
Figure 4 - Hardness and Young's modulus of the TiCN coating depending on the applied bias potential of the substrate [15]

It was shown that the tribological properties of the TiCN/SiC pair are better under friction in water than in air [[35], [36]]. Temperature is also one of the important parameters in studies of coating wear resistance. Polcar T. and others performed the work in this direction [18]. They investigated the tribological characteristics of the TiCN coating at elevated temperatures. The tests were performed according to the "pin-on-disc" scheme using balls made of bearing steel 100Cr6, Al₂O₃, and Si₃N₄ as a counter body. The results of testing specimens at temperatures below 200 ºC and up to 500 ºC are shown in Figure 5. All wear tests were performed at a normal load of 5 N at linear velocities from 0.04 m/s to 0.3 m/s for up to 30,000 cycles. The results showed that raising the temperature increased the CoF and WR of TiCN coating when sliding on 100Cr6 balls. In contrast, for Si₃N₄ balls, friction and wear were independent of temperature[[18], [35]]. In [19] the same authors showed results comparing the tribological behavior of TiN, TiCN, and CrN coatings under similar test conditions at temperatures up to 500 ºC, at a linear velocity of 4 cm/s, for 5000 cycles. These results indicate that the TiCN coating can perform as a wear resistant coating at high temperatures [19].

Thus, the wide range of studies on the preparation and study of the mechanical properties of TiCN coatings indicate a great interest in the scientific community for them as promising wear-resistant coatings.

Figure 5 - The dependency of coating wear rate on temperature using 100Cr6 ball (a) and Si_3N_4 ball [18]

Research on obtaining multilayer and alloyed TiCN coatings

Recently, coatings of a new generation based on TiCN have appeared, such as multi-component (TiAlCN, TiNCO) [[39] [40]], multilayer (TiN/TiCN/TiC) [41], gradient (Ti/TiN/TiCN) [42] and composite [17], [22] coatings. The authors of these studies believe that the properties of these new TiCN-based coatings are better than those of traditional TiCN coatings. 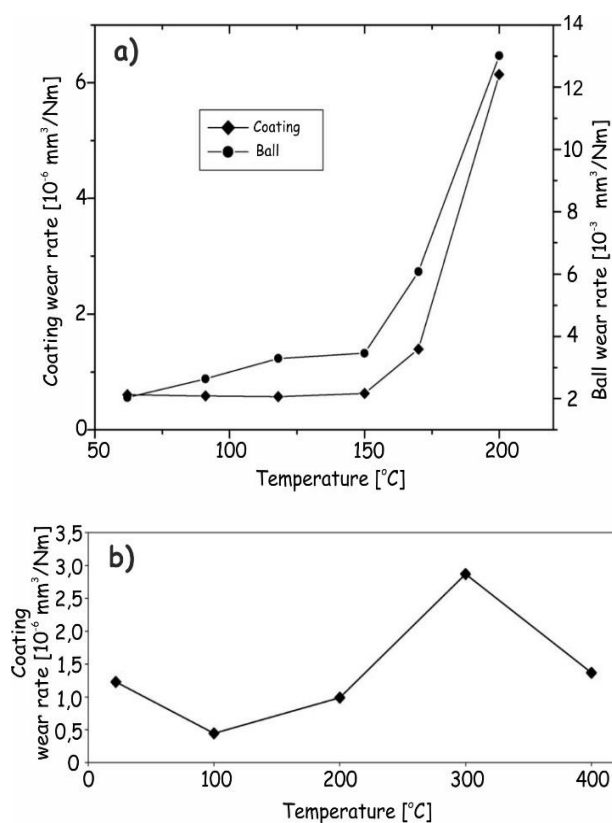Typically, the thickness of the TiCN coating varies from a few nanometers [17] to 4-5 microns [15]. In the case of multilayer coatings, this indicator can be higher and exceed several times, while they show good chemical stability, excellent mechanical properties, as well as excellent wear resistance and corrosion resistance. For example, Su Y.L. and his colleagues [43] found that multilayer TiN/TiCN/TiN coatings with a thickness of 7 μm, containing a two-layer TiN (2 μm) and TiCN (2 μm) with an upper TiN layer (3 μm), had high wear resistance, but coatings with a thickness of about 9 μm showed low wear resistance due to poor adhesion. A similar TiN/TiCN/TiC coating was obtained by the authors of [44]. The results of tests for scratching and nanoindentation showed the best mechanical properties for a coating on a Ti6Al4V substrate with a hardness of 19.96 GPa and a critical load of 25 N.

It is known that increasing the thickness of the coating not only contributes to the prolongation of the service life but also seriously affects the adhesion between the coating and the substrate. The authors of [45] argue that a possible solution to this problem is the formation of a gradient structure and the composition of a multilayer coating. They deposited a 23.5 μm thick TiN/TiCN multilayer coating on silicon and steel (Figure 6a). It was found that the inner TiCN layers consisted of a mixture of the nanocrystalline TiCN phase and amorphous carbon, while the TiN layers had a nanocolumnar structure. According to the results of scratching and nanoindentation tests, the coating showed high adhesion and satisfactory hardness even at a thickness of 23.5 μm (29.0 N and 21.4 GPa), as can be seen from the sclerometric result in Figure 6b. The results of tribological tests showed that the wear resistance of such a coating did not decrease in comparison with other thin hard films, but its service life was extended due to its large thickness (> 11 hours). Figure 6c shows the friction curve of a TiN/TiCN multilayer coating. It is noticeable that the CoF of such a coating exhibits good performance and has some variation due to the composition of the transition layer and the friction surface [45].

Alloying TiCN coatings with different elements, such as O, Al, Si, Cr, Zr, Ag, etc., makes it possible to influence their mechanical properties. The introduction of oxygen into the TiCN coating increases their resistance to friction and corrosion, which is justified by the inertness of the oxide and the small atomic size of oxygen, which creates high hardness and compressive stress [46]. In [[47], [48], [49]], the authors studied the effect of the oxygen fraction in the reaction atmosphere during MS on the properties of the TiCN coating. The results seen in Table 1 show that the TiCNO coating obtained at an oxygen consumption of 4 sccm is characterized by the lowest WR and the highest nanohardness. A further increase in oxygen consumption led to a decrease in hardness, adhesion, and wear resistance. Olteanu C. and her colleagues [49] deposited a TiCNO coating in an Ar, $C_2H_2/(O_2 + N_2)$ atmosphere. During deposition, the working pressure was kept constant at about 0.4 Pa, and the bias voltage of the substrate was -70 V. In all cases, the deposition time was 1 hour. The maximum CoF values were recorded for coatings deposited at a $C_2H_2/(O_2 + N_2)$ flux ratio of about 2.5.
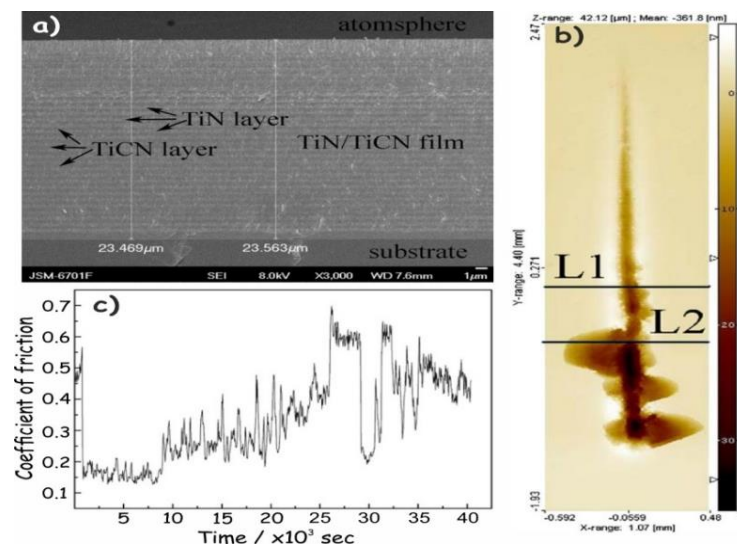
Figure 6 - SEM images of a cross-section (a), micrograph of a scratch (b) and a friction curve (c) of a multilayer TiN/TiCN coating [45]

The authors [50] obtained (Zr, Ti)CN coatings for medical applications by MS of two targets of Zr and Ti (purity 99.99 %). The substrates were placed at a distance of 17 cm from the targets, rotating them at a speed of 30 rpm. The reactive atmosphere was a mixture of N_2, CH_4, and Ar gases. It was found that the coatings have a composite structure in which the crystalline phase (Zr, Ti)CN coexists with the amorphous phase C. The measured thickness and hardness of the coating were in the ranges of 1.8-2.1 µm and 25-29 GPa, respectively.

Works [[51], [52], [53]] have focused on the study of TiSiCN nanocomposite coatings due to their excellent mechanical and tribological properties. Thus, the aim of work [51] was to compare the microstructural, mechanical, and tribological properties of TiSiCN coatings obtained by MS and plasma enhanced magnetron sputtering (PEMS) under practically identical conditions on Custom-450 and Ti-6Al-4V stainless steel for gas and steam turbines. During the deposition of both MS and PEMS, two Ti target magnetrons were used in an argon-nitrogen-trimethyl silane gas mixture. The results showed that the surface microhardness of the PEMS coating (24.65 GPa) is twice as high as that of the MS coating (11.77 GPa), which provided a much lower WR during the sliding and erosion rate of the TiSiCN coating (Figure 7a). In a study [52], TiSiCN coatings were deposited by PEMS in an Ar + N_2 + C_2H_2 atmosphere with the addition of two types of silicon precursors: gaseous trimethylsilane (TMS - $(CH_3)_3SiH$) and hexamethyldisilazane liquid (HMDSN - $(CH_3)6Si_2NH$). The flow rate for TMS was 0, 1.5, 3, 6, and 9 sccm, and for HDMSN it was maintained at 3 g/h. TiSiCN coatings obtained at a TMS flow rate of 6 and 9 sccm and for an HMDSN liquid of 3 g/h showed high wear resistance (Figure 7b).

A comparative study of the structure and properties of Al- and Cr-doped TiSiCN coatings was performed by the authors of [53]. The deposition of coatings was performed in a gas mixture of argon and nitrogen at a pressure of 0.1 Pa using targets made of TiAlSiCN and TiCrSiCN. The current and voltage supplied to the magnetron were 2 A and 500 V, respectively. The bias voltage of the substrate was -50 V, and the substrate temperature was kept constant at 300 °C (for TiCrSiCN coating) and 500 °C (for TiAlSiCN coating). To assess the thermal stability and resistance to oxidation, the coatings were annealed in vacuum at 1000, 1100, 1200, and 1300 °C or in the air at 1000 °C for 1 h. The results obtained show that the hardness of TiAlSiCN coatings increased from 41 to 46 GPa, reaching a maximum at 1000 °C, and then slightly decreased to 38 GPa at 1300 °C. TiCrSiCN coatings have demonstrated high thermal stability up to 1100 °C at a hardness above 34 GPa. TiAlSiCN coatings were more resistant to oxidation than TiCrSiCN coatings.

Tillmann W. et al. [54] compared TiAlCN coatings obtained by MS and high-power impulse magnetron sputtering (HiPIMS). The results showed that all MS coatings showed better adhesion than their HiPIMS counterparts. After that, the same authors presented the following study [55], where TiAlCN coatings were deposited using hybrid (MS/HiPIMS) technology with increasing acetylene flow. The results of tribological studies have shown that CoF does not depend as much on the carbon content as on the sliding speed and normal load.

Table 1 - Gas flow rate and some properties of TiCNO coatings [47]

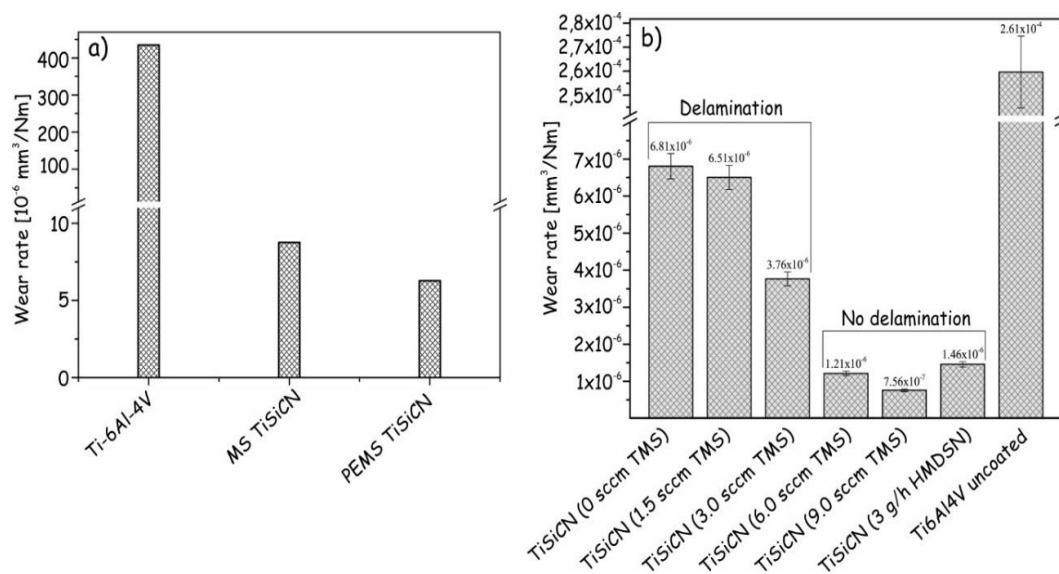| N_2 flow rate (sccm)	O_2 flow rate (sccm)	Hardness (GPa)	Adhesion (load, N)	C:N:O	Coating color
22	0	26	54	1:2:0	Pink brown
20	2	30	60	1:3.8:0.2	Pink purple
18	4	32	65	1:3.5:0.4	Red brown
16	6	30	45	1:5:0.4	Yellow brown
14	8	29	40	1:3.5:0.5	Red brown
12	10	24	38	1:3.5:0.6	Gray brown

Figure 7 - Wear rate of TiSiCN coating depending on: (a) deposition method [42], (b) silicon precursor flow [52]

It is known about alloying TiCN coating with silver [56] and deposition of the surface layer of hydroxyapatite (HA) [57] for use in biomedicine. In [56], the characteristics of thin coatings based on silver-containing carbonitrides (Ag-TiCN) obtained by DCMS were studied. The Ag content in the coatings was varied from 0 to 26.7 at. % by changing the targets and the proportion of C_2H_2 and N_2 in the gas mixture with Ar. As a result, when the Ag/Ti ratio was below 0.20, coatings were obtained with high mechanical properties (hardness ~ 18 GPa, WR ~ 10^{-6} mm^3/Nm, CoF ~ 0.3) and good biocompatibility. Thampi A. and her colleagues [57] deposited a HA layer on top of TiCN coatings, which were obtained using DCMS by deposition on substrates of medical grade 316 L SS. This study proves that HA-TiCN can provide better surface properties when used as a biocompatible coating on implant material.

Table 2 lists the target and substrate materials, deposition parameters, and tribological characteristics of some TiCN-based coatings published in the literature. The table shows the best selective tribological characteristics of the coating in the results of one work, regardless of the sample. From the data, it can be said that TiCN coatings deposited by sputtering a combined C/Ti target (~10^{-14} mm^3/Nm) have the best wear resistance [[17], [21]]. The best wear characteristics in terms of CoF were 0.06 [23].

Thus, studies on TiCN coatings indicate that their properties can be significantly affected by alloying them with different elements.

Table 2 - Deposition parameters of a TiCN-based coating by the MS method and its influence on the coating results

Coating	Deposition materials and parameters				Coating results			Reference
	Target material and	Target material and subject to the impact	Working gas atmosphere and flow	Working pressure, Pa	Coating thickness, μm	Coefficient of friction of the coating	Wear rate of the coating, mm^3/Nm	

	sputtering type							
TiCN	Ti RF	Steel XC38 and Si (100) U = 0,-30, -70, -100 B	Ar : 8 sccm N_2 : 4 sccm CH_4 : 4 sccm	1.33	2-4	0.13 and higher	1.12×10^{-4}	[15]
TiCN	C/Ti DC	Si (100) T = 200 °C U = -100 B	Ar/N_2 = 30 sccm N_2 = 0, 10, 20, 30 sccm	0.3	0.5	0.13 and higher	7.3×10^{-14}	[17]
TiCN	Ti DC	Steel T = 450 °C	Ar/N_2 = 50%/50% C_2H_2	10^{-3}	1.7	0.14 and higher	0.5×10^{-3}	[18]
TiCN	Ti DC	Steel T = 450 °C	Ar/N_2 = 50%/50% C_2H_2	0.1	–	0.14 and higher	0.8×10^{-6}	[19]
TiCN	C/Ti DC	Steel W6Mo5Cr4V2 T = 200 °C U = -80 B	Ar :4 sccm N_2 : 4 sccm	0.4	1.2	0.12 and higher	0.67×10^{-14}	[21]
TiCN	Ti DC	Titanium VT6 U = 0, -70, -100 B	Ar : 18 sccm N_2 : 2.6 sccm C_2H_2 : 4.6 sccm	0.4	0.8-1.4	0.06 (average)	1.4×10^{-6}	[23]
TiCN	Ti RF	Carbide-grade H-21 U = -90 B	$Ar/N_2/C_2H_2$	–	2.3	0.14	1.83×10^{-12}	[26]
TiCN	Ti RF	Steel XC38 U = 0-100 B	Ar: 8 sccm N_2: 4 sccm CH_4: 4 sccm	–	–	0.13	–	[27]
TiCN	Ti	WC	$Ar/N_2/CH_4$	0.8	3	0.2 (average)	–	[35]
TiCN	Ti, Al RF/DC	Ti6Al4V U = -80 B	Ar: 15 sccm N_2	0.6	~2	0.16	–	[37]
TiCN	TiC	Si (100), steel AISI 1045 T = 250 °C	Ar: 50 sccm N_2: 16 sccm	1.4	–	0.75 and higher	0.125×10^{-12}	[38]
TiN/TiCN/TiC	Ti DC	Ti and Ti6Al4V, Si U = -60 B	$Ar/N_2/C_2H_2$	0.3	1.7	0.1 and higher	–	[44]
TiN/TiCN	Ti DC	Steel 2520-310S and Si (100) T = 40-100 °C U = -100 B	Ar : 20 sccm N_2 : 0-6 sccm CH_4 : 0-10 sccm	0.4	23.5	0.15 and higher	–	[45]
TiCNO	Ti	Steel AISI 316 T = 260 °C	CO_2/N_2	0.1	~1	0.1 and higher	–	[46]
TiCNO	Ti DC	Steel M2 T = 300 ºC U = - 60 B	O/N_2 = 22 sccm N_2 = 22, 20, 18, 16, 14, 12 sccm, C_4H_{10}	0.44	3	0.2 and higher	1×10^{-9}	[47]
TiCNO	Ti DC	Steel M2 T = 200 °C U = - 70 B	$Ar/N_2+O_2 /C_2H_2$	0.4	–	0.2 and higher	2.47×10^{-6}	[49]
TiSiCN	Ti PEMS	Ti-6Al-4V and steel Custom-450 T = 400 °C U = - 40 B	$Ar/N_2/TMS$ N_2 : 45 sccm TMS : 6 sccm	10^{-4}	29.8	0.2 and higher	6.26×10^{-6}	[51]
TiSiCN	Ti PEMS	Ti-6Al-4V T = 200 °C U = - 60 B	Ar :190 sccm, N_2 : 45 sccm C_2H_2 : 30 sccm TMS : 0-9 sccm	0.4	8-10	0.15 and higher	7.5×10^{-7}	[52]
TiSiCN	Ti, Si, C	Si (100)	Ar/N_2=70%/30%	0.53	0.4-2.0	0.4 and higher	–	[60]

	DC	T = 500 °C						
TiCrSiCN	TiCrSiCN DC	WC, Si (100), Ni foil, Al_2O_3 T = 500 ºC U = - 50 B	Ar	0.1	1	0.4-0.45	1.5×10^{-6}	[53]
TiAlSiCN	TiAlSiCN DC	WC, Si (100), Ni foil, Al_2O_3 T = 300 °C U = - 50 B	Ar	0.1	1.7	0.5 and higher	6×10^{-6}	[53]
TiAlSiCN	TiAlSiCN DC	Si and Ni T = 500 °C U = - 250 B	Ar + 15% N_2	0.2	–	0.5 and higher	2.9×10^{-6}	[62]
TiAlCN	Ti DC	Steel AISI H11 T = 425 °C U = - 100 B	Ar: 295 sccm Kr: 200 sccm C_2H_2 : 20 sccm N_2	5×10^{-2}	3	~ 0.78	3.1×10^{-6}	[54]
TiAlCN	Ti HiPIMS	Steel AISI H11 U = - 80 B	Ar: 295 sccm Kr: 200 sccm C_2H_2 : 15 sccm N_2	5×10^{-2}	3	~ 0.4	1.5×10^{-6}	[54]
TiAlCN	Ti, Al, C DC	Steel AISI 316 and Si (111)	Ar/N_2=70%/30%	0.4	–	0.25 and higher	8×10^{-6}	[61]
TiAlN/ TiAlCN	Ti, TiAl48-12 MS/HiPIMS	Steel AISI H11 U = - 80 B	Ar: 295 sccm Kr: 200 sccm C_2H_2 : 5 и 10 sccm N_2	5×10^{-2}	–	0.5 and higher	1.42×10^{-6}	[55]
TiBCN	TiBC DC	Steel AISI 304 and Si (100) U = - 50 B	Ar+N_2: 20 sccm N_2: 0-7 sccm	0.27	2-3	0.54 and higher	2×10^{-6}	[58]
WTiCoCN	Ti (DC) WC (RF)	Steel H13 and Si (100) U = - 50 B	Ar/N_2	0.13	–	0.2 (average)	5×10^{-7}	[59]

Conclusions

Titanium carbonitride coatings are characterized by high wear resistance, relatively low coefficient of friction in various media, and corrosion resistance. This makes them promising for a wider application on the working surfaces of parts in the friction units of various mechanisms, on the surfaces of implants, as protective coatings providing corrosion protection at different temperatures.

Magnetron sputtering is a well established technique for the deposition of thin TiCN coatings, which is flexible, has a wide range of possibilities, and ensures a high level of adhesion of the coatings on the substrate. If you vary the ratio and composition of the reaction gases, the composition of the atomized target, the bias voltage on the substrate, the parameters of the current fed to the magnetron, and the number of magnetrons, you can vary the composition of the deposited coatings in a wide range, introduce alloying elements and deposit multilayer coatings. Such coatings are characterized by different levels of properties, including mechanical and tribological.

Further developments in the method of magnetron sputtering can relate to the upgrades of the method (HiPIMS, PEMS, RF and DC combined MS and others), which open up new possibilities for designing the microstructure and tuning the mechanical properties of TiCN-based coatings.

In addition, the elemental inclusion during alloying of TiCN coatings makes it possible to increase the tribological and mechanical properties. In the future, a number of elements such as O, Al, Cr, Si will be promising alloying elements that provide high wear resistance. However, to date, there is no universal TiCN coating that meets all the

requirements and is characterized by high tribotechnical characteristics in various environments. This indicates the need for further studies and, in particular, to investigate the effect of alloying with various elements on the properties of such coatings.

Магнетронды тозаңдату әдісімен титан карбонитридті жабындарын отырғызу және оның трибо-механикалық қасиеттеріне әсері

Мамаева А.А., Кенжегулов А.К., Паничкин А.В., Кшибекова Б.Б., Бахытулы Н.

«Металлургия және кен байыту институты» АҚ, Сәтбаев университеті, Алматы, Қазақстан

ТҮЙІНДЕМЕ

Техникадағы металл бөлшектер көбінесе тозудан туындаған зақымдардың салдарынан сәтсіздікке ұшырайды, бұл өнімнің функционалдығын жоғалтуға әкеледі. Бөлшектердің тозуға төзімділігі мен қызмет ету мерзімін арттыру үшін тиімді деп саналатын нитридті жұқа қатты жабындар қолданылады. Мақалада магнетронды тозаңдандыру әдісімен титан карбонитридінің тозуға төзімді жабындарын алу саласындағы қазіргі заманғы әдебиеттерге қысқаша шолу жасалды. Әдеби шолуда тозаңдандыру параметрлері мен жабындарды алу шарттарына байланысты алынған ғылыми нәтижелерді егжей-тегжейлі бағалау ұсынылды. Магнетронды тозаңдату әдісімен және оның модификацияларымен алынған жабындардың үйкеліс коэффициенті, жабынды мен контртелдің тозу жылдамдығы, наноқаттылық және адгезия күші нәтижелері көрсетілген. Легирленген элементтердің титан карбонитриді жабындарының механикалық және трибологиялық қасиеттеріне әсері қарастырылады. Жақсартылған тозу сипаттамалары бар титан карбонитридті жабындарды алу саласындағы соңғы жетістіктер талқыланды.

Түйін сөздер: титан карбонитриді, магнетрондық тозаңдандыру, жабынды, тозуға төзімділік, үйкеліс коэффициенті.

	Авторлар туралы ақпарат:
Мамаева Аксауле Алиповна	*Қауымдастырылған профессор, физика-математика ғылымдарының кандидаты, металтану зертханасының меңгерушісі, «Металлургия және кен байыту институты» АҚ, Алматы, Казахстан. ORCID ID: 0000-0002-9659-8152. Email: a.mamayeva@satbayev.university*
Кенжегулов Айдар Карауулович	*PhD, Ғылыми қызметкер, «Металлургия және кен байыту институты» АҚ, Алматы, Казахстан. ORCID ID: 0000-0001-7001-2654. Email: a.kenzhegulov@satbayev.university*
Паничкин Александр Владимирович	*Технических ғылымдардың кандидаты, заведующий Национальной научной лабораторией, АО «Институт металлургии и обогащения», Алматы, Казахстан. ORCID ID: 0000-0002-2403-8949. Email: a.panichkin@satbayev.university*
Кшибекова Балжан Булатовна	*Ғылыми қызметкер, «Металлургия және кен байыту институты» АҚ, Алматы, Казахстан. ORCID ID: 0000-0002-5944-7865. Email: b.kshibekova@satbayev.university*
Бахытулы Наурызбек	*Кіші ғылыми қызметкер, «Металлургия және кен байыту институты» АҚ, Казахстан. ORCID ID: 0000-0003-3087-0616. Email: n.bakhytuly@satbayev.university*

Осаждение покрытий карбонитрида титана методом магнетронного распыления и его влияние на трибо-механические свойства

Мамаева А.А., Кенжегулов А.К., Паничкин А.В., Кшибекова Б.Б., Бахытулы Н.

АО «Институт металлургии и обогащения», Satbayev University, Алматы, Казахстан

АННОТАЦИЯ

Металлические детали в технике часто выходят из строя в результате повреждений, вызванных износом, что приводит к потере функциональности изделий. С целью повышения износостойкости и срока службы деталей используют тонкопленочные твердые нитридные покрытия, считающиеся эффективными. В статье представлен краткий обзор современной литературы в области получения износостойких покрытий карбонитрида титана методом магнетронного распыления. В обзоре представляется детальная оценка полученных научных результатов в зависимости от параметров напыления и условий получения покрытий. Показаны результаты коэффициента трения, скорости износа покрытия и контртела, нанотвердости и силы адгезий покрытий, полученные методом магнетронного распыления и его модификациями. Рассматривается влияние легирующих элементов на механические и трибологические свойства покрытий карбонитрида титана. Обсуждаются последние достижения в области получения покрытий из карбонитрида титана с улучшенными характеристиками износа.

Ключевые слова: карбонитрид титана, магнетронное распыление, покрытие, износостойкость, коэффициент трения.

Информация об авторах:

Мамаева Аксауле Алиповна	*Ассоциированный профессор, кандидат физико-математических наук, заведующий лабораторией металловедения. АО «Институт металлургии и обогащения», Алматы, Казахстан. ORCID ID: 0000-0002-9659-8152. Email: a.mamayeva@satbayev.university*
Кенжегулов Айдар Караулович	*PhD, Научный сотрудник, АО «Институт металлургии и обогащения», Алматы, Казахстан. ORCID ID: 0000-0001-7001-2654. Email: a.kenzhegulov@satbayev.university*
Паничкин Александр Владимирович	*Кандидат технических наук, заведующий Национальной научной лабораторией, АО «Институт металлургии и обогащения», Алматы, Казахстан. ORCID ID: 0000-0002-2403-8949. Email: a.panichkin@satbayev.university*
Кшибекова Балжан Булатовна	*Научный сотрудник, АО «Институт металлургии и обогащения», Алматы, Казахстан.ORCID ID: 0000-0002-5944-7865. Email: b.kshibekova@satbayev.university*
Бахытулы Наурызбек	*Младший научный сотрудник, АО «Институт металлургии и обогащения», Алматы, Казахстан. ORCID ID: 0000-0003-3087-0616. Email: n.bakhytuly@satbayev.university*

References

[1] Ceschini L, Lanzoni E, Palombarini G, Sambogna G. Frictional behaviour and wear resistance of TiN-based PVD coatings dry sliding against a TiN coated tool steel. Metallurgia Italiana. 1999;91:45-51.

[2] Rodriguez RJ, Garcia JA, Medrano A, Rico M, Sanchez R, Martinez R, Labrugere C, Lahaye M, Guette A. Tribological behaviour of hard coatings deposited by arc-evaporation PVD. Vacuum 2002;67:559-566. https://doi.org/10.1016/s0042-207x(02)00248-8

[3] Yeshmanova GB, Smagulov DU, Blawert C. Plasma electrolytic oxidation technology for producing protective coatings of aluminum alloys. Complex Use of Mineral Resources. 2021;2(317):78-93. https://doi.org/10.31643/2021/6445.21

[4] Ramazanova JM, Zamalitdinova MG. Physical and mechanical properties investigation of oxide coatings on titanium. Complex Use of Mineral Resources 2019;2:34-41. https://doi.org/10.31643/2019/6445.14

[5] Kozyreva LV, Fadeev OV, Yudin AO. The algorithm of development safe methods for depositing metallic coatings by CVD-method of organometallic compounds. Complex Use of Mineral Resources 2020;1(312):5-10. https://doi.org/10.31643/2020/6445.01

[6] Uskenbayeva AM, Aubakirova RK, Panickin AV, Dzhumabekov DM. Polucheniye misheney na osnove alyuminidnykh sistem dlya magnetronnogo osazhdeniya zharostoykikh pokrytiy [Preparation of targets based on aluminide systems for magnetron deposition of heat-resistant coatings]. Kompleksnoe Ispol'zovanie Mineral'nogo Syr'a = Complex Use of Mineral Resources 2017;4:49-56. (in Russ.).

[7] Kapsalamova FR, Kenzhaliyev BK, Mironov VG, Krasikov SA. Structural and phase transformations in wear resistant Fe-Ni-Cr-Cu-Si-B-C coatings. Journal of the Balkan Tribological Association 2019;25:95-103.

[8] Arndt M, Westphal H. Influence of residual stresses and nanostructure on the properties and applications of PVD coatings. In: Institute of Production Engineering and Machine Tools, organizer. Proceedings of the 7th International Conference "THE Coatings" in Manufacturing Engineering and EUREKA partnering event; 2008 October 1-3; Kallithea of Chalkidiki, Greece. p. 151-155.

[9] Sagdoldina Zh, Skakov M, Rahadilov B, Zhadyranova A. Struktura poverkhnosti bystrorezhushchey stali R6M5 posle elektronno-luchevoy obrabotki [Preparation of TiN/Al2O3 coatings by mechanical fusion]. Kompleksnoe Ispol'zovanie Mineral'nogo Syr'a = Complex Use of Mineral Resources 2017;3:47-53. (in Russ.).

[10] Zhang GJ, Li B, Jiang BL, Chen DC, Yan FX. Microstructure and mechanical properties of multilayer Ti(C,N) films by closed-field unbalanced magnetron sputtering ion plating. Material Science Technology 2010;26:119-124.

https://doi.org/10.1016/s1005-0302(10)60019-9

[11] Martinez-Martinez D, Sanchez-Lopez JC, Rojas TC, Fernandez A, Eaton P, Belin M. Structural and microtribological studies of Ti-C-N based nanocomposite coatings prepared by reactive sputtering. Thin Solid Films 2005;472:64-70. https://doi.org/10.1016/j.tsf.2004.06.140

[12] Sedira S, Achour S, Avci A, Eskizeybek V. Physical deposition of carbon doped titanium nitride film by DC magnetron sputtering for metallic implant coating use. Applied Surface Science 2014;29515:81-85. https://doi.org/10.1016/j.apsusc.2014.01.010

[13] Anusha TVV, Subramanian B. Enhancement of bioactivity of pulsed magnetron sputtered TiCxNy with bioactive glass (BAG) incorporated polycaprolactone (PCL) composite scaffold. Journal of Alloys and Compounds 2015;649:1210-1219. https://doi.org/10.1016/j.jallcom.2015.06.250

[14] Bunshah RF. Handbook of Hard Coatings Deposition Technologies, Properties and Applications, Norwich: Noyes Publications / William Andrew Publishing LLC;2001.

[15] Saoula N, Madaoui N, Tadjine R, Erasmus RM, Shrivastava S, Comins JD. Influence of substrate bias on the structure and properties of TiCN films deposited by radio-frequency magnetron sputtering. Thin Solid Films 2016;616:521-529. https://doi.org/10.1016/j.tsf.2016.08.047

[16] Auciello O, Engemann J. Multicomponent and multilayered thin films for advanced microtechnologies: techniques, fundamentals and devices, Bad Windsheim: NATO ASI Series, Springer;1993.

[17] Chen R, Tu JP, et al. Microstructure, mechanical and tribological properties of TiCN nanocomposite films deposited by DC magnetron sputtering. Surface & Coatings Technology 2011;205:5228-5234. https://doi.org/10.1016/j.surfcoat.2011.05.034

[18] Polcar TR, Novak P, Siroky P. The tribological characteristics of TiCN coating at elevated temperatures. Wear. 2006;260:40-49. https://doi.org/10.1016/j.wear.2004.12.031

[19] Polcar T, Kubart T, Novak R, Kopecky L, Siroky P. Comparison of tribological behaviour of TiN, TiCN and CrN at elevated temperatures. Surface & Coatings Technology 2005;193:192-199. https://doi.org/10.1016/j.surfcoat.2004.07.098

[20] Schneider JM et al. X-Ray diffraction investigations of magnetron sputtered TiCN coatings. Surface and Coatings Technology 1995;74:312-319. https://doi.org/10.1016/0257-8972(95)08238-7

[21] Senna LF et al. Structural, chemical, mechanical and corrosion resistance characterization of TiCN coatings prepared by magnetron sputtering. Surface and Coatings Technology 1997;94-95:390-397. https://doi.org/10.1016/s0257-8972(97)00447-7

[22] Zheng XH, Tu JP, Gu B, Hu SB. Preparation and tribological behavior of TiN/a-C composite films deposited by DC magnetron sputtering. Wear 2008;26:261-265. https://doi.org/10.1016/j.wear.2007.10.007

[23] Mamaeva A, Kenzhegulov A, Panichkin A, Alibekov Z, Wieleba W. Effect of Magnetron Sputtering Deposition Conditions on the Mechanical and Tribological Properties of Wear-Resistant Titanium Carbonitride Coatings. Coatings 2022;12(2):193. https://doi.org/10.3390/coatings12020193

[24] Kenzhegulov, A.K.; Mamayeva, A.A.; Panichkin, A.V. Adgezionnyye svoystva kaltsiy-fosfatnykh pokrytiy na titane [Adhesion properties of calcium phosphate coatings on titanium]. Kompleksnoe Ispol'zovanie Mineral'nogo Syr'a = Complex Use of Mineral Resources 2017;3:35-41. (in Russ.).

[25] Saoula N, Madaoui N, Ait Djafer AZ, Annou K, Tadjine R, Shrivastava S, Erasmus RM, Comins JD. Mechanical proprieties of TiN, TiC and TiCN coatings deposited by magnetron sputtering deposition technique. In: Tampere University of Technology, organizer. Surface modification technologies XXVIII proceedings of the Twenty Eighth International Conference on Surface Modification Technologies; 2014 June 16-18; Tampere, Finland. p. 521-530.

[26] Bull SJ, Bhat DG, Staia MH. Properties and performance of commercial TiCN coatings. Part 2: tribological performance. Surface and Coatings Technology 2003;163-164:507-514. https://doi.org/10.1016/s0257-8972(02)00651-5

[27] Mechri H, Saoula N, Madaoui N. Friction and wear behaviors of TiCN coating treated by R.F magnetron sputtering. In: Research Center in Industrial Technologies CRTI, organizer. 7th African Conference on Non Destructive Testing ACNDT 2016 & the 5th International Conference on NDT and Materials Industry and Alloys (IC-WNDT-MI); 2016 July 31; Algiers, Algeria p. 16-20.

[28] Alfonso E, Olaya J, Cubillos G. Crystallization – Science and Technology. Rijeka:InTech, 2012.

[29] Sarakinos K, Alami J, Konstantinidis S. High power pulsed magnetron sputtering: A review on scientific and engineering state of the art. Surf Coat Technol 2010;204:1661-1684. https://doi.org/10.1016/j.surfcoat.2009.11.013

[30] Zhang GJ, Li B, Jiang BL, Yan FX, Chen DC. Microstructure and tribological properties of TiN, TiC and Ti (C, N) thin films prepared by closed-field unbalanced magnetron sputtering ion plating. Appl Surf Sci 2009;255:8788-8793. https://doi.org/10.1016/j.apsusc.2009.06.090

[31] Martinez-Martinez D, Lopez-Cartes C, Justo A, Fernandez A, Sanchez-Lopez JC, Garcia-Luis A, Brizuela M, Onate JI. Tailored synthesis of TiC∕a-CTiC∕a-C nanocomposite tribological coatings. Vac Sci Technol A 2005;23:1732-1736. https://doi.org/10.1116/1.2101810

[32] Sanchez-Lopez JC, Martinez-Martinez D, Abad M.D, Fernandez A. Metal carbide/amorphous C-based nanocomposite

coatings for tribological applications. Surf Coat Technol 2009;204:947-954. https://doi.org/10.1016/j.surfcoat.2009.05.038

[33] Saoula N, Henda K, Kesri R, Shrivastava S, Erasmus RM, Comins JD. Effect of the plasma deposition parameters on the properties of Ti/TiC multilayers for hard coatings applications. Acta Physica Polonica A 2012;121:172-174. https://doi.org/10.1063/1.2999950

[34] Saoula N, Djerourou S, Yahiaoui K, Henda K, Kesri R, Erasmus RM, Comins J.D. Study of the deposition of Ti/TiN multilayers by magnetron sputtering. Surf. Interface Anal 2010;42:1176-1179. https://doi.org/10.1002/sia.3299

[35] Wang Q, Zhou F, Chen K, Wang M, Qian T. Friction and wear properties of TiCN coatings sliding against SiC and steel balls in air and water. Thin Solid Films 2011;519:4830-4841. https://doi.org/10.1016/j.tsf.2011.01.038

[36] Santecchia E, Zalnezhad E, Hamouda AMS, Musharavati F, Cabibbo M, Spigarelli S. Wear resistance investigation of titanium nitride-based coatings. Ceramics International 2015;41:10349-10379. https://doi.org/10.1016/j.ceramint.2015.04.152

[37] Danısman S, Odabas D, Teber M. The Effect of Coatings on the Wear Behavior of Ti6Al4V Alloy Used in Biomedical Applications, In: IOP Publishing, organizer. 9th International Conference on Tribology; 2017 September 13-15, Nevsehir, Turkey, p. 1-12.

[38] Correa JF, Aperador W, Caicedo JC, Alba NC, Amaya C. Structural, mechanical and tribological behavior of TiCN, CrAlN and BCN coatings in lubricated and nonlubricated environments in manufactured devices. Materials Chemistry and Physics 2020;252:123164. https://doi.org/10.1016/j.matchemphys.2020.123164

[39] Shi Y, Peng H, Xie Y, Xie G, Zhao Ch, Li S. Plasma CVD of hard coatings Ti(CNO) using metallo-organic compound Ti(OC3H7)4. Surface and Coatings Technology 2000;132:26-30. https://doi.org/10.1016/s0257-8972(00)00743-x

[40] Endler I, Hohn M, Herrmann M, Holzschuh H, Pitonak R, Ruppi S, van den Berg H, Westphal H, Wilde L. Aluminium-rich TiAlCN coatings by low pressure CVD. Surface & Coatings Technology 2010;205:1307-1312. https://doi.org/10.1016/j.surfcoat.2010.09.002

[41] Behrens BA, Huskic A. Reduction of wear on dies for precision forging of gears through multi-layer hard material coating (TiN-TiCN-TiC). Materialwiss Werkst 2005;36:218-225.

[42] Agudelo LC, Ospina R, Castillo HA, Devia A. Synthesis of Ti/TiN/TiCN coatings grown in graded form by sputtering DC. Phys Scr 2008;T131:1-3. https://doi.org/10.1088/0031-8949/2008/t131/014006

[43] Su YL, Kao WH. Tribological behavior and wear mechanisms of TiN/TiCN/TiN multilayer coatings. Mater Eng Perform 1998;7:601-612. https://doi.org/10.1361/105994998770347440

[44] Razmi A, Yeşildal R. Microstructure and mechanical properties of TiN/TiCN/TiC multilayer thin films deposited by magnetron sputtering. International Journal of Innovative Research and Reviews 2018;5(1):15-20. https://doi.org/10.20944/preprints201807.0127.v1

[45] Zheng J, Hao J, Liu X, Gong Q, Liu W. A thick TiN/TiCN multilayer film by DC magnetron sputtering. Surface & Coatings Technology 2012;209:110-116. https://doi.org/10.1016/j.surfcoat.2012.08.045

[46] Stanishevsky A, Lappalainen R. Tribological properties of composite Ti(N,O,C) coatings containing hard amorphous carbon layers. Surf Coat Technol 2000;123:101-105. https://doi.org/10.1016/s0257-8972(99)00514-9

[47] Hsieh JH, Wu W, Li C, Yu CH, Tan BH. Deposition and characterization of Ti(C,N,O) coatings by unbalanced magnetron sputtering. Surface and Coatings Technology 2003;163:233-237. https://doi.org/10.1016/s0257-8972(02)00494-2

[48] Hsieh JH, Tan ALK, Zeng XT. Oxidation and wear behaviors of Ti-based thin films. Surf Coat Technol 2006;201:4094-4098. https://doi.org/10.1016/j.surfcoat.2006.08.026

[49] Olteanu C, Munteanu D, Ionescu C, Munteanu A. Tribological characterisation of magnetron sputtered Ti(C, O, N) thin films. Int J Materials and Product Technology 2010;39:186-194. https://doi.org/10.1504/ijmpt.2010.034270

[50] Braic V, Braic M, Balaceanu M, Vladescu A, Zoita CN, Titorencu I, Jinga V. (Zr,Ti)CN coatings as potential candidates for biomedical applications. Surface & Coatings Technology 2011;206:604-609. https://doi.org/10.1016/j.surfcoat.2011.03.074

[51] Abd El-Rahman AM, Wei R. A comparative study of conventional magnetron sputter deposited and plasma enhanced magnetron sputter deposited Ti–Si–C–N nanocomposite coatings. Surface & Coatings Technology 2014;241:74-79. https://doi.org/10.1016/j.surfcoat.2013.08.049

[52] Hatem A, Lin J, Wei R, Torres RD, Laurindo C, Biscaia de Souza G, Soares P. Tribocorrosion behavior of low friction TiSiCN nanocomposite coatings deposited on titanium alloy for biomedical applications. Surface & Coatings Technology 2018;347:1-12. https://doi.org/10.1016/j.surfcoat.2018.04.049

[53] Shtansky DV, Kuptsov KA, Kiryukhantsev-Korneev PhV, Sheveiko AN, Fernandez A, Petrzhik MI. Comparative investigation of Al- and Cr-doped TiSiCN coatings. Surface & Coatings Technology 2011;205:4640-4648. https://doi.org/10.1016/j.surfcoat.2011.04.012

[54] Tillmann W, Grisales D, Stangier D, et al. Residual stresses and tribomechanical behaviour of TiAlN and TiAlCN monolayer and multilayer coatings by DCMS and HiPIMS. Surface & Coatings Technology 2021;406:126664. https://doi.org/10.1016/j.surfcoat.2020.126664

[55] Tillmann W, Grisales D, Tovar CM, Contreras E, Apel D, Nienhaus A, Stangier D, Lopes Dias NF. Tribological behaviour of low carbon-containing TiAlCN coatings deposited by hybrid (DCMS/HiPIMS) technique. Tribology International

2020;151:106528. https://doi.org/10.1016/j.triboint.2020.106528

[56] Sanchez-Lopez JC, Abad MD, Carvalho I, Escobar GR, et. all. Influence of silver content on the tribomechanical behavior on Ag-TiCN bioactive coatings. Surface & Coatings Technology 2012;206:2192-2198. https://doi.org/doi:10.1016/j.surfcoat.2011.09.059

[57] Thampi VVA, Dhandapani P, Manivasagam G, Subramanian B. Enhancement of bioactivity of titanium carbonitride nanocomposite thin films on steels with biosynthesized hydroxyapatite. International Journal of Nanomedicine 2015;10:107-118. https://doi.org/10.2147/IJN.S79976

[58] Lin J, Moore JJ, Mishra B, Pinkas M, Sproul W.D. The structure and mechanical and tribological properties of TiBCN nanocomposite coatings. Acta Materialia 2010;58:1554-1564. https://doi.org/10.1016/j.actamat.2009.10.063

[59] Ataie SA, Soltanieh M, Naghizadeh R, Ahmadi M, Ghanaatshoar M. Effects of substrate temperature and reactive gas flow rate on the crystalline ceramic phases formation and tribological properties of W–Ti–Co–C–N thin films produced by co-sputtering. Ceramics International 2020;46:29137-29149. https://doi.org/10.1016/j.ceramint.2020.08.087

[60] Onoprienko AA, Ivashchenko VI, Dub SN, Khyzhun OYu, Timofeeva II. Microstructure and mechanical properties of hard Ti–Si–C–N films deposited by dc magnetron sputtering of multicomponent Ti/C/Si target. Surface & Coatings Technology 2011;205:5068-5072. https://doi.org/10.1016/j.surfcoat.2011.05.009

[61] Zhang X, Qiu Y, Tan Zh, Lin J, Xu A, Zeng Y, Moore JJ, Jiang J. Effect of Al content on structure and properties of TiAlCN coatings prepared by magnetron sputtering. Journal of Alloys and Compounds 2014;617:81-85. https://doi.org/10.1016/j.jallcom.2014.08.009

[62] Kiryukhantsev-Korneev FV, Kuptsov KA, Sheveiko AN, Levashov EA, Shtansky DV. Wear Resistant Ti–Al–Si–C–N coatings produced by magnetron sputtering of SHS targets. Russian Journal of NonFerrous Metals 2013;54:330-335. https://doi.org/10.3103/s106782121304007x

Substantiation of the specific energy intensity of drilling as a criterion characterizing the explosive destruction of rocks on the example of the Koktaszhal deposit

Ozhigin S.G. [1], Chunuev I.K. [2], Musin R.A. [1], Tyan S.G. [1*]

[1] Karaganda Technical University, Karaganda, Kazakhstan
[2] Kyrgyz State University of Geology, Mining and Natural Resources Development named after Academician U.A. Asanaliev, Kyrgyzstan.

* Corresponding author email: info@geo-in.kz

ABSTRACT

Drilling and blasting operations are one of the most important components of the mining industry. Currently, further improvement and optimization of technological processes at mining enterprises are possible mainly due to the determination and constant monitoring of the mining and technological properties of the rock mass – their drillability, explosivity and exaviability. A prospective assessment of the explosivity of rocks in the massif, which is the basis for designing and calculating the parameters of the DBO, is currently possible only using the energy parameters of technological work. The article provides information on methods for studying the strength and elastic characteristics of rocks in natural occurrence. The results of the study of the relationship between the specific energy intensity of drilling and explosive destruction of rocks are presented. The correlation between the specific energy intensity of drilling and the propagation velocity of elastic longitudinal waves is also considered. A comparative analysis is carried out between the traditional calculation of the explosive index using the results of laboratory studies on the physical and mechanical properties of the rocks of the Koktaszhal deposit and the calculation of the explosive destruction index taking into account the energy parameters of drilling. The validity of the use of the specific energy intensity of drilling as a criterion characterizing the explosive destruction of rocks in the design of drilling and blasting operations is shown.

Keywords: Drillability, energy intensity of drilling, explosiveness, rock strength.

	Information about authors:
Ozhigin Sergey Georgievich	*Doctor of Technical Sciences, Professor. Karaganda Technical University, Karaganda, Kazakhstan. ORCID ID: 0000-0003-2432-3851. Email: osg62@mail.ru*
Chunuev Ishimbay Karybayevich	*Doctor of Technical Sciences, Professor. Kyrgyz State University of Geology, Mining and Natural Resources Development named after Academician U.A. Asanaliev, Bishkek, Kyrgyzstan. Email: ichunuev@gmail.com*
Musin Ravil Altavovich	*PhD, senior lecturer. Karaganda Technical University, Karaganda, Kazakhstan. ORCID ID: 0000-0002-1206-6889. Email: r.a.mussin@mail.ru*
Tyan Stanislav Georgievich	*Doctoral student, Karaganda Technical University, Karaganda, Kazakhstan. . ORCID ID: 0000-0002-3566-1437. Email: info@geo-in.kz*

Introduction

Drilling and blasting operations are one of the most important components of the mining industry. Every year, the volume of exploding rocks is only growing, which increases the demand for technologies that accelerate the design process and calculate the efficiency of the work performed. Currently, further improvement and optimization of technological processes at mining enterprises are possible mainly due to the determination and constant monitoring of the mining and technological properties of the rock mass – their drillability, explosivity and exaviability. A prospective assessment of the explosivity of rocks in the massif, which is the basis for designing and calculating the parameters of the DBO, is currently possible only using the energy parameters of technological work.

According to morphostructural features, physical and geographical conditions and technical and economic parameters, the Koktaszhal copper-porphyry deposit is planned to be worked out in an open-pit manner with a depth of 300 m.

As shown in [1], the surface of the industrial areas of the Koktaszhal mining and Processing Plant is represented by a rocky base covered in areas with covers with low power within 10-30 cm of delvial-proluvial deposits. The rocks are represented by strong silica tuffs, plagiogranitic porphyry and porphyry, silicic acid-invasive rocks, monochrome and quartz-shimmering chlorite rocks.

Components included in the mineral composition:

1. Quartz 43-45%,
2. Sour plagioclase 31 - 33 %,
3. Chloride 9 - 11 %,
4. Hydrosluda 8-10 %,
5. Dolomite 2 – 3 %.

Zones of tectonic disturbances are mostly filled with differently oriented quartz veins, which has a positive effect on the stability of rocks. Ores and host rocks of the deposit have the same strength properties due to the fact that mineralization has no pronounced boundaries and the mineral grains of the rocks have a dense structural-crystallization relationship between them. Groundwater within the mountain drainage in the weathering crust does not spread. In rock formations they are deep enough (10 - 30 m) and do not affect the change of engineering and geological properties of rocks. That is why the category of complexity of engineering and geological criteria for the development of the Koktaszhal site, according to the "Methodological guidelines for the study of mining and geological conditions of deposits of solid minerals" belongs to the simple. The contract area is characterized by strong differences. Ores and rocks are not sensitive to spontaneous combustion and swelling, are not radioactive [1].

The experimental part

For blasting a rock mass under ideal conditions, the main physical and mechanical characteristics of rocks are: strength ($\sigma_{сж}$, $\sigma_{раст.}$, $\sigma_{сд}$), strength coefficient - f, elastic wave velocity - V_p, density - γ. Tests on the strength and elastic properties of rocks were carried out on the cores of six geotechnical wells drilled along the contour of the quarry to its design depth.

The determination of the tensile strength under uniaxial compression was carried out according to Gost 21153.2 -84.

Figure 1 shows the essence of the main method for determining the maximum destructive force ($P_{сж}$), which is applied to the ends of the sample of the correct shape through steel flat plates.

Figure 1 - Testing of rocks for tensile strength under uniaxial compression on a press

The compressive strength of the rock ($\sigma_{сж}$) for each test sample was calculated by the formula:

$$\sigma_{сж} = k_в \cdot \frac{P_{сж}}{F_0} \cdot 10, \tag{1}$$

where - $P_{сж}$ is the total maximum load on the sample at the time of its destruction, kN;

$F_0 = (\pi/4) \cdot d^2$ - initial cross-sectional area of the sample, cm^2;

d – sample diameter, cm;

$k_в$ – the dimensionless height coefficient of the sample, equal to 1.00 with the ratio of height to diameter m = 2 ± 0.5. For other values of the ratio m, the coefficient $k_в$ was set according to Table 1.

Table 1 - Determination of the dimensionless coefficient $k_в$

m	0,7	0,80	0,90	1,00	1,20	1,40	1,60	1,80	2,00
$k_в$	0,68	0,72	0,76	0,80	0,86	0,90	0,94	0,97	1,00

Determination of the rock strength limit under uniaxial tension was carried out according to GOST 21153.3 – 85.

Figure 2 shows the essence of the method, which consists in determining the maximum destructive force ($P_{рас}$) applied perpendicular to the generatrix of a cylindrical rock sample, as a result of which tensile stresses arise in the sample, leading to its destruction in the plane of the longitudinal section.

Figure 2 - Testing of rocks for tensile strength under uniaxial tension

The tensile strength of the rock (σ_p) was calculated by the formula:

$$\sigma_p = \frac{P_{pac}}{d \cdot h} \cdot 10 \ ,\qquad (2)$$

where – (P_{pac}) is the maximum load on the sample at which the sample ruptured, kN;

d - is the diameter of the sample, cm;

h - is the height of the sample.

The coefficient of rock strength on the scale of M.M. Protodyakonov and is determined on pieces of rock with a size of 20-40 mm in the POK device by dropping weights weighing 2.5 kg from a height of 60 cm. The number of drops varies from 5 to 15. After crushing, the material is sieved through a 0.5 mm sieve and the volume of the crushed material is measured in a volume meter.

$$f = \frac{20 \times n}{h}\qquad (3)$$

where n – the number of kettlebell drops during the test of one hitch;

h – the height of the column of the fine fraction (after sieving on a sieve of 0.5 mm) in the volume meter after testing five attachments, mm;

20 - an empirical numerical coefficient that provides the generally accepted values of the strength coefficient and takes into account the work spent on crushing [2].

In preparation for measurements of elastic parameters of rocks, the end surfaces of the core were carefully sanded, their length strictly corresponded to 100 mm, diameter 48 mm, the ratio l/d ≥ 2 was observed, where d - is the diameter of the sample.

For laboratory studies of the propagation velocity of longitudinal and transverse waves, the measurement equipment and methods described in the literature [[4], [5], [6]] were used. A MATRIX Corp. high-frequency generator was used as instruments. MFG-8216 and digital storage oscilloscope (DSO) from ACUTE Tecn. DS 1002. Piezoelectric converters PRIZ-12 [3], (Figure 3) are used as converters.

«The main measurement parameter in determining the elastic properties of rocks is the acoustic delay time Δt of the front of the first half-period of the received signal pulse, which, at a constant value of the rock sample L = 100mm, allows us to determine the propagation velocity of
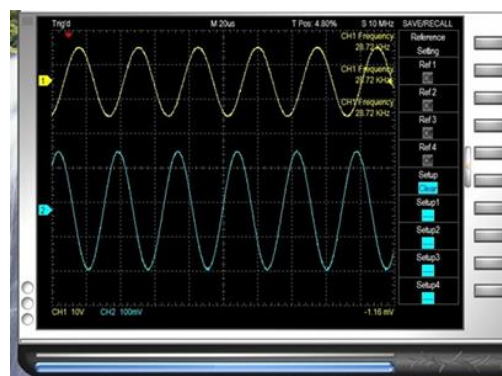

Figure 3 - Ultrasound examination method

the longitudinal wave Vp = L/ Δt. To determine the velocity of propagation of a transverse wave, a signal reception sensor (piezoelectric transducer - emitting or receiving) was located on the sample at an angle

$$90°Vs = L(90°)/ Δt,\qquad (4)$$

where L (90) - is the length of the sample, taking into account the displacement of sensors on the sample surface.

Figure 4 shows a block diagram of the measurement of elastic parameters by the pulse method».
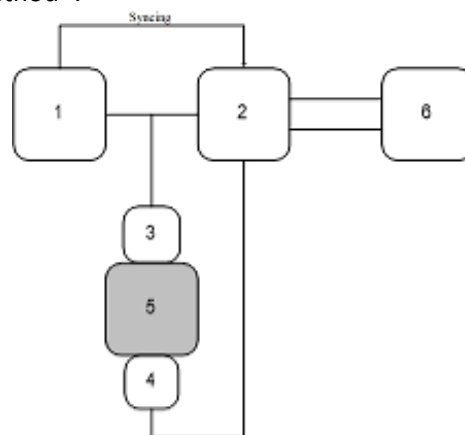
1 - generator; 2 - oscilloscope; 3 - radiating piezoelectric converter; 4 - receiving piezoelectric converter; 5 - acoustic load - rock sample made of core or reference; 6 - computer for data input and pulse observation.

Figure 4 - Block diagram of elastic parameters measurement by pulse method

«Laboratory tests for determining the density of rocks were carried out according to Gost 8269.0-97.

Also, the basic density in the framework of the experiment was determined by measuring the mass

Table 2 - Strength properties of rocks along the horizons

Horizon, m		γ, g/cm³	Ultimate strength			f	Wave speed	
from	to		$(\sigma_{сж})$, MPa	$(\sigma_{рс})$, MPa	$(\sigma_{сд})$, MPa		(V_p), m/sec	(V_s), m/sec
720	705	2,75	82,1	8,0	20,2	12	4548	2697
705	690	2,75	82,1	8,0	20,2	12	4548	2697
690	675	2,78	79,8	7,9	27,5	12	4552	2686
675	660	2,78	79,8	7,9	27,5	12	4552	2686
660	645	2,76	72,8	7,0	27,6	11	4139	2536
645	630	2,76	72,8	7,0	27,6	11	4139	2536
630	615	2,80	65,1	6,8	33,6	11	4212	2576
615	600	2,80	65,1	6,8	33,6	11	4212	2576

of a unit volume of solid pieces of rock using hydrostatic weighing scales.

The measurement of the average density (γ) of the test rock was carried out according to the formula:

$$\gamma = q/V, \ g/cm^3 \qquad (5)$$

where q – the mass of the sample, determined on technical scales with an accuracy of 0.01, g;

V – sample volume determined by hydrostatic weighing, cm³».

«3-5 parallel volume density determinations were performed for each sample. The arithmetic mean of all definitions was taken as the final test result.

The true (specific) density (γ_y) was determined by measuring the mass of a unit volume of crushed dried rock according to the formula:

$$\gamma_y = q_u/V_u, \ g/cm^3 \qquad (6)$$

where q_u – mass of the crushed sample (mineral part of the rock), g;

V_u – volume of crushed rock (mineral part of the rock), cm³.

Two parallel determinations of the true density were made for each rock, then the average value was calculated with an accuracy of 0.01 [2].

The results of the research are spread across the horizons and summarized in summary table 2.

To destroy the rock mass in the quarry, a drilling and blasting method is used, the main task of which is to ensure the necessary lumpiness of the rock mass (65% - dk ≤ 300 mm). Primary crushing is carried out by the method of borehole charges (mass explosions). Blast wells with a diameter of 215 mm are drilled using high-performance ball drilling rigs of the DML LPE 1600/110 brand. The development of the deposit is planned in an open way, with 15-meter ledges. Cutting of oversized items is carried out by the shpurov method, overhead and cumulative charges. The calculation of the design specific consumption of explosives was adopted according to the methodology proposed by Academician V.V. Rzhevsky [7]:

$$q_п = q_э К_т К_д К_{о.п.} К_з К_v К_{вв}, \qquad (7)$$

where $q_э$ - reference consumption of explosives [8]:

$$q_э = К_1(\sigma_{сж} + \sigma_{рс} + \sigma_{сд}) + К_2 \gamma g, \qquad (8)$$

$К_т$ - coefficient that takes into account the effect of fracturing of the mountain range,

$К_д$ - coefficient that takes into account the degree of crushing,

$К_{о.п.}$ - correction factor that takes into account the number of open surfaces,

$К_з$ - correction factor for the degree of charge concentration in the array,

$К_у$ - correction factor for the height of the ledge,

$К_{вв}$ - correction factor for the consumption of explosives, taking into account the required degree of crushing,

$К_1$ и $К_2$ – empirical coefficients [7].

Table 3 - Calculated values of the design specific consumption of explosives

Horizon, m		$q_э$	$K_т$	$K_д$	$K_{о.п.}$	$K_з$	$K_у$	$K_{вв}$	$q_п$ (g/cm³)
from	to								
720	705	0,124							**0,69**
705	690	0,124							**0,69**
690	675	0,124							**0,69**
675	660	0,124	0,45	1,667	4,750	1,026	1,000	1,533	**0,69**
660	645	0,120							**0,67**
645	630	0,120							**0,67**
630	615	0,106							**0,62**
615	600	0,106							**0,62**

It follows from the data obtained that the rocks forming horizons of 720-600 m at the Koktaszhal deposit belong to the average degree of explosivity and to the category of explosivity - II [9].

Discussion of the results

To substantiate the specific energy intensity of drilling as a universal criterion for the strength of rocks and massifs, it is necessary to compare it with the specific energy intensity of explosive destruction [10].

Comprehensive research in this direction in production conditions in the 70-80-ies of the 20th century was conducted by Professor I.A. Tangaev, as a result, the following was noted:

1. the specific consumption of BB- q (kg/m³) of energy q_e (Mcal /m³) is the coefficient of proportionality between the energy of the charge and its load, reflecting the strength properties of the medium:

$$Q=qV \qquad (9)$$

2. the relationship between the specific energy intensity of drilling - e (kW·h/m³) and explosive destruction - q_e (Mcal/m³) is approximated by the linear equation:

$$q_e=0,15+0,011e \qquad (10)$$

3. in accordance with the value e, kW·h/m, the value of the specific consumption of explosive q, kg/m³, can be calculated by the formula:

$$q_п=0,24e+0,16 \qquad (11)$$

There is an unambiguous dependence of the explosivity on the velocity of propagation of longitudinal waves in rocks.

This is due to the close correlation with such characteristics of the medium as density, fracturing, anisotropy, etc. [[10], [11]].

Applying data on the velocity of longitudinal waves of rocks of the Koktaszhal deposit and indicators of the specific energy intensity of drilling of rocks similar in lithological, strength and elastic properties, we determine the relationship between them. (Figure 5).
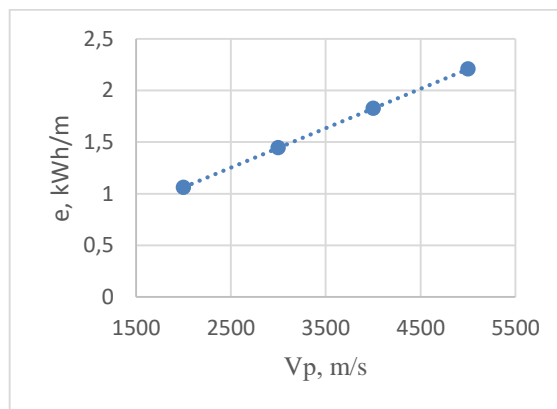

Figure 5 - The relationship between the specific energy intensity of drilling and the propagation velocity of elastic waves.

This dependence can be represented by the following linear function:

$$e=0.0004V_p+0,2967 \qquad (12)$$

Solving equations (12) and (11) together, we obtain the value of the specific explosive consumption q, kg/m³, taking into account the specific energy intensity of drilling. Table 4.

Table 4 - Calculated values of the design specific consumption of explosives

Horizon, m		Velocity of longitudinal waves (Vp), m/sec	Specific energy intensity of drilling, e, (kW·h/m)	Design specific consumption of explosive qп according to the Rzhevsky method (kg/m3)	Design specific consumption of explosive qп by drilling energy intensity, (kg/m³)	Difference, %
from	to					
720	705	4547,69	2,116	**0,69**	**0,68**	**-1,5**
705	690	4547,69	2,116	**0,69**	**0,68**	**-1,5**
690	675	4552,46	2,118	**0,69**	**0,67**	**-2,9**
675	660	4552,46	2,118	**0,69**	**0,67**	**-2,9**
660	645	4139,51	1,952	**0,67**	**0,63**	**-6,0**
645	630	4139,51	1,952	**0,67**	**0,63**	**-6,0**
630	615	4211,92	1,981	**0,62**	**0,64**	**3,2**
615	600	4211,92	1,981	**0,62**	**0,64**	**3,2**

Conclusions

Comparative analysis shows good convergence of the results and suggests the legitimacy of using the specific energy intensity of drilling as a criterion characterizing the explosive destruction of rocks.

It should be noted that the data under consideration on the strength and elastic properties of rocks were obtained by laboratory means in samples, which does not guarantee their identity in the array.

The use of specific energy capacities of drilling and blasting makes it possible to obtain information for each well directly on the block and, in accordance with the characteristics of the array, set or adjust the energy and detonation parameters of charges and geometric parameters of the location of wells.

Conflict of interest

On behalf of all the authors, the correspondent author declares that there is no conflict of interest.

Acknowledgements

Көктасжал кен орны мысалында тау жыныстарының жарылғыш бұзылуын сипаттайтын өлшем ретінде бұрғылаудың меншікті энергия сыйымдылығын негіздеу

Ожигин С.Г. [1], Чунуев И.К. [2], Мусин Р.А. [1], Тян С.Г. [1]

[1] Қарағанды Техникалық Университеті, Қарағанды, Қазақстан
[2] Қырғыз мемлекеттік Геология, тау-кен ісі және табиғи ресурстарды игеру университеті. академик Ө. А. Асаналиева, Қырғызстан.

ТҮЙІНДЕМЕ

Бұрғылау-жару жұмыстары Тау-кен өнеркәсібінің маңызды құрамдас бөлігі болып табылады. Қазіргі уақытта тау-кен кәсіпорындарындағы технологиялық процестерді одан әрі жетілдіру және оңтайландыру, негізінен, тау жыныстары массивінің тау – технологиялық қасиеттерін-олардың бұрғылануын, жарылғыштығын және эксавирациялануын анықтау және үнемі бақылау есебінен мүмкін болады. БВР параметрлерін жобалау мен есептеудің негізі болып табылатын массивтегі жыныстардың жарылғыштығын перспективалық бағалау қазіргі уақытта технологиялық жұмыстардың энергетикалық параметрлерін пайдалану арқылы ғана мүмкін болады. Мақалада тау жыныстарының табиғи жатыс кезіндегі беріктік

және серпімділік сипаттамаларын зерттеу әдістері туралы мәліметтер келтірілген. Бұрғылаудың нақты энергия сыйымдылығы мен тау жыныстарының жарылғыш бұзылуы арасындағы байланысты зерттеу нәтижелері келтірілген. Бұрғылаудың нақты энергия сыйымдылығы мен серпімді бойлық толқындардың таралу жылдамдығы арасындағы корреляциялық байланыс қарастырылған. "Көктасжал" кен орны жыныстарының физикалық-механикалық қасиеттері бойынша зертханалық зерттеулердің нәтижелерін пайдалана отырып, жарылғыштық көрсеткішінің дәстүрлі есебі мен бұрғылаудың энергетикалық параметрлерін ескере отырып, жарылғыштық көрсеткішінің есебі арасында салыстырмалы талдау жүргізілді. Бұрғылау-жару жұмыстарын жобалау кезінде тау жыныстарының жарылғыш бұзылуын сипаттайтын өлшем ретінде бұрғылаудың меншікті энергия сыйымдылығын пайдаланудың негізділігі көрсетілген.

Түйін сөздер: Бұрғылау, бұрғылаудың энергия сыйымдылығы, жарылғыштық, тау жыныстарының беріктігі.

Авторлар туралы ақпарат:	
Ожигин Сергей Георгиевич	*Техника ғылымдарының докторы, профессор. Қарағанды Техникалық Университеті, Қарағанды, Қазақстан. ORCID ID: 0000-0003-2432-3851. Email: osg62@mail.ru*
Чунуев Ишимбай Карыбаевич	*Техника ғылымдарының докторы, профессор. Қырғыз мемлекеттік Геология, тау-кен ісі және табиғи ресурстарды игеру университеті. академик Ө. а. Асаналиева, Бішкек, Қырғызстан. Email: ichunev@gmail.com*
Мусин Равиль Альтавович	*PhD, аға оқытушы. Қарағанды Техникалық Университеті, Қарағанды, Қазақстан. ORCID ID: 0000-0002-1206-6889. Email: r.a.mussin@mail.ru*
Тян Станислав Георгиевич	*Докторант, Қарағанды Техникалық Университеті, Қарағанды, Қазақстан. ORCID ID: 0000-0002-3566-1437. Email: info@geo-in.kz*

Обоснование удельной энергоемкости бурения как критерия, характеризующего взрывное разрушение горных пород на примере месторождения Коктасжал

Ожигин С.Г. [1], Чунуев И.К. [2], Мусин Р.А. [1], Тян С.Г. [1]

[1] *Карагандинский Технический Университет, Караганда, Казахстан*
[2] *Кыргызский государственный университет геологии, горного дела и освоения природных ресурсов им. академика У.А. Асаналиева, Кыргыстан*

АННОТАЦИЯ

Буровзрывные работы являются одной из важнейших составляющих горнодобывающей промышленности. В настоящее время дальнейшее совершенствование и оптимизация технологических процессов на горных предприятиях возможны преимущественно за счет определения и постоянного контроля горно-технологических свойств массива горных пород – их буримости, взрываемости и эксавируемости. Перспективная оценка взрываемости пород в массиве, являющаяся основой проектирования и расчетов параметров БВР, на данный момент возможна только с использованием энергетических параметров технологических работ. В статье приведены сведения о методах изучения прочностных и упругих характеристик горных пород в естественном залегании. Приведены результаты исследования взаимосвязи между удельной энергоемкостью бурения и взрывного разрушения горных пород. Также рассмотрена корреляционная зависимость между удельной энергоемкостью бурения и скоростью распространения упругих продольных волн. Проведен сравнительный анализ между традиционным расчетом показателя взрываемости с использованием результатов лабораторных исследований по физико-механическим свойствам пород месторождения «Коктасжал» и расчетом показателя взрывного разрушения с учетом энергетических параметров бурения. Показана обоснованность использования удельной энергоемкости бурения как критерия, характеризующего взрывное разрушение горных пород при проектировании буровзрывных работ.

Ключевые слова: Буримость, энергоемкость бурения, взрываемость, прочность пород.

Информация об авторах:	
Ожигин Сергей Георгиевич	*Доктор технических наук, профессор. Карагандинский Технический Университет, Караганда, Казахстан. ORCID ID: 0000-0003-2432-3851. Email: osg62@mail.ru*
Чунуев Ишимбай Карыбаевич	*Доктор технических наук, профессор. Кыргызский государственный университет геологии, горного дела и освоения природных ресурсов им. академика У.А. Асаналиева, Бишкек, Кыргыстан. Email: ichunuev@gmail.com*
Мусин Равиль Альтавович	*PhD, старший преподаватель. Карагандинский Технический Университет, Караганда,*

	Казахстан. ORCID ID: 0000-0002-1206-6889. Email: r.a.mussin@mail.ru
Тян Станислав Георгиевич	Докторант, Карагандинский Технический Университет, Караганда, Казахстан. ORCID ID: 0000-0002-3566-1437. Email: info@geo-in.kz

References

[1] Proekt promyshlennoj razrabotki mestorozhdeniya Koktaszhal [Industrial development project of the Koktaszhal deposit]. TOO Altaj polimetally, 2014. [in Russ.].

[2] Otchet po NIR po teme Issledovaniya ustojchivosti bortov kar'era Koktaszhal v svyazi s korrektirovkoj gorno-geologicheskoj situacii [Research report on the topic of the study of the stability of the sides of the Koktaszhal quarry in connection with the adjustment of the mining and geological situation]. NAO KarTU, Karaganda, 2020. [in Russ.].

[3] Otchet o NIR po teme Provedenie laboratornyh testov dlya opredeleniya fiziko-mekhanicheskih harakteristik obrazcov porod [Research report on the topic conducting laboratory tests to determine the physical and mechanical characteristics of rock samples]. Ministerstvo industrii i novyh tekhnologij RK, Komitet promyshlennoj bezopasnosti Filial RGP Nacional'nyj centr po kompleksnoj pererabotke mineral'nogo syr'ya RK, Institut gornogo dela imeni D.A. Kunaeva, Almaty, 2014. [in Russ.].

[4] Zurabishvili I.I., Nadirashvili N.R., Mataradze E.D. Geofizicheskie issledovaniya napryazhenno-deformirovannogo sostoyaniya gornogo massiva pri razrabotke rudnyh mestorozhdenij plastovogo tipa [Geophysical studies of the stress-strain state of the rock mass during the development of ore deposits of the formation type]. Tbilisi: Mecniereba. 1971. 120. [in Russ.].

[5] Bajkonurov O.A. Metody kontrolya fiziko-tekhnicheskih parametrov podzemnoj razrabotki rud [Methods of control of physical and technical parameters of underground ore mining]. Alma-Ata: Nauka AN Kaz.SSR. 1979. [in Russ.].

[6] Savich A.I. i dr. Sejsmoakusticheskie metody izucheniya massivov skal'nyh porod (Seismoacoustic methods for studying rock massifs). Moscow: Nedra. 1969; 240. [in Russ.].

[7] Rzhevskij V.V. Otkrytye gornye raboty. CHast' 1 [Open-pit mining. Part 1]. Moscow: Nedra. 1985; 509. [in Russ.].

[8] Kutuzov B.N., Belin V.A. Proektirovanie i organizaciya vzryvnyh rabot [Design and organization of blasting operations]. Moscow: Gornaya kniga. 2012; 416. [in Russ.].

[9] Kutuzov B.N. i dr. Spravochnik vzryvnika (The Bomber's Handbook). Moscow: Nedra. 1988; 511. [in Russ.].

[10] Tangaev I.A. Burimost' i vzryvaemost' gornyh porod. (Drillability and explosiveness of rocks). Moscow: Nedra. 1978; 184. [in Russ.].

[11] Krasil'nikov V.A. Zvukovye i ul'trazvukovye volny v vozduhe, vode i tverdyh telah. (Sound and ultrasonic waves in air, water and solids). Moscow: Fizmatgiz. 1960; 560. [in Russ.].

EVAPORATION THERMODYNAMICS AND SUBLIMATION OF ALUMINUM TELLURIDE

Burabaeva N.M.*, Volodin V.N., Nitsenko A.V., Tuleutai F. Kh.

"Institute of Metallurgy and Ore Beneficiation" JSC, Satbayev University, Almaty, Kazakhstan

* Corresponding author email: Nuri_eng@mail.ru

ABSTRACT

The analysis of the researches completed by now showed the lack of information concerning the definition of quantity of the vapor pressure values over the molten and crystalline aluminum chalcogenide. In the work presented here, the saturated vapor pressure over liquid and crystalline aluminum sesquitelluride was determined for the first time by the boiling point method (isothermal version). The compound was synthesized from elements, with a purity of 99.99 wt. %, identified by X-ray phase analysis as a monophase Al_2Te_3 was used as a research object. Certain vapor pressure of liquid Al_2Te_3 corresponds to the dependence, $\ln p_{Al_2Te_3}[\Pi a] = 18{,}828 - 11865 \cdot T^{-1}$ vapor pressure over crystalline telluride is $\ln p_{Al_2Te_3}[\Pi a] = 19{,}869 - 13077 \cdot T^{-1}$ Based on the values of saturated vapor, the temperature dependence of the Gibbs free energy of evaporation and sublimation was determined, by differentiating which concerning temperature, the entropies of the condensed phase - vapor transformation were calculated, and then the enthalpy. Thermodynamic functions were as follows: entropy of evaporation of the liquid phase - 60.71 ± 4.08 J/(mol K), enthalpy - 98.65 ± 6.64 kJ/mol; entropy of sublimation of the crystalline phase - 69.37 ± 4.67 J/(mol K), enthalpy - 108.73 ± 7.31 kJ/ mol. The low value of entropy of the aluminum telluride transfer to the vapor phase indicates the presence of associates in the vapor and of the congruent character of evaporation and sublimation of Al_2Te_3 indirectly. Defined as the difference between the sublimation enthalpies and evaporation, the enthalpy of aluminum telluride melting was 10.08 ± 0.68 kJ/mol, the entropy calculated similarly was 8.66 ± 0.58 J/(mol K). The data obtained coincide with the thermodynamic values found by other authors by calorimetric methods.

Keywords: aluminum telluride, vapor pressure, melting, evaporation, sublimation

Burabaeva Nurila Muratovna	*Candidate of Technical Sciences, Senior researcher, JSC "Institute of Metallurgy and Ore Beneficiation", Almaty, Kazakhstan. ORCID ID: 0000-0003-2183-2239, Email: Nuri_eng@mail.ru, Almaty, Kazakhstan.*
Volodin Valerij Nikolaevich	*Doctor of technical sciences, professor, doctor of physical and mathematical sciences, professor, Chief scientific employee JSC "Institute of Metallurgy and Ore Beneficiation", Almaty, Kazakhstan. ORCID ID: 0000-0001-9543-5944, Email: volodinv_n@mail.ru*
Nitsenko Alina Vladimirovna	*Candidate of Technical Sciences, Head of of the laboratory of vacuum processes JSC "Institute of Metallurgy and Ore Beneficiation", Almaty, Kazakhstan. ORCID ID: 0000-0001-6753-0936. Email: nitc@inbox.ru*
Tuleutai Farkhat Khanafiyauly	*Master of Technical Sciences, Engineer, JSC "Institute of Metallurgy and Ore Beneficiation", Almaty, Kazakhstan, Email: farkhat_kaldybek@mail.ru.*

Introduction

A retrospect of seventy years showed a limited number of researches devoted to the physicochemical study of aluminum chalcogenides, compared with similar compounds of other metals [[1],[2],[3],[4],[5],[6],[7]], and the most of these few studies are associated with the aluminum-tellurium system.

Under the equilibrium state diagram [8], there is one compound, aluminum sesquitelluride selenide (Al_2Te_3) in the tin-selenium system in the condensed phase, which melts congruently at temperatures of 895 °C.

The authors of [9] found the heat of formation of aluminum sesquichalcogenides, for a compound with tellurium – 326.3 ± 21 kJ/mol by direct determination of the heat of interaction of metal with chalcogenes in the Berthelot-Roth microbomb.

A close value of the enthalpy of formation of aluminum telluride (–318.8 ± 4 kJ/mol) based on calorimetric measurements was obtained in [10].

As a result of the approximate calculation [11], the heat of gaseous Al_2Te_3 formation was 364 kJ/mol.

Mass spectrometric studies [12] of the composition of the vapor phase over aluminum telluride found the presence of AlTe +, Al_2Te +, Al_2Te_2 +, and $AlTe_2$ + ions with a low relative intensity and found the enthalpies and entropies of formation of compounds of the indicated composition at a temperature of 1,292K (1,019 °C). The dissociation energy of AlS was determined to be 359.8 ± 12.6 kJ/mol.

A group of authors first determined the enthalpies of formation and melting of alloys with a concentration of up to 70 at. % Those, where the congruent character of melting of Al_2Te_3 was established, and then, using differential thermal analysis [14], the presence of a stratification region of liquid solutions was found.

Mass spectrometric studies and the values of the formation enthalpies obtained in the same study confirmed the presence of two liquid phases.

When studying the pressure and composition of vapor by mass spectroscopic, static, and torsion-effusion methods [15] in the temperature range 538-760 K, it was found that the only component of the gas phase over crystalline AL_2Te_3 is the Te_2 dimer, and the temperature dependence of the dissociation pressure ($\bar{p}_{Te_2}$) turned out to be equal

$$\lg \bar{p}_{Te_2}[\kappa\Pi a] = (5,079 \pm 0,297) - (8270 \pm 152) \cdot T^{-1},$$

where T is the temperature, K.

Partial and integral thermodynamic functions of metals were determined in [16] paper, using the method of measuring the electromotive forces of concentration chains at 700 - 820 K (427 – 547 °C) in the range of alloy compositions of the aluminum-tellurium system up to 20 atom percentte.

When studying phase equilibria and intermediate phases in the Al-Te system, the authors of [17] paper found the presence of a superstructure in the α - Al_2Te_3 compound. The [18] paper gives excess thermodynamic functions in the concentration range 0-60 atom percent tellurium for 1190 K (917 °C), indicating very low values of its thermodynamic activity.

The study [19] is devoted to thermodynamic modeling and optimization of the Al-Te system based on and using previously performed experiments, including [[13], [14]].

No later publications concerning the study of the thermodynamics of the aluminum-tellurium system have been found. The analysis of the research results outlined above shows a clear lack of Information about the aluminum-tellurium system in respect to the technologies of tellurium purification by physical and physicochemical methods. There is no information regarding the thermodynamics of evaporation and sublimation of aluminum sesquitelluride Al_2Te_3.

The purpose of this study was to determine the thermodynamic functions of the sublimation of crystalline telluride, its evaporation from the liquid phase, and the melting of the compound.

Research object and methodology

The object of research was aluminum telluride synthesized by fusing the amounts of tellurium (99.99 wt.%) and aluminum (99.99 wt.%) corresponding to the composition of the compound in sealed quartz ampoules, from which air was previously evacuated. Heating was performed at a rate of 100 °C per hour to a temperature of 1000 °C, the melt was kept at this temperature for 12 hours, followed by quenching in water. The alloy was identified by X-ray phase analysis as a monophase Al_2Te_3.

When considering the Al-Te system, the congruent nature of melting and the existence of aluminum telluride in solution was noted [13], a very low value of Te activity in the liquid phase at concentrations of 0-60 atom percent, that, apparently, refers to the element obtained as a result of the dissociation of AL_2Te_3, as well as its low value of the dissociation pressure at a melting temperature of 1168 K (895 °C) - 9.97 10^{-3} kPa (we calculated from the data [15].

This fact, as well as the significant value of the free energy of aluminum telluride formation, gives grounds to assume the congruent character of the compound evaporation. thermodynamic characteristics were calculated based on the values of the saturated vapor of Al_2Te_3.

To determine the vapor pressure values, the boiling point method (isothermal version) was chosen; the method was based on a sharp increase in the evaporation rate when the external pressure and saturated vapor pressure of the investigated component are equal with a decrease in pressure above the melt, which was described in detail by the authors earlier [[20], [21], [22], [23], [24], [25]].

The advantage of the method is that there is no need to establish the molecular composition of the vapor, which introduces significant errors in calculations when determining the saturated vapor

Table -1 – Experimentally determined and calculated values of the saturated vapor of aluminum telluride

Temperature, K	Experiment steam pressure, kPa.	Calculated steam pressure, kPa	Relative error, %	Temperature, K	Experiment steam pressure, kPa.	Calculated steam pressure, kPa	Relative error, % (Δ),
1,473	46.40	47.72	-2.77	1,123	3.73	3.73	±0.0
	49.06		+2.81		3.47		-6.97
	47.72		±0.0		4.00		+7.24
1,373	27.52	26.54	+3.69	1,033	1.33	1.35	-1.48
	26.73		+0.72		1.27		-5.93
	25.43		-4.18		1.47		+8.89
1,173	5.73	6.08	-5.76	973	0.67	0.62	8.06
	6.11		-0.49		0.67		+8.06
	6.42		+5.59		0.53		-14.52
							$|\Delta|_{average}$=5.13

pressure by other methods. due to the high aggressiveness of tellurium and telluride concerning metals, quartz was used as the material of the device and the container for the test charge and suspension device material in its high-temperature part. The pressure was measured with a vacuum gauge in mm Hg with subsequent transfer to Pa.

Experimental results and their discussion

The experimental conditions and the values of the vapor pressure of aluminum telluride determined in this case are given in the table 1.

The total measurement error is defined as the sum of the errors of independent measurements: temperature – 1 %, weighing –0.1 %, pressure – 0.5 %, approximation of experimental data –5.13 %, equal to 6.73 %.

The experimentally determined vapor pressure of liquid Al_2Te_3 corresponds to the dependence: $\ln p_{Al_2Te_3}[\Pi a] = 18,828 - 11865 \cdot T^{-1}$, vapor pressure over crystalline telluride – $\ln p_{Al_2Te_3}[\Pi a] = 19,869 - 13077 \cdot T^{-1}$

The results of the values of the saturated vapor pressure over liquid and crystalline aluminum sesquitelluride in the coordinates lnp – T^{-1} (figure 1) graphically, by the intersection of linear dependences (*1000·T⁻¹*=0.8591) determine the melting point equal to 1,164 K (891 °C) that only differs by 4°C from the one shown on the equilibrium phase (895 °C) diagram [8] and indicates the correctness of the experimental data.

Based on the values of the saturated vapor pressure over aluminum telluride (Al_2Te_3), the thermodynamic functions of evaporation were calculated, which amounted to entropy of the liquid phase – 60.71 ± 4.08 J/(mol K), enthalpy – 98.65 ±

6.64 kJ/mol; entropy of sublimation of the crystalline phase - 69.37 ± 4.67 J/(mol K), enthalpy − 108.73 ± 7.31 kJ/mol. The low enthalpy value of the aluminum telluride transfer to the vapor phase indicates the presence of associates in the vapor and, indirectly, the congruent character of Al_2Te_3 evaporation under Truton's rule.
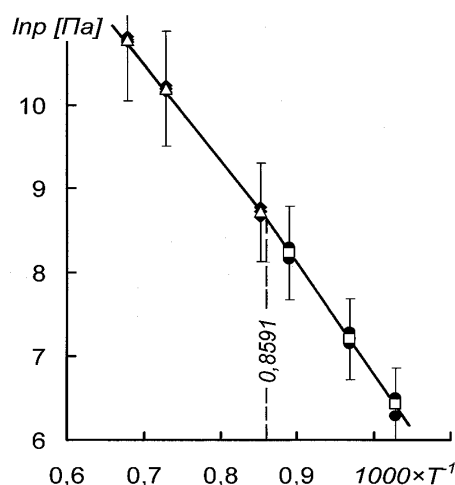
Dark marks are experimental data and light marks are calculated data

Figure 1 - Dependence of the vapor pressure of aluminum telluride on temperature

Based on the simplest relationship: $\Delta H_{mel} = \Delta H_{subl.} - \Delta H_{evap}$, where ΔH_{mel}, $\Delta H_{subl.}$ and ΔH_{evap} are enthalpies of melting, sublimation and evaporation, respectively, the thermodynamic functions of melting of aluminum telluride were determined: enthalpy is 10.08 ± 0.68 kJ/mol, entropy is 8.66 ± 0.58 J/(mol K).

The latter coincides with the data of the study [14], where, using calorimetry, the melting entropy

was determined equal to 8.6 ± 0.9 J/(mol K), and the enthalpy is 10 ± 1 kJ/mol.

Conclusions

As a result of this research, the pressure of saturated vapor over liquid and crystalline aluminum sesquitelluride using the boiling point method was determined for the first time and on this grounds, the thermodynamic functions of evaporation and sublimation of Al₂Te₃ were calculated.

The enthalpy of liquid compound vaporization was determined as 98.65 ± 6.64 kJ/mol, of crystalline sublimation was 108.73 ± 7.31 kJ/mol; the evaporation entropy of telluride was found to be equal to 60.71 ± 4.08 J/(mol K), the sublimation entropy was 69.37 ± 4.67 J/(mol K).

The low value of entropy indicates the presence of associates in the vapor and the congruent character of evaporation and sublimation. The melting functions determined in this study: entropy − 8.6 ± 0.9 J/(mol K), enthalpy − 10 ± 1 kJ/mol, coincide with the results of determinations performed with the calorimetric method.

The obtained values of the functions will supplement the currently missing information in the thermodynamic database.

Алюминий теллуридінің булану және сублимациясының термодинамикасы

Бурабаева Н.М., Володин В.Н., Ниценко А.В., Тулеутай Ф.Х.

«Металлургия және кен байыту институты» АҚ, Сәтбаев университеті, Алматы, Қазақстан

ТҮЙІНДЕМЕ

Осы уақытқа дейін жүргізілген зерттеулерді талдау нәтижесінде балқытылған және кристалды алюминий халбкогенидінің бу қысымының мәндерін анықтауға қатысты ақпарат жоқ екені анықталды. Ұсынылған жұмыста қайнау нүктелері әдісімен (изотермиялық нұсқа) алғаш рет қаныққан будың сұйық және кристалды алюминий сесквителлуридіне қысымы анықталды. Зерттеу нысаны ретінде элементтерден синтезделген тазалығы 99,99 мас. %, Al₂Te₃ монофаза ретінде рентген-фазалық талдау арқылы анықталған қосылыс қолданылды. Сұйық Al₂Te₃ белгілі бу қысымы: $\ln p_{Al_2Te_3}[\Pi a] = 18,828 - 11865 \cdot T^{-1}$ - тәуелділікке сәйкес келеді, кристалды теллурид үстіндегі бу қысымы: $\ln p_{Al_2Te_3}[\Pi a] = 19,869 - 13077 \cdot T^{-1}$ тең. Қаныққан будың мәндеріне сүйене отырып, Гиббстің булану мен сублимацияның бос энергиясының температураға тәуелділігі, оны температураға қатысты дифференциалдау арқылы конденсацияланған фазаның энтропиялары – будың түрленуі алдымен есептеледі, содан кейін энтальпия. Термодинамикалық функциялар келесі мәндерді құрады: сұйық фазаның булану энтропиясы - 60,71±4,08 Дж/(моль·К), энтальпия – 98,65± 6,64 кДж/моль; кристалды фазаның сублимация энтропиясы – 69,37±4,67 Дж/(моль·К), энтальпиясы – 108,73±7,31 кДж/моль. Алюминий теллуридінің бу фазасына өту энтропиясының төмен мәні буда ассоциаттардың болуын және жанама түрде Al₂Te₃ булануы мен сублимациясының конгруентті сипатын көрсетеді. Сублимация және булану энтальпияларының айырмашылығы ретінде анықталған алюминий теллуридінің балқу энтальпиясы 10,08±0,68 кДж/моль, осыған ұқсас әдіспен есептелген энтропия 8,66±0,58 Дж/(моль·К) болды. Алынған деректер калометриялық әдістермен басқа авторлар тапқан термодинамикалық мәндермен сәйкес келеді.

Түйін сөздер: алюминий теллуриді, бу қысымы, балқу, булану, сублимация, энтропия, энтальпия.

	Авторлар туралы ақпарат:
Бурабаева Нурила Муратовна	Техника ғылым кандидаты, «Металлургия және байыту институты» АҚ, Алматы, Қазақстан. ORCID идентификаторы: 0000-0003-2183-2239 Электрондық поштасы: Nuri_kaz@mail.ru
Володин Валерий Николаевич	Техника ғылымдарының докторы, профессор, физика-математика ғылымдарының докторы, профессор, «Металлургия және байыту институты» АҚ бас ғылыми қызметкері, Алматы, Қазақстан. ORCID идентификаторы: 0000-0001-9543-5944 Электрондық поштасы: volodinv_n@mail.ru
Ниценко Алина Владимировна	Техника ғылымдарының кандидаты, «Металлургия және байыту институты» АҚ вакуумдық процестер зертханасының меңгерушісі, Алматы қ., Қазақстан. ORCID идентификаторы: 0000-0001-6753-0936. Электрондық поштасы: nitc@inbox.ru
Тулеутай Фархад Ханафияұлы	Магистр, инженер, «Металлургия және байыту институты» АҚ, Алматы, Қазақстан, Электрондық поштасы: farkhat_kaldybek@mail.ru.

Термодинамика испарения и сублимации теллурида алюминия

Бурабаева Н.М., Володин В.Н., Ниценко А.В., Тулеутай Ф.Х.

АО «Институт металлургии и обогащения», Satbayev University, Алматы, Казахстан

АННОТАЦИЯ

В результате анализа выполненных к настоящему времени исследований установлено отсутствие сведений, касающихся определений величин давления пара над расплавленным и кристаллическим халькогенидом алюминия. В представленной работе впервые методом точек кипения (изотермический вариант) определено давление насыщенного пара над жидким и кристаллическим сесквителлуридом алюминия. В качестве объекта исследования использовано синтезированное из элементов, чистотой 99,99 мас. %, соединение, идентифицированное рентгенофазовым анализом как монофаза Al_2Te_3. Определенное давление пара жидкого Al_2Te_3 соответствует зависимости: $\ln p_{Al_2Te_3}[\Pi a] = 18{,}828 - 11865 \cdot T^{-1}$, давление пара над кристаллическим теллуридом - $\ln p_{Al_2Te_3}[\Pi a] = 19{,}869 - 13077 \cdot T^{-1}$. На основании величин насыщенного пара определена температурная зависимость свободной энергии Гиббса испарения и сублимации, дифференцированием которой по температуре рассчитаны вначале энтропии превращения конденсированная фаза – пар, а затем энтальпия. Термодинамические функции составили величину: энтропия испарения жидкой фазы – 60,71±4,08 Дж/(моль·К), энтальпия – 98,65± 6,64 кДж/моль; энтропия сублимации кристаллической фазы – 69,37±4,67 Дж/(моль·К), энтальпия – 108,73±7,31 кДж/моль. Малая величина энтропии перевода теллурида алюминия в паровую фазу свидетельствует о наличии ассоциатов в паре и косвенно – о конгруэнтном характере испарения и сублимации Al_2Te_3. Определенная как разница энтальпий сублимации и испарения энтальпия плавления теллурида алюминия составила величину 10,08±0,68 кДж/моль, энтропия, рассчитанная аналогично, – 8,66±0,58 Дж/(моль·К). Полученные данные совпадают с термодинамическими величинами, найденными другими авторами калориметрическими методами.

Ключевые слова: теллурид алюминия, давление пара, плавление, испарение, сублимация

Бурабаева Нурила Муратовна	*Информация об авторах: Кандидат технических наук, АО "Институт металлургии и обогащения", Алматы, Казахстана. ORCID ID: 0000-0003-2183-2239, Email: Nuri_eng@mail.ru*
Володин Валерий Николаевич	*Доктор технических наук, профессор, доктор физико – математических наук, профессор, главный научный сотрудник АО "Институт металлургии и обогащения", Алматы, Казахстан. ORCID ID: 0000-0001-9543-5944, Email: volodinv_n@mail.ru*
Ниценко Алина Владимировна	*Кандидат технических наук, заведующая лабораторией вакуумных процессов АО "Инстит металлургии и обогащения", Алматы, Казахстан. ORCID ID: 0000-0001-6753-0936. Email: nitc@inbox.ru*
Тулеутай Фархад Ханафияулы	*Магистр, инженер, АО "Институт металлургии и обогащения", Алматы, Казахстан. Email: farkhat_kaldybek@mail.ru.*

References

[1] Isakova R.A., Nesterov V.N., Chelokhsaev L.S. Fundamentals of vacuum pyroselection of polymetallic raw materials. Alma-Ata: Nauka. 1973: 255.

[2] Chemistry and physics of chalcogenides. Eds. Obolonchik V.A. Kiev: Naukova Dumka. 1977: 140.

[3] Vanyukov A.V., Isakova R.A., Bystrov V.P. Thermal dissociation of metal sulfides. Alma-Ata: Nauka. 1978: 272.

[4] Novoselova A.V., Pashinkin A.S. Vapor pressure of volatile metal chalcogenides. Moscow.: Nauka. 1978: 112.

[5] Vaysburd S.E. Physicochemical properties and structural features of sulfide melts. Moscow: Metallurgiya. 1996: 304.

[6] Kopylov N.I., Lata V.A., Polyvyanny I.R., Khegay L.D. State diagrams of double and triple thiosystems. Komsomolsk-on-Amur: Zhuk Industrial and Commercial Enterprise. 1999: 177.

[7] Volodin V.N., Trebukhov S.A. Distillation processes of selenium extraction and refining. Karaganda: Tengri Ltd. 2017: 220.

[8] Diagrams of the state of binary metal systems. Eds. Lyakisheva N.P. Moscow: Mashinostroyeniye. 1996; 1: 992.

[9] Kapustinsky A.F., Golutvin Yu.M. Thermo-chemistry and the structure of atoms. Report 5. The heat of aluminum compounds formation with elements of Group VI of the D.I. Mendeleev Periodic System // Proceedings of the Academy of Sciences of the USSR. Chemical Sciences Department 1951; 2: 192-200.

[10] Joël H.A., Schneider A. Die Bildungsentalpie von Aluminiumtellurid// Naturwissenschaften. 1967; (54) 22: 587.

[11] Gattow Dr. G. Orientierende Berechnung der Bildungwärmen von Aluminium (I,II)-chalkogeniden //Angew. Chem. 1956; (68) 16: 521.

[12] Ficalora P.J., Hastie J.W., Margrave J.L. Mass Spectrometric Studies at High Temperatures. XXVII. The Reactions of Aluminum Vapor with S2(g), Se2(g), and Te2(g) // J. Phys. Chem. 1968; (72) 5: 1660-1663.

[13] Said H., Castanet R., Kehiaian H.V. Étude calorimétrique du systéme binaire aluminium-tellure // J. Less-Comm. Met. 1976; (46)2: 209-215.

[14] Said H., Chastel R., Bergman C., Castanet R. Said H., Chastel R., Bergman C., Castanet R. Ther-modynamic investigation on Al – Te Alloys by dif-ferential thermal analysis and Knudsen-cell mass-spectrometry // Z. Metallkunde. 1981; (72)5: 360-365.

[15] Ferro D., Nappi B.M., Balducci G., Placente V. A vaporization study of Al2Te3 // Thermochim. Acta. 1980; 35: 35-41.

[16] Blot J., Rogez J., Castanet R. Étude potenti-ométrique des alliages liquids aluminium – étain et aluminium – tellure // J. Less-Comm. Met. 1986; 118: 67-82.

[17] Kniep R., Blees P. Phasengleichgewichte und intermediäre Phasen im System Al – Te // Z. Naturforsch. 1988. (43b): 182-188.

[18] Prabhu N., Howe J.M. The Al – Te (Alumini-um – Tellurium) System //Bull. Alloy Phase Dia-grams. 1990; (11)2: 202-206.

[19] Oh C.-S., Lee D.N. Thermodynamic assess-ments of the In – Te and Al – Te systems // CALPHAD. 1993; (17)2: 175-187.

[20] Volodin V.N., Khrapunov V.E., Kenzhaliyev B.K., Isakova R.A., Moldabaev M. Thermodynamic study of the silver-cadmium system with the deter-mination of the upper limit of liquid alloys existence. Proceedings of the Universities. Nonferrous-metals Industry. 2005; 3: 22-28.

[21] Volodin V.N., Tuleushev Yu.Zh. The Liquid-Vapor Phase Transition in a Copper-Calcium System // Russian Journal of Physical Chemistry A. 2020; (94)8: 1526-1531.

[22] Volodin V.N., Tuleushev Yu.Zh., Kenzhaliyev B.K., Trebukhov S.A. Thermal degradation of hard alloys of the niobium-cadmium system at low pressure. Kompleksnoe ispol'zovanie mineral'nogo syr'a. 2020; 1: 41-47. DOI: 10.31643/2020/6445.05

[23] Volodin, V.N., Trebukhov, S.A., Kenzhaliyev, B.K., Nitsenko, A.V., Burabaeva, N.M. Melt–Vapor Phase Diagram of the Te–S System. Russian Journal of Physical Chemistry A. (92) 3: 407-410. DOI: 10.1134/S0036024418030330

[24] Volodin V.N., Tuleushev Yu.Zh., Kenzhaliyev B.K., Trebukhov S.A. Thermal degradation of hard alloys of the niobium-cadmium system at low pressure. Kompleksnoe ispol'zovanie mineral'nogo syr'a. 2020; 1: 41-47. DOI: 10.31643/2020/6445.05

[25] Volodin V.N., Tuleushev Yu.Zh., Nitsenko A.V., Burabaeva N.M. Concentration limits of niobi-um and existence of cadmium alloys formed by ultrafine particles. Kompleksnoe ispol'zovanie mineral'nogo syr'a. 2019; 1. P. 30-36. DOI: 10.31643/2019/6445.

Cluster-associate model of the viscosity of potassium carbonat

[1]* Bekbayeva L.A., [2] Malyshev V.P., [3] Mamyachenkov S.V., [1] Makasheva A.M.

[1] Karaganda Technical University, Kazakhstan, Karaganda
[2] Chemical and Metallurgical Institute named after Zh. Abishev, Kazakhstan, Karaganda
[3] Ural Federal University named after the first President of Russia B. N. Yeltsin, Russian Federation, Yekaterinburg

* Corresponding author email: lyazzat.bekbaeva@mail.ru

ABSTRACT

In the article, the temperature dependence of the viscosity of a complex inorganic substance - potassium carbonate was obtained and the proposed mathematical model was verified. Viscosity is considered as a chaosensitive property of a liquid inherent in it in motion and at rest. The mathematical model of viscosity was developed using the Boltzmann distribution and the concept of chaotic particles. On this basis, a hierarchical cluster-associate viscosity model is constructed, which takes into account not only the formation of primary clusters, but also secondary associates with respect to them, with the possibility of identifying the degree of cluster association. To adapt the cluster-associated model to experimental data, certain data processing techniques have been developed to identify unknown parameters of the model. The method of processing viscosity data using the entire set of three reference points allows you to determine the indicator of the degree of aggregation of associates. When processing the data on the viscosity of potassium carbonate, a high correlation coefficient was established calculated in comparison with reference values, which indicates the adequacy of the new relationship. This model makes it possible to predict the behavior of the viscosity of potassium carbonate in a higher temperature range. The degree of association of clusters with an increase in temperature decreases, corresponding to the dynamics of the destruction of associates and viscosity in general.

Keywords: concept of randomized particles, Boltzmann distribution, dynamic viscosity, potassium carbonate, cluster, associate.

	Information about authors:
Bekbayeva Lazzat Akylbaevna	*M. Sc., a doctoral student of the Department of NTM of Karaganda Technical University, Karaganda, Kazakhstan. Email: lyazzat.bekbaeva@mail.ru, ORCID ID: 0000-0003-2543-6380.*
Malyshev Vitaly Pavlovich	*Doctor of Technical Sciences, Professor, Zh. Abishev Chemical and Metallurgical Institute, Karaganda, Kazakhstan. Email: eia_hmi@mail.ru, ORCID ID: 0000-0002-3996-1533.*
Mamyachenkov Sergey Vladimirovich	*Doctor of Technical Sciences, Professor, Head of the Department "Metallurgy of Non-ferrous Metals" of the Ural Federal University named after the first President of Russia B. N. Yeltsin, Yekaterinburg, Russia. Email: svmamyachenkov@yandex.ru, ORCID ID: 0000-0001-6070-8746.*
Makasheva Astra Mundukovna	*Doctor of Technical Sciences, Professor of the Department of NTM of Karaganda Technical University, Karaganda, Kazakhstan. Email: astra_mun@mail.ru, ORCID ID: 0000-0003-2249-3435.*

Introduction

Viscosity is an important characteristic of a liquid substance. The nature of the viscous state is insufficiently studied, there is a disparity of temperature dependences of viscosity, fragmentary and narrowness of experimental determination of this characteristic and the impossibility of displaying it in the full temperature range of the liquid state, especially for melts. This determines the relevance of these studies, in particular, complex compounds [[1], [2], [3], [4], [5], [6], [7], [8], [9]].

In addition to its practical importance, the study of the viscosity of melts of inorganic compounds is also of great scientific interest, since viscosity is the most structurally sensitive characteristic of a substance that gives an idea of the forces of intermolecular interaction and the mechanism of molecular transfer processes in liquids. The accumulation of knowledge in this field allows us to solve many issues related to the theory of the liquid state [[10], [11], [12], [13], [14], [15], [16], [17]].

Based on the Boltzmann's distribution and the normalized dependence of particles on temperature, the authors [[18], [19], [20], [21], [22]] developed a semi-empirical cluster-associate model of viscous fluid flow, which allows us to evaluate the aggregation of clusters into associates.

This model for determining the regularity of viscosity by temperature based on the concept of chaotic particles does not contradict, but even complements the classical theory of viscosity [18-22]. According to the proposed concept, developers rely on the virtual presence of liquid and gaseous phases in the solid state of matter.

The experimental part

The cluster-associate model of fluid viscosity makes it possible to estimate the degree of association of clusters or their number based on the temperature dependence of viscosity [[18], [19], [20], [21], [22]].

The viscosity equation according to the concept of chaotic particles is expressed by the formula:

$$\eta = \eta_1 (T_1/T)^a, \qquad (1)$$

where η_1 – reference point of dynamic viscosity at temperature T_1 (К); a – degree of cluster association. The value of a is determined by:

$$a = a_2 \left(\frac{T_2}{T}\right)^b, \qquad (2)$$

where b – the measure of lowering the degree of cluster association. Values a_2 and b:

$$a_2 = \frac{ln\,(\eta_2/\eta_1)}{ln\,(T_1/T_2)}, \qquad (3)$$

$$a_3 = \frac{ln\,(\eta_3/\eta_1)}{ln\,(T_1/T_3)}. \qquad (4)$$

$$b = \frac{ln\,(a_3/a_2)}{ln\,(T_2/T_3)}. \qquad (5)$$

Thus, the general form of a two-level hierarchical model will be presented as follows:

$$\eta = \eta_1 (T_1/T)^{a_2(T_2/T)^b}, \qquad (6)$$

Reference points η_1, T_1, η_2, T_2, η_3, и T_3 should be chosen at the beginning, middle and end of the entire experimental array, respectively [[21], [22], [23]]. In this case, we can limit ourselves to calculating a_2, a_3 and b, without processing the

entire experimental array, with further introduction of the necessary values into the model (6) and calculation of η for comparison with all experimental values by the correlation coefficient.

We will check the adequacy of the cluster-associate viscosity model on such an inorganic substance as potassium carbonate.

Discussion of the results

Potassium carbonate is produced by carbonation of КОН solutions obtained by electrolytic means, or $MgCO_3$ suspensions in КСl, solution, as well as a by-product during the processing of nepheline into alumina [24, pp. 189-190].

Potassium carbonate is used as a starting product for the production of various potassium compounds and as a potassium fertilizer [24, pp. 187-188].

It easily reacts with sulfur carbon monoxide, upon completion of which crystallohydrates are formed. This interaction is possible only in saline solution.

When the substance is heated to 1200 ℃ and above, it decomposes into two components - potassium oxide and carbon dioxide. The substance reacts perfectly with non-oxidizing acids, bases, carbon (under high temperature conditions) and with sulfur oxide.

Potassium carbonate is actively used in various industries in calcined and 1.5-in one form, 1st, 2nd and 3rd grades. The chemical industry, glass production, agricultural complex, fire fighting, light industry, photo production and other industrial areas cannot do without it.

The presented data array and melting point T_m = 1169 К of potassium carbonate were taken from the reference [25]. There is no boiling point in this handbook. In the source [26] indicated that at a temperature above the melting point, potassium carbonate decomposes. From the presented values [25], the following were selected as reference values: T_1 = 1190 К, η_1 = 3,03 mPa·s, T_2 = 1220 К, η_2 = 2,23 mPa·s, T_3 = 1250 К, η_3 = 1,66 mPa·s. The data is given only up to 1250 K.

The necessary values were calculated using formulas (3)-(5): a_2 = 12,3129; a_3 = 12,2330; b = 0,2679. Then a_2 and b were substituted into expression (6)

$$\eta = 3,03 \left(\frac{1190}{T}\right)^{12,3129\,(1220/T)^{0,2679}}, \qquad (7)$$

In addition to this, the exponential equation is given in the reference book [25]

$$\eta = 1{,}161 \cdot 10^{-5} exp(29487/RT),\qquad (8)$$

derived from data [27] (5 points in the temperature range 1186,2-1257,2 К; torsional vibration method [17] of a hollow cylinder). The accuracy corresponds to the standard deviation $s = 0{,}0272$ (1,23%). The uncertainty is estimated at ∼ 3,0 %. The authors [25] additionally give the viscosity value at one temperature (1173,2 K), obtained by S.V. Karpachev and collaborators [28] using the method of torsional vibrations of the ball. This value is lower than the corresponding value in [27], so it was not used when comparing reference and calculated data.

The calculation results for all viscosity values, reference [25] and calculated by (7) and (8), together with the calculations of the temperature dependence of the degree of association (2) are shown in Table 1 and Figure 1.

Table 1 - Reference [25] and calculated by formulas (7) and (8) data on dynamic viscosity for potassium carbonate

T, K	η [25], mPa·s	η (7), mPa·s	η (8), mPa·s	a
T_m = 1169	–	3,78	0,000241	12,46
1190	3,03	3,03	0,000229	12,40
1200	2,73	2,73	0,000223	12,37
1210	2,46	2,47	0,000218	12,34
1220	2,23	2,23	0,000213	12,31
1230	2,02	2,02	0,000208	12,29
1240	1,83	1,83	0,000203	12,26
1250	1,66	1,66	0,000198	12,23
1300	-	1,04	-	12,11
1350	-	0,67	-	11,98
1400	-	0,44	-	11,87
1450	-	0,30	-	11,76
1460	-	0,28	-	11,73
1470	-	0,26	-	11,71
1473	-	0,25	-	11,71

It should be noted that the values obtained from equation (8) are very different from the reference values [25] and calculated from equation (7). Apparently, there is a typo in the first coefficient of equation (7), so these values were not taken for comparison with experimental data.

The correlation coefficient when comparing the reference data [25] with the proposed cluster-associate model (7) of viscosity is quite high R = 0,999979 with its significance t_R = 52091 >> 2, which indicates the adequacy of the new dependence.

The degree of association of clusters decreases with increasing temperature, amounting to the value a_m = 12,46, at the melting point, corresponding to the general dynamics of the destruction of associates and the behavior of viscosity as a whole.
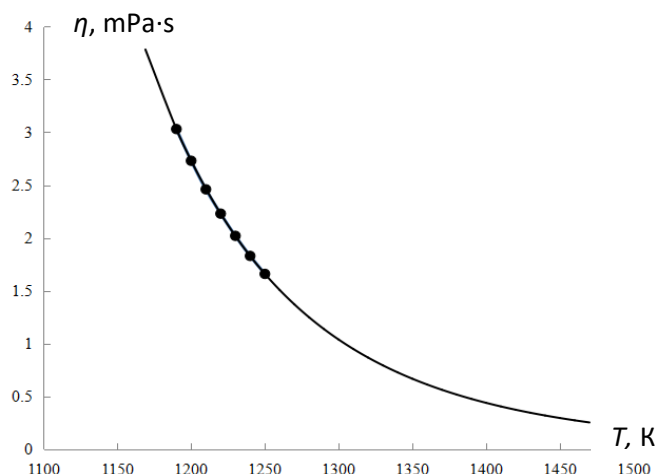

Figure 1 - Dependence of the dynamic viscosity of potassium carbonate on temperature

Conclusions

The cluster-associate viscosity model made it possible to construct a model for potassium carbonate. Comparison of the reference data with the newly developed model establishes the high adequacy of the presented cluster-associate model of dynamic viscosity of a complex inorganic substance.

The correlation coefficient of potassium carbonate is high, which indicates the possible application of the developed viscosity models in the future.

In addition, an exponential equation was given, the value of which was significantly lower than the corresponding value, so it was not used when comparing reference and calculated data.

One of the most important characteristics of the cluster-associate model – the degree of cluster association – naturally decreases with increasing temperature, corresponding to the dynamics of the destruction of associates.

The proposed viscosity model adequately describes the entire range of the liquid state of a substance, and thus allows predicting behavior at higher temperatures up to the boiling point.

Conflict of interest

On behalf of all the authors, the correspondent author declares that there is no conflict of interest.

Калий карбонаты тұтқырлығының кластерлі-ассоциаттық моделі

[1] Бекбаева Л.А., [2] Малышев В.П., [3] Мамяченков С.В., [1] Макашева А.М.

[1] Қарағанды техникалық университеті, Қазақстан, Қарағанды
[2] Ж. Әбішев атындағы химия-металлургия институты, Қазақстан, Қарағанды
[3] Ресейдің Тұңғыш Президенті Б. Н. Ельцин атындағы Орал федералдық университеті, Ресей Федерациясы, Екатеринбург

ТҮЙІНДЕМЕ

Мақалада күрделі бейорганикалық заттың - калий карбонатының тұтқырлығының температуралық тәуелділігі алынды және ұсынылған математикалық модель тексерілді. Тұтқырлық сұйықтықтың қозғалыста және тыныштықта өзіне тән хаосқа сезімтал қасиеті ретінде қарастырылады. Тұтқырлықтың математикалық моделі Больцманның таралуын және хаотикалық бөлшектер тұжырымдамасын қолдана отырып жасалды. Осы негізде тұтқырлықтың иерархиялық кластерлі-ассоциаттық моделі құрылған, ол тек бастапқы кластерлердің құрылуын ғана емес, сонымен қатар кластерлер қауымдастығының дәрежесін анықтау мүмкіндігімен оларға қатысты қайталама ассоциацияларды да ескереді. Кластерлі-ассоциаттық модельді эксперименттік деректерге бейімдеу үшін белгісіз модель параметрлерін анықтау үшін деректерді өңдеудің белгілі әдістері жасалды. Тұтқырлық туралы мәліметтерді үш нүктенің жиынтығын қолдана отырып өңдеу әдісі ассоциаттардың агрегация дәрежесін анықтауға мүмкіндік береді. Калий карбонатының тұтқырлығы туралы мәліметтерді өңдеу кезінде анықтамалық мәндермен салыстырғанда есептелген жоғары корреляция коэффициенті анықталды, бұл жаңа тәуелділіктің жеткіліктілігін көрсетеді. Бұл модель калий карбонатының тұтқырлығын жоғары температура диапазонына дейін болжауға мүмкіндік береді. Кластерлердің қауымдастық дәрежесі температураның жоғарылауымен төмендейді, ассоциаттардың бұзылу динамикасына және тұтастай тұтқырлыққа сәйкес келеді.

Түйін сөздер: ретсіз бөлшектер туралы түсінік, Больцманның таралуы, динамикалық тұтқырлық, калий карбонаты, кластер, ассоциат.

	Авторлар туралы ақпарат:
Бекбаева Ләззәт Ақылбайқызы	*т.ғ.м., Қарағанды техникалық университетінің НТМ кафедрасының докторанты, Қарағанды, Қазақстан. ORCID ID: 0000-0003-2543-6380.. Email: lyazzat.bekbaeva@mail.ru*
Малышев Виталий Павлович	*т.ғ.д., профессор, Ж. Әбішев атындағы химия-металлургия институты, Қарағанды, Қазақстан. ORCID ID: 0000-0002-3996-1533. Email: eia_hmi@mail.ru*
Мамяченков Сергей Владимирович	*т. ғ.д., профессор, Ресейдің Тұңғыш Президенті Б. Н. Ельцин атындағы Орал федералдық университетінің «Түсті металдар металлургиясы» кафедрасының меңгерушісі, Екатеринбург, Ресей. ORCID ID: 0000-0001-6070-8746. Email: svmamyachenkov@yandex.ru*
Макашева Астра Мундуковна	*Қарағанды техникалық университетінің НТМ кафедрасының профессоры, т.ғ.д., Қарағанды, Қазақстан. ORCID ID: 0000-0003-2249-3435. Email: astra_mun@mail.ru*

Кластерно-ассоциатная модель вязкости карбоната калия

[1] Бекбаева Л.А., [2] Малышев В.П., [3] Мамяченков С.В., [1] Макашева А.М.

[1] Карагандинский технический университет, Казахстан, Караганда
[2] Химико-металлургический институт им. Ж.Абишева, Казахстан, Караганда
[3] Уральский федеральный университет имени первого Президента России Б. Н. Ельцина, Российская Федерация, Екатеринбург

АННОТАЦИЯ

В статье авторами была получена температурная зависимость вязкости сложного неорганического вещества - карбоната калия и проведена проверка предложенной математической модели. Вязкость рассматривается как хаосочувствительное свойство жидкости, присущее ей в движении и в покое. Математическая модель вязкости была разработана с использованием распределения Больцмана и концепции хаотизированных частиц. На этой основе построена иерархическая кластерно-ассоциатная модель вязкости, которая учитывает не только образование первичных кластеров, но и вторичных по

отношению к ним ассоциатов с возможностью выявления степени ассоциации кластеров. Для адаптации кластерно-ассоциатной модели к экспериментальным данным разработаны определенные приемы обработки данных для идентификации неизвестных параметров модели. Метод обработки данных по вязкости с использованием из всего множества трех реперных точек позволяет определить показатель степени агрегации ассоциатов. При обработке данных по вязкости карбоната калия был установлен высокий коэффициент корреляции рассчитанных по сравнению со справочными величинами, что указывает на адекватность новой зависимости. Данная модель позволяет прогнозировать поведение вязкости карбоната калия в более высокий температурный диапазон. Степень ассоциации кластеров с повышением температуры понижается, соответствуя динамике разрушения ассоциатов и вязкости в целом.

Ключевые слова: концепция хаотизированных частиц, распределение Больцмана, динамическая вязкость, карбонат калия, кластер, ассоциат.

Информация об авторах:

Бекбаева Ләззәт Ақылбайқызы — м.т.н., докторант кафедры НТМ Карагандинского технического университета, Караганда, Казахстан. ORCID ID: 0000-0003-2543-6380. Email: lyazzat.bekbaeva@mail.ru

Малышев Виталий Павлович — д.т.н., профессор, Химико-металлургический институт им. Ж. Абишева, Караганда, Казахстан. ORCID ID: 0000-0002-3996-1533. Email: eia_hmi@mail.ru

Мамяченков Сергей Владимирович — д.т.н., профессор, заведующий кафедрой «Металлургия цветных металлов» Уральского федерального университета имени первого Президента России Б.Н. Ельцина, Екатеринбург, Россия. ORCID ID: 0000-0001-6070-8746. Email: svmamyachenkov@yandex.ru

Макашева Астра Мундуковна — д.т.н., профессор кафедры НТМ Карагандинского технического университета, Караганда, Казахстан. ORCID ID: 0000-0003-2249-3435. Email: astra_mun@mail.ru

References

[1] Denisov VM, Istomin SA, Denisova LT, Kuchumova OV, Ryabov VV. Vyazkost rasplavov Bi2O3-CaO [Viscosity of Bi2O3-CaO melts]. Rasplavy = Melts, 2014;2:12-16. (In Rus.)

[2] Konstantinova NYu, Kurochkin AR, Borisenko AV, Filippov VV, Popel PS. Vyazkost rasplavov med-alyumini [Viscosity of copper–aluminum melts]. Rasplavy = Melts, 2016;2:157. (In Rus.)

[3] Ryabina AV, Shevchenko VG. O vyazkosti zhidkikh metallov [On the viscosity of liquid metals]. Rasplavy = Melts, 2017;6:522. (In Rus.)

[4] Beltyukov AL, Olyanina NV, Ladianov VI. Osobennosti izmereniya vyazkosti zhidkikh splavov So–Si [Peculiarities of measurement of viscosity of liquid Co–Si alloys]. Rasplavy = Melts, 2017;6:470 (In Rus.)

[5] Dobosz Alexandra, Gancarz Tomasz. Reference Data for the Density, Viscosity, and Surface Tension of Liquid Al-Zn, Ag-Sn, Bi-Sn, Cu-Sn, and Sn-Zn Eutectic Alloys. Journal of Physical and Chemical Reference Data, 2018;47(1). https://doi.org/10.1063/1.5010151

[6] Nunes V.M.B., Queiros C.S.G.P., Lourenco M.J.V., et al. Viscosity of Industrially Important Zn-Al Alloys Part II: Alloys with Higher Contents of Al and Si. International Journal of Thermophysics, 2018;39(5). https://doi.org/10.1007/s10765-018-2388-x

[7] Zhao Yan, Hou Xiaoxia, Bai Yanwen. Viscosity, structure and fragility of Ag-Si melts. Aip Advances, 2018;8(8). https://doi.org/10.1063/1.5046317

[8] Tyagunov A G, Baryshev EE, Tyagunov GV, Shmakova KYu, Mushnikov VS. Struktura i svoystva Ni–Al splavov v zhidkom sostoyanii [Structure and properties of Ni–Al alloys in the liquid state]. Rasplavy = Melts, 2019;1:24-28. (In Rus.) https://doi.org/10.7868/S0235010619010213

[9] Tasidou KA, Chliatzou ChD, Assael MJ, et al. Reference Correlations for the Viscosity of 13 Inorganic Molten Salts. Journal of Physical and Chemical Reference Data, 2019;48(1). https://doi.org/10.1063/1.5091511

[10] Chikova OA, Tkachuk GA, V'yukhin VV. Viscosity of Cu-Ni Melts. Russian Journal of Physical Chemistry A, 2019;93(2). https://doi.org/10.1134/S0036024419020067

[11] Zhang Fan, Wen Shiyi, Liu Yuling, et al. Modelling the viscosity of liquid alloys with associates. Journal of Molecular Liquids, 2019;291. https://doi.org/10.1016/j.molliq.2019.111345

[12] Uddin Md Salah, Gosh RC, Bhuiyan GM. Investigation of surface tension, viscosity and diffusion coefficients for liquid simple metals. Journal of Non-Crystalline Solids, 2019;499:426-433. https://doi.org/10.1016/j.jnoncrysol.2018.07.014

[13] Gao Shanchao, Jiao Kexin, Zhang Jianliang. Review of viscosity prediction models of liquid pure metals and alloys. Philosophical Magazine, 2019;99(7):853-868. https://doi.org/10.1080/14786435.2018.1562281

[14] Meyer N, Xu H, Wax J-F. The role of chemical order in the temperature and composition dependence of the viscosity of liquid alloys. Journal of Chemical Physics, 2019;150(17). https://doi.org/10.1063/1.5092694

[15] Filippov VV, Shunyaev KYu, Leont'ev LI. Temperature and Time Dependences of the Viscosity of InBi-Pb Melts. Doklady Physical Chemistry, 2020;494(1), 139-142. https://doi.org/10.1134/S0012501620090018

[16] Filippov VV, Shunyayev KYu. Vyazkost rasplavov InBi–Pb [Viscosity of InBi–Pb melts]. Rasplavy = Melts, 2020;5:541-547. (In Rus.) https://doi.org/10.31857/S0235010620050059

[17] Beltyukov AL, Olyanina NV. Ladianov V.I. Osobennosti izmereniya vyazkosti metallicheskikh rasplavov metodom krutilnykh kolebaniy. Rasplavy = Melts, 2016;2:176. (In Rus.)

[18] Makasheva AM, Malyshev VP. Klasterno-assotsiatnaya model vyazkosti ftorida natriya v sopostavlenii s modelyu Frenkelya [Cluster-associate model of the viscosity of sodium fluoride in comparison with the Frenkel model]. Rasplavy = Melts, 2020;5:480-488. (In Rus.) https://doi.org/10.31857/S0235010620050060

[19] Malyshev VP, Makasheva AM. Vyazkost' i tekuchest' rasplavov v aspekte ih haotizacii (neorganicheskie soedineniya i splavy) [Viscosity and fluidity of melts in terms of their randomization (inorganic compounds and alloys)]. Lambert: Academic Publishing (Germany), 2020;153. (In Rus.)

[20] Malyshev VP, Bekturganov NS, Turdukozhayeva (Makasheva) AM. Vyazkost, tekuchest i plotnost veshchestv kak mera ikh khaotizatsii [Viscosity, fluidity and density of substances as a measure of their chaos]. M.: Nauchnyy mir. 2012;288. (in Russ).

[21] Makasheva AM. Klasterno-associatnaya model' vyazkosti i metody opredeleniya ee parametrov [Cluster-associated viscosity model and methods for determining its parameters]. Kompleksnoe ispol'zovanie mineral'nogo syr'ya = Complex Use of Mineral Resources, 2020;2(313):27-37. (In Rus.) https://doi.org/10.31643/2020/6445.14

[22] Malyshev VP, Makasheva AM. Vzaimosvyaz' klasterno-associatnoj modeli vyazkosti zhidkosti s model'yu vyazkosti Frenkelya-Andrade [Relationship between the cluster-associate model of fluid viscosity and the Frenkel-Andrade viscosity model]. Izvestiya Rossijskoj Akademii nauk = Russian Chemical Bulletin, Ser. him. 2020;7:1296-1305.. (In Rus.) https://doi.org/10.1007/s11172-020-2901-9

[23] Aleksandrov VD, Frolova SA, Pokintelitsa EA, Zozulya AP, Amerkhanova ShK. Dinamika izmeneniya klasternoy struktury rasplavov v protsesse ravnovesnoy i neravnovesnoy kristallizatsii [Dynamics of changes in the cluster structure of melts during equilibrium and non-equilibrium crystallization]. Rasplavy = Melts, 2017;6:484. (In Rus.)

[24] Pozin ME. Tekhnologiya mineralnykh soley (udobreniy, pestitsidov, promyshlennykh soley, okislov i kislot) [Technology of mineral salts (fertilizers, pesticides, industrial salts, oxides and acids)] Ch. I i II, 4-e, ispr., L.: Khimiya. 1974;792. (in Russ).

[25] Morachevskiy AG. Elektroprovodnost. plotnost i vyazkost individualnykh rasplavlennykh soley: spravochnik po rasplavlennym solyam [Electrical conductivity, density and viscosity of individual molten salts: Handbook of molten salt] T. 1. Perevod s angl. i s dop. – Leningradskoye otd-e: Khimiya. 1971**;**168. (In Rus.)

[26] Volkov AI, ZHarskij IM. Bol'shoj himicheskij spravochnik [Big chemical reference book]. – Mn.: Sovremennaya shkola, 2005:608. (In Rus.)

[27] Janz GJ, Saegusa F. Molten Carbonates as Electrolytes: Viscosity and Transport Properties J. Electrochem. Soc. 1963;110: 452.

[28] Vorobyev GV, Palguyev SF, Karpachev SV. Trudy Instituta elektrokhimii UFAN SSSR [Proceedings of the Institute of Electrochemistry UFAN USSR]. 1965;6:39. (in Russ).

МАЗМҰНЫ
СОДЕРЖАНИЕ
CONTENTS

Технические редакторы:
Г.К. Касымова, Н.М. Айтжанова, Т.И. Кожахметов, Н.Ж. Артыкбаев

Верстка на компьютере:
Г.К. Касымова

Дизайнер:
Г.К. Касымова, Н.Ж. Артыкбаев

Институт металлургии и обогащения, Satbayev University

Алматы, Казахстан

18.02.2022 г.